UNIVERSITI TEKNOLOGI MARA

UNRAVELLING POROUS SILICON (PSI)-BASED SURFACE-ENHANCED RAMAN SPECTROSCOPY (SERS) SUBSTRATE FABRICATION FORMULA SENSITIVE TO SALIVARY DENGUE NON-STRUCTURAL PROTEIN 1 (NS1)

NOOR FADZILAH BINTI ISMAIL

MSc

May 2026

UNIVERSITI TEKNOLOGI MARA

UNRAVELLING POROUS SILICON (PSI)-BASED SURFACE-ENHANCED RAMAN SPECTROSCOPY (SERS) SUBSTRATE FABRICATION FORMULA SENSITIVE TO SALIVARY DENGUE NON-STRUCTURAL PROTEIN 1 (NS1)

NOOR FADZILAH BINTI ISMAIL

Thesis submitted in fulfilment
of the requirements for the degree of
Master of Science
(Electrical Engineering)

Faculty of Electrical Engineering

May 2026

CONFIRMATION BY PANEL OF EXAMINERS

I certify that a Panel of Examiners has met on 10 December 2025 to conduct the final examination of Noor Fadzilah binti Ismail on her Masters of Science thesis entitled "Unravelling Porous Silicon (PSi)-Based Surface-Enhanced Raman Spectroscopy (SERS) Substrate Fabrication Formula Sensitive to Salivary Dengue Non-Structural Protein 1 (NS1)" in accordance with Universiti Teknologi MARA Act 1976 (Akta 173). The Panel of Examiners recommends that the student be awarded the relevant degree. The Panel of Examiners was as follows:

Irni Hamiza Hamzah, PhD
Associate Professor
Faculty of Electrical Engineering
Universiti Teknologi MARA
(Chairman)

Puteri Sarah Mohamad Saad, PhD
Associate Professor
Faculty of Electrical Engineering
Universiti Teknologi MARA
(Internal Examiner)

Noor Hasmiza Harun, PhD
Associate Professor
Medical Engineering Technology Section
University of Kuala Lumpur
British Malaysian Institute
(External Examiner)

PROFESSOR DR HJH ZURAEDA IBRAHIM
Dean
Institute of Postgraduates Studies
Universiti Teknologi MARA

Date: 26 May 2026

AUTHOR'S DECLARATION

I declare that the work in this thesis was carried out in accordance with the regulations of Universiti Teknologi MARA. It is original and is the results of my own work, unless otherwise indicated or acknowledged as referenced work. This thesis has not been submitted to any other academic institution or non-academic institution for any degree or qualification.

I, hereby, acknowledge that I have been supplied with the Academic Rules and Regulations for Postgraduate, Universiti Teknologi MARA, regulating the conduct of my study and research.

Name of Student	:	Noor Fadzilah binti Ismail
Student ID. No.	:	2020548251
Programme	:	Master of Science (Electrical Engineering) – EE750
Faculty	:	Electrical Engineering
Thesis Title	:	Unravelling Porous Silicon (PSi)-Based Surface-Enhanced Raman Spectroscopy (SERS) Substrate Fabrication Formula Sensitive to Salivary Dengue Non-Structural Protein 1 (NS1)
Signature of Student	:	…… ……..
Date	:	May 2026

ABSTRACT

Dengue fever remains a major public health issue in Malaysia, with annual cases consistently exceeding 100,000 since 2014. Although the mortality rate is relatively low at around 0.2%, timely diagnosis is essential for effective treatment. One of the most promising biomarkers for early detection is the non-structural protein 1 (NS1), which can be detected as early as the first day of infection, well before the production of antibodies such as IgM, IgG and IgA. This makes NS1 an attractive target for diagnostic assays. Blood-based tests are commonly used, but their invasive nature may discourage early medical consultation. Since NS1 is also present in saliva, it offers a less invasive diagnostic alternative; however, reported sensitivity in saliva detection remains limited at only 64.7%. This limitation underscores the need for more sensitive and reliable detection methods. In this study, a surface-enhanced Raman spectroscopy (SERS) substrate coated with silver nanoparticles (AgNPs) was fabricated using an electrochemical etching method combined with drop-casting deposition, with the aim of detecting low concentrations of NS1 in saliva. Etching durations were varied to optimize the porous silicon structure, with the optimum condition determined from the highest Raman peak intensity and narrowest full width at half maximum (FWHM). AgNPs of various sizes (5 nm, 25 nm, 50 nm, 75 nm and 110 nm) were also tested to identify the most effective configuration for SERS enhancement. The resulting substrates were characterized using Raman spectroscopy, field emission scanning electron microscopy (FESEM) and energy-dispersive X-ray spectroscopy (EDX). Performance evaluation using Rhodamine 6G (R6G) as a model analyte showed that the substrate coated with 75 nm AgNPs exhibited the best enhancement, achieving an enhancement factor (EF) of 148.56 and a limit of detection (LOD) of 0.01 mg/mL. For NS1 detection, the 75 nm AgNPs-coated PSi SERS substrate was functionalized with dengue antibodies. This functionalized substrate achieved a detection limit of 0.001 mg/mL (equivalent to 1000 ng/mL), which lies within the clinically relevant detection range. Overall, this work highlights the potential of 75 nm AgNPs-coated PSi SERS substrate as a sensitive, non-invasive platform for dengue detection in saliva. These findings provide a foundation for developing portable and cost-effective diagnostic tools that could facilitate early disease detection and timely intervention.

ACKNOWLEDGEMENT

Firstly, I wish to thank Allah for giving me the opportunity to embark on my MSc and for completing this long and challenging journey successfully. My deepest gratitude goes to my supervisor Dr Afaf Rozan binti Mohd Radzol, whose expertise and unwavering support have been instrumental in the completion of this thesis. Your guidance and encouragement have inspired me to push my boundaries and strive for excellence.

My appreciation goes to my co-supervisors, Dr. Lyly Nyl binti Ismail and Prof. Lee Yoot Khuan for their valuable insights and constructive feedback, which have significantly enhanced the quality of my work.

I extend my sincere thanks to the staffs who provided essential facilities and assistance during sampling process. The support from Center of System Studies, Faculty of Electrical Engineering, Universiti Teknologi MARA Shah Alam, Selangor, Center for Electrical Engineering Studies, Universiti Teknologi MARA, Cawangan Pulau Pinang, Pulau Pinang and the laboratory staff of the Institute of Nano Optoelectronics Research and Technology (INOR), Universiti Sains Malaysia, Pulau Pinang is gratefully acknowledged.

I would like to acknowledge the financial support from the Ministry of Higher Education Malaysia (MOHE) through the Fundamental Research Grant Scheme (600-IRMI/FRGS 5/3 (294/2019)), which enabled me to pursue my research.

I also wish to extend my special thanks to everyone who contributed, both directly and indirectly, with the full willingness of contributing their effort, time, energy and idea in completing this thesis.

Finally, I am profoundly thankful to my family for their unwavering support, love and understanding. Your encouragement has been my foundation and I could not have achieved this milestone without you. Alhamdulillah.

TABLE OF CONTENTS

LIST OF TABLES

LIST OF FIGURES

LIST OF SYMBOLS

Symbols

Ag	Silver
Au	Gold
C	Carbon
C_2H_5OH	Ethanol
Cu	Copper
GPTS	Glycidoxypropy Trimethoxysilane
H_2	Hydrogen Gas
HF	Hydrofluoric Acid
NS1	Non-Structural Protein 1
O	Oxygen
PBS	Phosphate-Buffered Saline
R6G	Rhodamine 6G

LIST OF ABBREVIATIONS

Abbreviations

AFM	Atomic Force Microscopy
AgNPs	Silver Nanoparticles
Arboviral	Arthropod-borne Viral
COVID-19	Coronavirus Disease 2019
DC	Direct Current
DCPEC	Double Cell Photo Electrochemical Cell
DENV	Dengue Virus
DI	Deionized
EDX	Energy Dispersive X-ray Spectroscopy
EF	Enhancement Factor
ELISA	Enzyme-Linked Immunosorbent Assay
FESEM	Field Emission Scanning Electron Microscope
FWHM	Full Width at Half Maximum
HCT	Hematocrit
ICT	Immuno-Chromatographic
IgA	Immunoglobulin A
IgG	Immunoglobulin G
IgM	Immunoglobulin M
LOD	Limit of Detection

LSPR	Localized Surface Plasmon Resonance
NPs	Nanoparticles
PCA-SVM	Principal Component Analysis and Support Vector Machine
PSi	Porous Silicon
RCT	Rapid Combo Test
RIE	Reactive Ion Etching
RNA	Ribonucleic Acid
RT-PCR	Reverse Transcription Polymerase Chain Reaction
SERS	Surface Enhanced Raman Spectroscopy
Si	Silicon
WCC	White Cell Count

LIST OF NOMENCLATURE

Nomenclatures

a.u.	Arbitrary Units, The Measurement Scale Used to Represent Raman Signal Intensity
cm^{-1}	Reciprocal Centimeters, The Unit Employed to Express Raman Shift for Peak Position; The Unit for FWHM to Describe Spectral Linewidth of the Peak
mA/cm^2	Milliampere per Square Centimeter, Electric Current Density Unit
M	Molarity, The Concentration Unit Defined the Number of Moles of Solute per Liter of R6G Solutions
mg/mL	Milligrams per Milliliter, The Volume Concentration Unit
nm	Nanometer, Unit of Length Used to Describe The Size of Nanoparticles
Ω·cm	Ohm-Centimeter, The Resistivity Unit Representing The Electrical Resistance of a Material

CHAPTER 1
INTRODUCTION

1.1 Research Background

Dengue is a disease caused by viral infection. In 2023, a record breaking 6.5 million dengue cases were reported globally, resulting in over 7,300 deaths ("Dengue and Severe Dengue," 2014). In Malaysia alone, 123,133 cases and 100 deaths were recorded in the same year (Hassan, 2024). By 2024, the number of cases slightly decreased to 122,423; however, fatalities rose to 117 (Hassan, 2025). Early detection of dengue infection particularly within the initial days of illness is crucial for effective patient monitoring and management, which can significantly contribute to reducing the mortality rate.

The non-structural protein 1 (NS1) of the dengue virus (DENV) serves as an early biomarker for detecting DENV infection. It can be detected between days 1 and 5 of illness (Malaysia Health Technology Assessment Section (MaHTAS), 2015). Currently, NS1 detection is commonly performed using enzyme-linked immunosorbent assay (ELISA) (Costa et al., 2014) and immunochromatographic (ICT) rapid test kits (S. M. Wang & Sekaran, 2010). Both methods require blood samples, which are invasive and carry a risk of bloodborne infections.

Saliva has emerged as a promising non-invasive alternative for DENV detection, particularly because the NS1 protein an early biomarker of infection has been shown to be detectable in this medium (Anders et al., 2012). The use of saliva offers several advantages over traditional blood-based methods, such as increased patient comfort, reduced risk of infection and simplified sample collection, especially in resource-limited or mass-screening settings. However, one of the primary challenges lies in the considerably lower concentration of NS1 in saliva compared to blood, which can compromise the sensitivity and reliability of current detection methods. This necessitates the development of more sensitive diagnostic tools tailored for salivary diagnostics to effectively harness its potential for early dengue detection.

In this study, Surface-Enhanced Raman Spectroscopy (SERS) is proposed as a promising technique for the detection of low-concentration NS1 protein in saliva. Renowned for its high sensitivity and specificity, the effectiveness of SERS is largely

influenced by the properties of the substrate employed. A typical SERS substrate consists of nanostructured noble metals capable of adsorbing analyte molecules, thereby significantly enhancing Raman scattering signals to detectable levels. The degree of signal amplification is highly dependent on the structural characteristics of the substrate, including parameters such as size, shape and dimensional modifications (length and width). To this end, the study aims to fabricate nanostructured porous silicon (PSi) based substrates coated with silver nanoparticles (AgNPs), introducing variations in their structural features. The core objective is to develop an optimized SERS substrate that enhances detection sensitivity for low concentrations of dengue NS1 protein. The structural and optical properties of the fabricated substrates are characterized using field emission scanning electron microscopy (FESEM), energy-dispersive X-ray spectroscopy (EDX) and Raman spectroscopy. The sensing performance of the substrates is evaluated using Rhodamine 6G (R6G) and NS1 protein.

1.2 Problem Statement

Early and accurate detection of DENV is crucial for timely medical intervention and the prevention of severe complications or fatalities. Currently, standard diagnostic methods rely on blood-based techniques such as ELISA and rapid diagnostic tests. While effective, these methods are invasive and often require trained personnel, making them less suitable for mass screening or point-of-care applications.

To address these limitations, researchers have explored non-invasive alternatives such as saliva-based diagnostics. Saliva sampling offers significant advantages in terms of ease of collection, patient comfort and reduced risk of infection transmission. However, existing approaches for detecting DENV in saliva have shown limited success. For instance, ELISA-based detection in saliva has achieved only about 64.7% sensitivity (Anders et al., 2012), while rapid tests have failed to detect the virus altogether (Machado et al., 2012).

In response to these challenges, SERS has emerged as a promising alternative due to its high sensitivity and molecular specificity. Recent studies utilizing SERS, in combination with advanced signal processing and machine learning algorithms, have demonstrated improved detection of the dengue NS1 in saliva, achieving up to 83.22% accuracy using commercially available substrate (Radzol et al., 2024). Despite these

advancements, a significant portion of misclassified cases has been attributed to low concentrations of NS1 protein in the saliva samples.

In clinical diagnostics, low-concentration NS1 samples are defined as antigen levels at or below the detection limits of conventional ELISA methods, typically ≤40 ng/mL during the acute phase and ≤4 ng/mL during the convalescent phase in serum samples (Alcon et al., 2002; Anand et al., 2016; Moi et al., 2013; Vazquez et al., 2010). Because most studies have focused on serum, the challenges of detecting NS1 are expected to be even greater in saliva, where antigen levels are substantially lower. It is therefore hypothesized that enhancing the affinity of the SERS substrate for NS1 could significantly improve detection accuracy, particularly within this clinically relevant low-concentration range.

To date, no reported studies have focused on the development of a SERS substrate specifically designed to selectively target NS1 in saliva. Therefore, the fabrication of a novel affinity-enhanced SERS substrate is proposed as a promising strategy to advance non-invasive dengue diagnostics and address the limitations of current detection methods.

1.3 Research Objectives

The primary goal of this study is to fabricate a SERS substrate capable of improving the detection of low-concentration NS1 (ranging from 0.1 mg/mL to 0.001 mg/mL), thereby enabling salivary-based, non-invasive detection for dengue. The following sub-objectives are structured toward achieving the goal:

a) To fabricate AgNPs-coated PSi SERS substrate using electro-chemical technique.
b) To characterize the structural and Raman properties of AgNPs-coated PSi SERS substrate.
c) To evaluate the performance of the AgNPs-coated PSi SERS substrate in detecting low concentration of the Raman marker, Rhodamine (R6G), DENV NS1 in term of limit of detection (LOD) and enhancement factor (EF).

1.4 Scope and Limitation of Study

This study focuses on the development and evaluation of a SERS substrate for the non-invasive detection of DENV NS1 protein using saliva samples. The substrate is based on PSi fabricated through a direct current (DC) electrochemical etching method, which is selected for its simplicity, low-cost and ability to produce nanostructured surfaces suitable for SERS applications.

Following the fabrication of PSi, AgNPs are deposited onto the porous structure surface to serve as Raman signal enhancers. The AgNPs play a critical role in amplifying the Raman signals of target molecules, thereby improving the sensitivity of the substrate. The study includes systematic characterization of the AgNPs-coated PSi SERS substrates, with particular focus on optimizing key fabrication parameters such as etching time and AgNPs size to achieve maximum SERS enhancement.

The scope of the study includes:

i) Fabrication of PSi using a DC electrochemical etching process, where etching time are varies for optimum setting.
ii) Deposition of various sizes of AgNPs on the PSi surface to enhance Raman scattering signals.
iii) Characterization of the structural properties of the AgNPs-coated PSi SERS substrates using Field Emission Scanning Electron Microscopy (FESEM) and Energy Dispersive X-ray Spectroscopy (EDX) and Raman properties using Raman spectroscopy.
iv) Performance evaluation of the optimized SERS substrate using two analytes: R6G as a standard probe molecule and DENV NS1 protein as the target biomarker. The substrate's performance will be assessed in terms of LOD and EF.

However, the study also recognizes certain limitations:

- The fabrication process may be affected by variability in etching uniformity, which can impact reproducibility.
- The study focuses exclusively on silver nanoparticles, although other plasmonic materials such as gold or hybrid nanostructures might offer different or improved enhancement profiles.

- Detection experiments are conducted under controlled laboratory conditions and further validation using clinical saliva samples under real-world conditions would be required for practical deployment.
- The study is limited to the detection of DENV NS1 protein and the specificity of the substrate against other viral or salivary proteins is not within the scope of this investigation.

Despite these limitations, the study provides a foundational framework for the development of a low-cost, highly sensitive and non-invasive diagnostic platform, potentially contributing to early dengue detection and improved disease surveillance.

1.5 Significance of Study

This study focuses on the fabrication of a SERS substrate specifically designed to detect low concentrations of the DENV NS1 in saliva, a non-invasive sample medium. Saliva-based diagnostics offer significant advantages in terms of patient comfort, ease of collection and safety, making them ideal for early screening and point-of-care testing.

To enhance the practicality and scalability of the detection platform, the SERS substrate will be fabricated using silicon, an abundant and cost-effective material that is compatible with established fabrication processes. The use of a simple and low-cost electrochemical fabrication method further supports the initial development of an affordable diagnostic tool.

By addressing the limitations of current diagnostic technologies, this study has the potential to significantly advance the field of dengue diagnostics. The successful development of a sensitive, specific and low-cost SERS-based platform for NS1 detection in saliva could pave the way for non-invasive, accessible and accurate diagnostic solutions, ultimately contributing to improved disease surveillance and timely clinical intervention in dengue-endemic regions.

1.6 Organization of Thesis

This thesis is organized in five main chapters which are Introduction, Literature Review, Methodology, Results and Discussions and Conclusion.

Chapter 1 provides an essential foundation for the thesis by outlining the key components of the research. It begins with the research background, offering context and highlighting the importance of the study. The problem statement identifies the core issue the research aims to address. This is followed by the research objectives, which clearly define what the study intends to achieve. The scope and limitations section delineates the boundaries of the research and acknowledges any constraints. Next, the significance of the study emphasizes the potential contributions and impact of the findings. Lastly, the organization of the thesis presents a brief overview of the structure of the remaining chapters, guiding the reader through the thesis layout.

Chapter 2 presents a comprehensive review of the existing literature relevant to the study, beginning with an introduction to the topic. It focuses on two main areas: dengue fever and SERS. The section on dengue fever explores various detection methods, including saliva-based non-invasive techniques and the use of NS1 antigen for early diagnosis. The following section delves into SERS, highlighting its application in disease diagnosis, especially for enhancing sensitivity and specificity. It covers the development of silicon-based SERS substrates, electrochemical etching techniques and the use of plasmonic metals to boost Raman signals. The concept of surface functionalization is also discussed to improve the performance of detection platforms. The chapter concludes with a summary that ties together the relevance of these technologies to the research problem.

Chapter 3 outlines the research methodology employed in the study, beginning with an introduction to the overall approach. It provides a detailed methodology overview, starting with the electrochemical fabrication of PSi, which serves as the base for further modifications. This is followed by the drop casting deposition of AgNPs to create an active SERS surface. Subsequent sections describe the Raman characterization techniques used to evaluate the substrate's Raman properties and the structural characterization to analyze its morphology and material composition. Lastly, the chapter details the surface functionalization of the SERS substrate for the specific detection of the dengue NS1 antigen, a crucial step to ensure sensitivity and specificity in biosensing. The chapter concludes with a summary of the procedures, emphasizing their role in achieving the research objectives.

Chapter 4 presents the results and analysis of the study, beginning with an overview of the PSi-based SERS substrate and how etching time influences its Raman and structural properties. It then explores the Raman characteristics of AgNPs-coated

PSi SERS substrates, particularly focusing on how different sizes of AgNPs deposition affect their performance. The detection performance of these substrates is evaluated, comparing EF between AgNPs-coated bare silicon and AgNPs-coated PSi SERS substrates and determining their respective LOD. The chapter further demonstrates the effectiveness of the developed AgNPs-coated PSi SERS substrate in detecting low concentrations of dengue NS1 antigen, culminating in a conclusion that summarizes the findings and their implications for sensitive biosensing applications.

Finally, Chapter 5 concludes the research by summarizing key achievements and outlining directions for future development. The study successfully demonstrated the fabrication and optimization of AgNPs-coated PSi SERS substrates for sensitive detection of low-concentration dengue NS1 antigens. Building on these findings, the chapter recommends future works aim to advance the practicality and versatility of the developed biosensor system for real-world clinical and environmental applications.

CHAPTER 2
LITERATURE REVIEW

2.1 Introduction

This review chapter is divided into 4 subsections. After the introduction, it reviews the fundamental concepts and related studies that form the basis of this research. Section 2.2 discusses dengue fever, highlighting existing detection methods, the potential of salivary-based non-invasive approaches and the importance of NS1 protein in early diagnosis. Section 2.3 focuses on SERS, emphasizing its application in disease diagnosis and the development of silicon-based SERS substrates. The section also reviews electrochemical etching techniques, the role of plasmonic metals in enhancing Raman signals and approaches for surface functionalization. Finally, Section 2.4 provides a conclusion summarizing the key insights from the literature and identifying research gaps addressed in this study.

2.2 Dengue Fever

Dengue fever is the most common Arthropod-borne Viral (arboviral) illness in humans which is the infections caused by a group of viruses spread to people by the bite of infected arthropods (insects) such as mosquitos ("Dengue and Severe Dengue," 2014). It is an outbreak and a major national health concern in Malaysia. Table 2.1 presents the statistical information of reported and fatal dengue cases in Malaysia from 2020 to 2024. The data reveals notable fluctuations over the five-year period. In 2020 (Rusli et al., 2020), there were 88,845 reported cases and 142 fatalities, the highest number of deaths recorded during this period. However, a sharp decline was observed in 2021 (Abdullah, 2022), with only 26,365 reported cases and 20 fatalities. This significant drop is likely attributed to the Coronavirus disease 2019 (COVID-19) pandemic, during which widespread movement restrictions and lockdowns may have reduced mosquito breeding grounds and human-vector contact. From 2022 onward, the number of dengue cases began to rise again, reaching 66,102 cases in 2022 (Abdullah, 2023) and peaking at 123,133 in 2023 (Hassan, 2024), with fatal cases increasing from 56 to 100 over the same span. In 2024 (Hassan, 2025),

the number of reported cases slightly decreased to 122,423, with 117 fatalities, suggesting a marginal improvement.

Table 2.1
The Statistical Information of Dengue Cases in Malaysia

Year	Reported Cases	Fatal Cases
2020	88,845	142
2021	26,365	20
2022	66,102	56
2023	123,133	100
2024	122,423	117

Note: Statistical information of dengue cases in Malaysia was adapted from Abdullah (2022, 2023), Hassan (2024, 2025) and Rusli et al. (2020)

The fatal cases of dengue reported in recent years are largely attributed to delays in diagnosis and the subsequent late initiation of appropriate medical treatment (Malaysia Health Technology Assessment Section (MaHTAS), 2015). Dengue can progress rapidly from mild symptoms to severe complications such as dengue hemorrhagic fever or dengue shock syndrome, both of which can be fatal if not addressed promptly (Malaysia Health Technology Assessment Section (MaHTAS), 2015). In many instances, early symptoms are mistaken for common viral infections, leading to underestimation of the severity and delayed healthcare-seeking behaviour. This highlights the critical importance of early detection and timely intervention. Early diagnosis enables close monitoring, proper fluid management and supportive care, all of which significantly reduce the risk of complications and mortality (Malaysia Health Technology Assessment Section (MaHTAS), 2015).

2.2.1 Dengue Detection Method

Table 2.2 outlines the various diagnostic and monitoring tests utilized by physicians to detect dengue infection as outlined in the Clinical Practice Guidelines: Management of Dengue Infection in Adults published by Ministry of Health Malaysia (Malaysia Health Technology Assessment Section (MaHTAS), 2015). The disease monitoring tests, such as white cell count (WCC), platelet count and hematocrit (HCT), are essential for tracking disease progression. A rapid decline in WCC and platelets typically indicates the worsening phase of dengue, while an elevated HCT level suggests plasma leakage a key indicator of severe dengue. In terms of diagnostic tests,

the Rapid Combo Test (RCT) is widely used due to its ability to detect both the NS1 antigen and dengue-specific IgM and IgG antibodies in whole blood, serum or plasma. It provides a quick turnaround with high sensitivity (93.9%) and specificity (92%), making it suitable for early diagnosis. The ELISA-based dengue antigen and serology tests offer more detailed insights by distinguishing between primary and secondary infections. NS1 antigen detection is most reliable between days 1 to 5 of illness (Malaysia Health Technology Assessment Section (MaHTAS), 2015), while IgM antibodies appear around day 6 and are indicative of a primary infection. IgG antibodies, on the other hand, become more prominent in secondary infections and are typically detected after day 7. Lastly, Real-time Reverse Transcription Polymerase Chain Reaction (RT-PCR) is a molecular diagnostic tool used to identify dengue viral RNA. This test is capable of detecting the virus up to five days after symptom onset, targeting specific serotypes of the DENV. However, it is limited by cost and availability, often being reserved for research or complex diagnostic cases.

All the listed tests require blood samples as the primary diagnostic medium. The invasive nature of blood sample collection can hinder early detection of dengue, as many individuals may be reluctant to undergo needle pricks or venipuncture. This hesitation often stems from fear of pain, discomfort or past negative experiences with blood draws. As a result, some patients may delay seeking medical attention until symptoms worsen, potentially missing the optimal window for early diagnosis and intervention. This delay can increase the risk of complications, especially in cases that progress to severe dengue. To improve early case detection, there is a need to raise public awareness, improve patient comfort during testing and explore the development of less invasive diagnostic alternatives such as using salivary medium.

Table 2.2
Dengue Monitoring and Diagnostic Tests

Method	Test	Criteria
Disease monitoring tests	White cell count (WCC) and Platelet count	Rapid decrease in WCC is accompanied by platelet reduction as disease progresses
	Haematocrit (HCT)	Plasma leakage in dengue infection cause rising in HCT value.
Diagnostic tests	Rapid Combo Test (RCT)	Detect the present of dengue NS1 antigen and dengue IgM and IgG antibodies using whole blood, serum and plasma. The sensitivity is 93.9% and specificity is 92%
	Dengue antigen and serology test by ELISA	NS1 antigen detection The sensitivity of NS1 antigen detection drops from day 4-5 of illness onwards and usually becomes undetectable in the convalescence phase.
		Dengue IgM test Almost 93%-99% of cases will have detectable IgM from day 6 through day 10. More suitable for primary dengue infection.
		Dengue IgM test IgG is recommended if IgM is still negative after day 7. More suitable for secondary dengue infection.
	Dengue viral RNA detection (Real time RT-PCR)	Target specific genome of DENV. Detect the viral RNA target up to 5 days after onset of the symptoms. Limited facilities and expensive.

Note: Information on dengue monitoring and diagnostic tests was adapted from the *Clinical Practice Guidelines: Management of Dengue Infection in Adults* (3rd ed.; Malaysia Health Technology Assessment Section [MaHTAS] (2015)

2.2.2 Salivary Based Non-Invasive DENV Detection Method

Saliva offers several distinctive advantages that make it a preferable alternative diagnostic fluid compared to other non-invasive biofluids such as sweat, tears and urine. Among its most notable benefits are the non-invasive, painless and straightforward nature of sample collection, which reduces patient discomfort and improves compliance (Madalli, 2013). Furthermore, saliva sampling is highly cost-effective for mass screening efforts in large populations, especially in resource-limited settings (Mittal et al., 2011). Unlike blood, which requires trained personnel and sterile equipment for venipuncture, saliva can be self-collected, minimizing the need for clinical infrastructure. Additionally, it is both cheaper and more practical to store and transport than blood or urine due to its reduced biohazard risk and less stringent cold chain

requirements (Madalli, 2013; Mittal et al., 2011). Biochemically, saliva consists of approximately 99.5% water and 0.5% enzymes, organic and inorganic molecules and dissolved gases. Many of the diagnostic constituents present in blood serum can also be found in whole saliva, having diffused from the local vasculature of salivary glands and gingival crevicular fluid. However, their concentrations in saliva are typically much lower than in serum, which presents a considerable limitation for its widespread use in diagnostic applications (Schenkels et al., 1995).

This challenge is particularly evident in dengue diagnostics. For example, Anders et al. (2012) explored the detection of dengue non-structural protein 1 (NS1) in saliva using ELISA, but only achieved a sensitivity of 64.7%, a level considered inadequate for clinical use. Similarly, another study employing a rapid NS1 test reported complete failure to detect NS1 even in saliva samples from acute dengue cases, reinforcing the difficulty of saliva-based antigen detection (Machado et al., 2012). In contrast, a more recent study by (Humaidi et al., (2021) evaluated saliva samples from hospitalized dengue patients collected between days 2 and 10 post-onset of fever. Their findings showed that RT-PCR detection of dengue RNA had a relatively high positivity rate of 82.1% during days 2 to 4, which then declined to 51.3% between days 5 and 10. However, when NS1 antigen detection was assessed using ELISA, the sensitivity dropped significantly to just 36%, underscoring the inadequacy of current methods for detecting NS1 in saliva. These limitations clearly highlight the need for an improved, more sensitive alternative technique for saliva-based NS1 detection.

Despite these challenges, saliva remains a highly attractive sample medium and emerging techniques offer new promise. Mizuno et al. (2007) and Poloni et al. (2010) successfully detected the dengue virus genome in saliva using real-time reverse transcription PCR (RT-PCR), supporting the feasibility of using saliva for molecular diagnostics. Further supporting this approach, Banavar and Vidya (2014) achieved 100% sensitivity and specificity using an IgG ELISA kit in saliva samples from seropositive patients, indicating strong potential for antibody-based dengue diagnosis using oral fluids.

Innovative sensor-based technologies are also being explored to enhance diagnostic performance. Wasik et al. (2018) developed a label-free chemiresistive immunosensor composed of a network of single-walled carbon nanotubes functionalized with anti-dengue NS1 monoclonal antibodies. This sensor successfully detected and quantified DENV NS1 protein in artificial human saliva within a clinically

relevant concentration range (1-1000 ng/mL), demonstrating the feasibility of high-sensitivity detection in a saliva-based platform. Additionally, Radzol et al. (2024) showed that combining surface-enhanced Raman spectroscopy (SERS) with a principal component analysis-support vector machine (PCA-SVM) algorithm achieved a diagnostic accuracy of 83.22%, sensitivity of 88.27% and specificity of 78.13% in identifying dengue infections from Raman spectra of saliva samples collected during the early stages (days 1 to 5) of illness. These findings underscore the potential of SERS, especially when enhanced with machine learning, as a powerful tool for non-invasive, early-stage dengue diagnostics. The development of a SERS substrate specifically optimized for NS1 detection in saliva could further elevate the sensitivity and reliability of such platforms, ultimately moving closer to practical, point-of-care dengue diagnosis.

2.2.3 NS1 for Early Dengue Detection

The non-structural protein 1 (NS1) is a highly conserved glycoprotein produced by all flaviviruses, including DENV, during viral replication (Muller & Young, 2013). Unlike other non-structural proteins, NS1 is actively secreted into the bloodstream in a hexameric form and becomes detectable in-patient serum during the early phase of infection, often as early as the first day of fever onset (Fisher et al., 2023). Crucially, NS1 can be identified in both primary and secondary dengue infections and does not rely on the host's immune response or antibody production for detection (Fisher et al., 2023; Muller & Young, 2013). This makes it an invaluable biomarker for early and accurate dengue diagnosis. Its early presence in circulation and stability across all four DENV serotypes further enhance its suitability for rapid diagnostic applications, particularly in point-of-care settings where timely clinical decisions are critical.

Table 2.3 provides a comparative evaluation of NS1 antigen detection assays used for early dengue diagnosis. A pivotal study conducted by Alcon et al. (2002) demonstrated that the DENV NS1 protein is detectable in serum as early as the first day of fever and can persist up to day nine, even in cases where viral RNA is no longer identifiable through RT-PCR. Their use of an ELISA-based assay revealed high sensitivity and showed efficacy in both primary and secondary infections, positioning NS1 as a key biomarker for early dengue diagnosis. Supporting this finding, Vazquez et al. (2010) investigated the temporal dynamics of NS1 in patients with

confirmed DENV-4 infections. Utilizing the Platelia™ NS1 ELISA, they reported detection sensitivities of 83.3% in primary and 96.4% in secondary cases, with peak detection occurring between days 2 and 4 following symptom onset. These results reinforced the utility of NS1 as a virologic marker during the acute phase of illness.

Further evidence was provided by Moi et al. (2013), who assessed NS1 detection in international travelers diagnosed with dengue. Their findings indicated that NS1 remained detectable in 88-96% of patients within the first five days of illness and showed extended persistence relative to viral RNA. This study underscored the broader applicability of NS1 assays across all DENV serotypes and geographic regions.

In a comparative evaluation, Anand et al. (2016) reported that NS1 antigen detection exhibited superior sensitivity (96.8%) compared to RT-PCR (68.1%) in early infection stages. Moreover, combining NS1 antigen with IgM ELISA significantly enhanced diagnostic sensitivity to 97.8%, highlighting the benefit of multiplexed approaches in clinical diagnostics (Anand et al., 2016). Additionally, the commercial Platelia™ dengue NS1 Ag ELISA was validated by Dussart et al. (2006), who documented sensitivity rates of 88.7%. Their results demonstrated strong concordance with RT-PCR outcomes and emphasized the test's utility for early dengue detection, beginning from the first day of clinical symptoms.

Collectively, these studies provide substantial evidence that NS1 serves as a highly sensitive and practical biomarker for early dengue diagnosis, with demonstrated effectiveness in both individual and combined diagnostic platforms during the acute phase of infection.

Table 2.3
Comparative Evaluation of NS1 Antigen Detection Assays

Reference	Study Focus	Methodology	Sample Type	NS1 Concentration Range	Sensitivity / Specificity	Key Findings
Alcon et al. (2002)	NS1 antigen detection window	ELISA (NS1-specific polyclonal Abs)	Serum	0.04 to 2 ug/ml in acute-phase serum convalescent phase serum (day 8 and later) was 0.04 g/ml	Detected NS1 from day 1-9	NS1 detectable earlier than IgM or PCR; useful for both primary and secondary cases
Vazquez et al. (2010)	NS1 kinetics in DENV-4	NS1 ELISA (Platelia™)	Serum (days 2-7)	Primary infections: 10 to 50 ng/mL	83.3% (primary); 96.4% (secondary)	Highest NS1 positivity between days 2-4; supports early virologic diagnosis
Moi et al. (2013)	Travelers with dengue	NS1 ELISA + RT-PCR	Serum (days 1-10+)	0.04 to 2 µg/mL	88-96% (day 1-5); 36-60% (after day 10)	NS1 detection lasts longer than RT-PCR; useful across all serotypes
Anand et al. (2016)	ELISA vs RT-PCR	NS1 ELISA, RT-PCR, IgM	Serum	0.004 to 2 µg/ml in acute phase serum ≤0.004 µg/mL in convalescent phase serum samples	96.8% (ELISA); 68.1% (RT-PCR)	NS1 superior for early diagnosis; NS1 + IgM offers highest sensitivity (97.8%)
Dussart et al. (2006)	Commercial ELISA validation	Platelia™ NS1 vs RT-PCR	Serum		Sensitivity: 88.7%	Strong agreement with RT-PCR; suitable for day 1 detection

2.3 Surface Enhanced Raman Spectroscopy (SERS)

Raman spectroscopy is a highly specific analytical technique that produces a unique Raman spectrum for each molecule based on the vibrational modes of its molecular structure (Gardiner & Graves, 1989). The spectrum can be regarded as spectral fingerprints that allow precise identification of chemical compounds and biological molecules.

When a monochromatic light interacts with molecule, the photons absorb and release energy from undergoing rotational and vibrational motion of the molecule producing Raman scattering (Raman & Krishnan, 1928) captured as Raman shift resulting the Raman spectrum.

The Raman shift, which represents the energy difference between the incident and scattered photons, is given by:

$$\Delta\omega = \omega_{incident} - \omega_{scattered} \tag{2.1}$$

where $\omega_{incident}$ is the frequency of the incoming light and $\omega_{scattered}$is the frequency of the scattered light. The intensity of the Raman signal is directly related to how the polarizability of molecule changes during vibration, described by:

$$I_R \propto \left(\frac{d\alpha}{dq}\right)^2 \tag{2.2}$$

where I_R is the Raman intensity, α is the polarizability and q is the normal coordinate of molecular vibration. This means that vibrations causing significant changes in a molecule's polarizability result in stronger Raman signals.

However, a major limitation of conventional Raman spectroscopy is its inherent insensitivity. The occurrence of Raman scattering is extremely weak, as only a small fraction (~1 in 10^6 ~ 10^8) of incident photons undergo inelastic scattering(Gardiner & Graves, 1989). This results in low signal intensity, making Raman spectroscopy less effective for detecting low-concentration analytes. To overcome this limitation, SERS is employed to significantly amplify the Raman signal. SERS was first observed in 1974 by Fleischmann et al. (1974), who noticed an unexpectedly strong Raman signal from pyridine molecules adsorbed onto a roughened silver electrode. Initially, they attributed this enhancement to an increased surface area, but later in 1977, Jeanmaire and Van Duyne, (1977) as well as Albrecht and Creighton, (1977) independently proposed that the enhancement was due to electromagnetic and chemical interactions at the metal surface.

The first mechanism is electromagnetic enhancement where light interacts with nanostructured metallic surfaces such as silver (Ag), gold (Au) and copper (Cu) nanoparticles inducing localized surface plasmon resonance (LSPR). This phenomenon generates a strong local electromagnetic field, which significantly intensifies the scattered Raman signal (Jeanmaire & Van Duyne, 1977). The second mechanism is chemical enhancement, which arises from charge transfer between the analyte and the metal surface. This interaction increases the molecule's polarizability, further boosting the Raman signal (Albrecht & Creighton, 1977). By combining these two effects, SERS transforms an otherwise weak Raman response into a highly sensitive analytical tool, enabling precise molecular detection for various scientific and biomedical applications. Since then, SERS has evolved into a powerful analytical technique, finding applications in biomedical diagnostics, environmental monitoring and chemical sensing.

2.3.1 SERS for Diseases Diagnosis

SERS is a label-free, rapid, non-destructive and water-compatible technique, making it highly suitable for biomedical applications. It enables ultra-sensitive detection of biomolecules, including proteins (H. Chen et al., 2022; Costrada et al., 2024; Kaladharan et al., 2023; M. Kim et al., 2024; Lan et al., 2025; Mustapa et al., 2025; Zhao et al., 2022), nucleic acids (M. G. Kim et al., 2023; Song et al., 2020) and metabolites (Gu et al., 2024). Due to its superior sensitivity, SERS has been extensively explored in disease detection, as reported in various literature reviews tabulated in Table 2.4. These studies demonstrate substantial progress in detecting various diseases, including Alzheimer's disease, several cancers, Severe Acute Respiratory Syndrome Coronavirus (SARS-CoV-2), influenza A and dengue, through diverse SERS methodologies and substrates. In Alzheimer's disease research by M. Kim et al. (2024), a surface-functionalized SERS approach utilizing a gold nanowire array achieved a high diagnostic accuracy of 99.5% when integrated with a deep learning model. Another study by Lan et al. (2025) employed a direct SERS method based on a graphitic carbon nitride/metal-organic framework (g-C_3N_4@MOF), attaining detection limits of 2.5×10^{-8} mg/mL for beta-amyloid proteins 40 (Aβ40) and 6.2×10^{-8} mg/mL for beta-amyloid proteins 42 (Aβ42) biomarkers.

In cancer diagnostics, Gu et al. (2024) demonstrated that a label-free SERS method employing AgNPs colloids achieved a classification accuracy of 84.4% for

bladder cancer detection from urine samples using a Random Forest model. Another investigation targeting prostate cancer biomarkers by Zhao et al. (2022) utilized aptasensor-based SERS with a PS@Ag-Porous Silicon substrate, enabling precise detection in clinical serum samples.

For viral infections, a SERS-immune assay using a nanostructured DVD substrate achieved a detection limit of 400 pg/mL for SARS-CoV-2 (Kaladharan et al., 2023), while a dual-mode Deoxyribonucleic Acid (DNA) aptasensor method employing a gold nanocomposite substrate yielded detection limits of 0.78 PFU/mL for SARS-CoV-2 and 0.68 HAU/mL for H1N1 (H. Chen et al., 2022).

Table 2.4
Emerging SERS Technologies for Diseases Diagnosis

Reference	Disease	Targeted Analyte	SERS Technique	SERS Substrate	Detection Performance
M. Kim et al. (2024)	Alzheimer	Blood-based amyloid ϐ (1-42)	Surface-functionalized SERS	Au nanowire array	99.5% of accuracy using deep learning model
Lan et al. (2025)	Alzheimer	Aβ40 and Aβ42 biomarkers	Direct SERS	(SERS) platform based on graphitic carbon nitride@metal-organic framework (g-C3N4@MOF)	LOD of Aβ40: 2.5 x 10^{-8} mg/mL LOD of Aβ42: 6.2 x 10^{-8} mg/mL
Gu et al. (2024)	Bladder cancer	Urine	Label-free SERS	AgNPs colloid	84.4% accuracy with Random Forest Model
Zhao et al. (2022)	Prostate cancer biomarker	Prostate-specific antigen (PSA) and free prostate-specific antigen (f-PSA)	SERS based aptasensors	PS@Ag - Porous Silicon	Accurate detection from clinical serum samples.
Kaladharan et al. (2023)	SARS-CoV-2	VLP protein spiked in untreated saliva	SERS-immune assay	Ag-deposited nanostructured DVD functionalized with SARS-CoV-2 antibody	LOD up to 400pg mL^{-1}
H. Chen et al. (2022)	SARS CoV-2 and influenza A/H1N1	Diluted SARS CoV-2 and influenza A/H1N1	SERS-based dual-mode DNA aptasensors	Au nanopopcorn substrate	SARS CoV-2 LOD: 0.78 PFU/mL H1N1 LOD: 0.68 HAU/mL
M. G. Kim et al. (2023)	COVID-19	Nucleic acid (DNA, RNA)	Direct SERS	ZnO Au-SERS based direct amplification (ZADA)	DNA (1×10^{0} CFU/mL) RNA (0.96×10^{-1} PFU/mL) Sensitivity with deep learning: 100% Specificity with deep learning: 100%
Mustapa et al. (2025)	Dengue	Diluted NS1 and IgG	Surface-functionalized SERS	Hybrid Au nanorods and Au nanospheres	EF of 8.544 x 10^{4} LOD of 25 fg/mL
Costrada et al. (2024)	Dengue	Envelope Glycoprotein Domain III (ED III)	Label-free SERS	Grating-Au surface polycarbonate DVD, Silicon and On-Spec-lite SERS	The OnSpec-lite SERS substrate, enhances intensity by a factor of 3.90, whereas the grating-Au SERS substrate achieves a 1.72-fold increase in intensity.
Song et al. (2020)	Dengue	DENV gene	SERS assay via cascade LCHA and HCR	SERS-active Ag Nanorod	LOD up to 0.49M Sensitivity is about 4.5 times that of CHA. S/N improved to 5.4 relative to 1.8 of the individual CHA.

Recently, M. G. Kim et al. (2023) reported the development of a novel deep learning-assisted SERS platform, known as ZADA (ZnO-Au Direct Amplification), for the rapid and label-free detection of viral RNA, particularly for COVID-19 diagnosis. The system uses gold-coated zinc oxide nanorods as the SERS substrate, enabling direct amplification of nucleic acids on the surface without the need for hybridization probes or labeling agents. By combining this with a deep learning algorithm, the platform achieved 100% sensitivity and specificity when tested on clinical COVID-19 samples, with a detection time of under 20 minutes. The integration of machine learning significantly improved result interpretation and diagnostic accuracy, highlighting the ZADA system's potential for fast, accurate and scalable molecular diagnostics in clinical and point-of-care settings.

Dengue diagnostics have also seen significant advances. A surface-functionalized SERS platform using hybrid gold nanorods and nanospheres detected diluted NS1 and IgG with a sensitivity of 25 fg/mL and an enhancement factor of 8.544 $\times 10^4$ (Mustapa et al., 2025). Costrada et al. (2024) further demonstrated a label-free SERS approach targeting the envelope glycoprotein domain III (ED III) of DENV using a grating-Au substrate on polycarbonate DVDs, which resulted in a 3.9-fold enhancement in signal intensity. Additionally, a cascade amplification strategy integrating localized catalytic hairpin assembly (LCHA) and hybridization chain reaction (HCR) with SERS-active Ag nanorods achieved a detection limit of up to 0.49 M and improved sensitivity by a factor of 4.5 over conventional enzyme-free catalyzed hairpin assembly (CHA) methods (Song et al., 2020).

Recently, Y. Chen et al. (2023) reviewed recent advancements in SERS strategies for early disease diagnosis, highlighting its potential as a highly sensitive, label-free and non-invasive analytical tool. The paper outlines developments in both label-free and label-based SERS methods, emphasizing their growing use in detecting disease biomarkers across a range of conditions including cancer, neurodegenerative, cardiovascular and infectious diseases. It also discusses the integration of SERS with multimodal diagnostic techniques, artificial intelligence and portable Raman systems, which collectively enhance detection accuracy and enable point-of-care applications. These innovations position SERS as a promising platform for clinical translation in early diagnostic settings.

Overall, these studies highlight the increasing versatility and sensitivity of SERS-based platforms. The combination of advanced nanostructured materials such as

Au and Ag nanoparticles, PSi and metal-organic frameworks (MOFs) with innovative detection modalities, including aptasensors, immunoassays and machine learning algorithms, has significantly elevated diagnostic performance. These developments have led to the realization of ultralow detection thresholds, supporting the application of SERS as a robust, non-invasive tool for early-stage disease diagnostics with high clinical relevance.

2.3.2 Silicon-Based SERS Substrate

This section highlights PSi-based SERS substrates that have been extensively reported in the literature. Silicon remains one of the most widely utilized materials for constructing solid-state SERS platforms because it offers a unique blend of structural, chemical and fabrication-related benefits (Bandarenka et al., 2018; Vendamani et al., 2022). From a materials availability perspective, silicon is abundant in nature, relatively inexpensive to source and fully compatible with well-established semiconductor manufacturing technologies, which collectively make it highly suitable for large-scale, reproducible and cost-efficient substrate fabrication. Furthermore, the crystallographic properties of silicon are exceptionally well understood, enabling researchers to exercise precise control over its surface morphology, an important factor for tuning and maximizing plasmonic enhancement in SERS-based measurements. This capability is especially valuable when designing nanostructured surfaces, as the geometry and arrangement of these features directly influence the density and intensity of "hot spots", the localized regions of strong electromagnetic field concentration that drive Raman signal amplification.

In terms of fabrication versatility, silicon can be patterned and etched into a diverse array of nanostructures, including nanowires, porous matrices, nanopillars and nanorods, using various methods such as metal-assisted chemical etching (MACE) (Das et al., 2023; Kumar et al., 2024; Nazarovskaia et al., 2025), electrochemical etching (Abood & Mutlak, 2020; Jakubowicz, 2007) and advanced lithographic approaches (D. Lin et al., 2017). These fabrication strategies make it possible to produce surfaces with extremely high specific surface areas and tunable nanoscale roughness, which are essential characteristics for generating intense SERS responses (Low & Voelcker, 2018). Beyond topographical optimization, silicon substrates can also be readily functionalized with noble metal nanoparticles, such as Ag,

Au and Cu, to induce strong LSPR effects that are critical for amplifying Raman scattering signals (Jeanmaire & Van Duyne, 1977).

Another important advantage is the inherent chemical stability and mechanical durability of silicon, which contribute to the long-term reliability and reproducibility of the substrate during repeated analytical cycles. Additionally, the material exhibits notable biocompatibility (Low & Voelcker, 2018; Zeng et al., 2019), broadening its utility for biosensing applications such as disease diagnostics (Zhao et al., 2022) and extending its applicability to environmental monitoring scenarios (Al-Syadi et al., 2021; Srivastava et al., 2024; Terry et al., 2022). Collectively, these characteristics position silicon as a versatile, high-performance foundation for the development of advanced SERS substrates capable of addressing a wide spectrum of analytical challenges across scientific, biomedical and environmental domains.

Recent advancements in silicon-based SERS substrates have significantly enhanced the sensitivity and selectivity of chemical and biological detection platforms. Various fabrication methods and silicon morphologies have been engineered to optimize EF and minimize LOD, illustrating the adaptability of silicon as a SERS substrate. Table 2.5 tabulates studies that used silicon as the base of SERS substrate. H. Lin et al. (2004) employed electrochemical etching to fabricate silver-plated porous silicon, achieving a LOD of up to 1 nM, establishing a baseline for SERS performance using conventional methods. Building upon this, D. Lin et al. (2017) integrated Au nanoparticles onto silicon nanorods using nanosphere lithography and MACE, which yielded a high EF ($>10^7$) and spatial uniformity (standard deviation: 3.9-7.2%). This approach proved especially valuable in biomedical applications, such as the detection of amyloid-beta aggregates, relevant to Alzheimer's disease diagnosis, demonstrating how nanostructure uniformity directly influences diagnostic reliability.

In a related study, Kumar et al. (2024) explored the application of silver-decorated dendritic porous silicon (D-PSi) structures as highly effective SERS substrates, achieving remarkable ultrasensitive detection of R6G molecules at concentrations as low as 10^{-15} M, with an exceptionally high EF of 6.1×10^{12}. These results strongly indicate that the intricate architecture and increased surface area provided by such dendritic nanostructures play a decisive role in amplifying Raman signals to an extraordinary degree. Similarly, Shlaga et al. (2025) investigated the role of surface chemistry in SERS performance by employing a potassium hydroxide (KOH)-assisted ion reduction technique to synthesize AgNPs-coated PSi.

This approach enabled the sensitive detection of ciprofloxacin, producing EF values of 6.3×10^{12} and 7.78×10^{10}, with the variation directly linked to differences in the etching sequence used during fabrication. Their findings emphasize that fine-tuning the chemical etching parameters is essential for optimizing the plasmonic properties and, consequently, the SERS efficiency of the substrate. Extending the potential applications of silicon-based SERS platforms, Das et al. (2023) developed silver-coated silicon nanowires capable of detecting not only chemical dyes, with a LOD as low as 10^{-12} M, but also biological targets, successfully identifying bacterial samples down to 100 colony-forming units per milliliter (CFU/mL). This dual-functionality underscores the versatility of nanowire-based architectures in both chemical sensing and microbiological diagnostics.

Within the scope of environmental sensing applications, Al-Syadi et al. (2021) developed a PSi substrate coated with palladium nanoparticles that demonstrated the capability to detect the neonicotinoid pesticide imidacloprid at concentrations as low as 10^{-9} M, corresponding to an EF of 1.2×10^5. Although this EF value is relatively modest when compared to the significantly higher enhancement factors achieved by other, more complex SERS platforms, the approach offers a noteworthy balance between fabrication simplicity, operational stability and detection sensitivity. Such a trade-off is particularly advantageous for field-deployable analytical devices, where portability, cost-effectiveness and ease of fabrication often outweigh the need for maximum possible signal enhancement.

In the domain of clinical diagnostics, Nazarovskaia et al. (2025) engineered a gold-deposited porous silicon nanowire array that provided a substantial reduction in antibody susceptibility testing (AST) times, from the conventional 24 hours typically required by standard laboratory methods to only 3 hours. This remarkable decrease in analysis time illustrates the practical potential of SERS-based systems in point-of-care diagnostic workflows, underscoring their ability to deliver rapid, accurate and actionable results in real-world healthcare environments without sacrificing analytical performance.

The most recent advancement in this area comes from Nirala et al. (2025), who reported the fabrication of a reusable porous silicon substrate coated with AgNPs and further functionalized with 4-aminothiophenol (4-ATP) to enhance molecular recognition capabilities. This platform was employed for the detection of the mycotoxin Fumonisin B_1 (FB_1), achieving an impressively low LOD of just 0.05 ppb along with

an enhancement factor exceeding 5×10^7. Beyond its impressive analytical figures, the study highlights the growing emphasis on reusability and targeted surface functionalization in the design of modern SERS substrates, reflecting broader trends toward sustainability, reduced operational costs and extended device lifespans in both food safety monitoring and broader analytical chemistry applications.

Table 2.5
Silicon-Based SERS Substrate

Reference	Substrate	Silicon type	Fabrication technique	Performance
H. Lin et al. (2004)	Silver-plated Porous Silicon	Si type: *p*-type, boron-doped, Resistivity: <0.005 Ω cm, Crystal orientation: ⟨100⟩ oriented, Thickness: 525± 25 µm	Electrochemical etching	LOD up to 1 nM
D. Lin et al. (2017)	Silicon Nanorods (SiNR) functionalized with gold and nanoparticles (AuNPs)	Si type: *p*-type boron-doped Crystal orientation: <100> oriented, Resistivity: 1-10 and 10-40 Ω cm (Huang et al., 2014)	Nanosphere lithography and metal-assisted chemical etching	EF > 10^7 Small standard deviation across the substrate (3.9-7.2%) Detection of amyloid aggregates related to Alzheimer's disease.
Kumar et al. (2024)	AgSLD-PSi SERS	Si type: *n*-type, Resistivity: 1-10 Ω·cm	MACE	They have shown high detection sensitivity for 10^{-15} M R6G with an EF of 6.1×10^{12}
Shlaga et al. (2025)	AgNPs/PSi	Si type: *n*-type, Resistivity: 10 Ω·cm, Thickness: 514 µm	Ion reduction and KOH method (potassium hydroxide solution)	CIPRO antibiotic detection EF of Pre-etching/ion reduction: 6.3×10^{12} EF of KOH: 7.78 x 10^{10}
Das et al. (2023)	Ag Silicon Nanowire (SiNW)	Si type: *p*-type, Crystal orientation: <100> oriented, Resistivity: 5 Ω·cm	MACE	LOD of 10^{-12} M R6G Detection of bacteria down to a concentration of 100 CFU/mL
Al-Syadi et al. (2021)	PSi (plated palladium) Pd NPs SERS	Si type: *p*-type, c Crystal orientation: <100> oriented, Resistivity: 0.0045-0.006 Ω·cm, Thickness: 450± 25µm	Electrochemical anodization, simple immersion plating technique for deposition of Pd NPs	LOD: 10^{-9} M imidacloprid pesticide EF of 1.2 x 10^5
Nazarovskaia et al. (2025)	Au Ag deposited on Porous Silicon Nanowire (PS NW)	Si type: *p*-type, Crystal orientation: <100> oriented, Resistivity: 100 Ω·cm	MACE	Significantly speeds up bacterial detection and antibody susceptibility testing (AST), reducing the testing time to just 3 hours instead of the usual 24 hours.
Nirala et al. (2025)	AgNPs PSi	Si type: *p*-type, Crystal orientation: <100> oriented, Resistivity: 1.0 mΩ·cm	Electrochemical etching, immersion of $AgNO_3$ solution and functionalization with ethanoic solution of 4-ATP	EF: >5 x 10^7 LOD of Fumonisin B_1 (FB_1): 0.05 ppb

Collectively, these studies clearly demonstrate that the analytical performance and overall sensitivity of silicon-based SERS platforms are determined by the interplay of three fundamental and interdependent factors: (i) the nanoscale architecture and morphological characteristics of the silicon surface, (ii) the selection, distribution and precise placement of plasmonic materials such as Ag, Au or other noble metals and (iii) the nature and effectiveness of any chemical treatments or surface functionalization strategies applied to target specific analytes. Each of these factors exerts a significant influence on the generation and localization of electromagnetic “hot spots”. which in turn governs how effectively the platform can amplify Raman signals and detect even trace quantities of substances.

Because of this interdependence, it becomes crucial to adopt a carefully tailored design strategy, one that considers the intended end-use, operating environment and target molecule, when choosing the fabrication approach, the plasmonic material and the functionalization chemistry. For instance, in the case of non-invasive dengue detection, the SERS platform must be optimized to reliably enhance signals from dengue-specific biomarkers present in easily accessible biological fluids such as saliva or urine. Achieving this requires not only engineering nanostructures that maximize signal amplification but also selecting plasmonic metals with high stability under physiological conditions and applying highly specific surface functionalization capable of selectively binding to dengue-associated molecular signatures. When these design considerations are systematically integrated, the resulting platform offers a powerful combination of sensitivity, selectivity and practicality for real-world biomedical diagnostics.

2.3.3 Electrochemical Etching

The fabrication of PSi generally relies on methods that selectively remove silicon atoms from the bulk crystal, thereby generating a highly porous network with a tunable internal architecture. Among the various approaches developed over the past decades, the electrochemical etching method has emerged as the most common and widely implemented technique. This popularity can be attributed to several advantages, including procedural simplicity, cost-effectiveness and most importantly its ability to exercise precise control over pore size, depth and overall morphology (Kuntyi et al., 2022).

In a typical electrochemical etching process, a crystalline silicon wafer is immersed in an electrolyte solution composed primarily of hydrofluoric (HF) acid mixed with ethanol (C_2H_5OH), which serves to improve wetting of the silicon surface and ensure uniform etching. A direct current (DC) is applied between the silicon wafer, functioning as the anode and an inert counter electrode, often fabricated from platinum due to its excellent chemical stability. When current is applied, the silicon atoms at the wafer surface undergo oxidation and are subsequently dissolved through interaction with fluoride ions, progressively forming a continuous and interconnected porous framework.

For *n*-type silicon wafers, the electrochemical etching process often incorporates photo-assisted mechanisms, in which light illumination generates electron-hole pairs that facilitate the anodic oxidation step. This photo-enhanced approach, described in detail in Sailor (2011) and discussed further in this section, allows for greater uniformity and control over the pore structure, thereby enabling the fabrication of PSi substrates with properties tailored to specific sensing, photonic or catalytic applications.

Upon illumination, electron-hole pairs are generated within the silicon substrate and the holes migrate to the surface describe by equation (2.3) and enabling the oxidation of silicon atoms.

$$h\nu \rightarrow e^- + h^+ \tag{2.3}$$

where h is Planck's constant = $6.626 \times 10^{-34} J.s$, ν is frequency of incident light (in Hz), $e^-$is electron and $h^+$is hole.

The oxidization of silicon is described by equation (2.4)

$$Si + 2h^+ + 6F^- \rightarrow SiF_6^{2-} + 4H^+ + 2e^- \tag{2.4}$$

where *Si* is silicon, $2h^+$are hole $6F^-$are fluoride ions, $SiF_6^{2-}$is hexafluorosilicate ion, $4H^+$are protons $2e^-$are electrons.

These oxidized silicon species react with fluoride ions to form soluble hexafluorosilicate ions which are remove from the surface resulting in the dissolution of silicon. Concurrently, protons (H+) and electrons (e-) are released to maintain charge neutrality. This process leads to the formation of PSi structure.

The overall chemical reaction can be described as equation (2.5)

$$Si + 6HF \rightarrow H_2SiF_6 + H_2 \uparrow + 2H^+ + 2e^- \tag{2.5}$$

where *Si* is silicon, *6HF* is aqueous of hydrofluoric acid, H_2SiF_6 is hexafluorosilicic acid, $H_2$is hydrogen gas, $2H^+$are protons and $2e^-$are electrons.

In this process, Si reacts with HF to produce hexafluorosilicic acid (H_2SiF_6), hydrogen gas (H_2), protons (H^+) and free electrons (e^-). The generation of H_2SiF_6 indicates the dissolution of Si, while the release of H_2 signifies active surface reactions, typically seen as bubbling. The electrons liberated during this oxidation can contribute to current flow in the electrochemical cell.

Table 2.6 provides a comprehensive summary of published studies that employ the electrochemical etching method for fabricating PSi-based from *n*-type wafers, detailing a variety of parameters that influence the resulting nanostructure. These parameters include intrinsic silicon properties such as crystal orientation, resistivity and wafer thickness as well as electrochemical process variables like current density, etching duration, electrolyte composition and mixing ratio and the method of current supply. Additionally, different illumination sources and configurations are considered, as light-assisted etching plays a critical role in modifying pore formation kinetics and structural uniformity.

Jakubowicz (2007) systematically investigated *n*-type silicon with different crystallographic orientations and resistivity values, finding that *n*-type <111> silicon displayed approximately ten times higher current compared to the <100> orientation under identical conditions. Their results further indicated that topside halogen illumination yielded the largest pore diameters and the highest critical current density, whereas the absence of illumination produced the smallest pores and the lowest measurable current density. Abood and Mutlak, (2020) applied a green laser (532 nm, 200 mW) during the etching of *n*-type <111> silicon wafers and demonstrated that fine-tuning the current density in the range of 6-50 mA/cm^2 enabled precise control over both porosity levels and photoluminescence properties of the resulting PSi. Similarly, Suryana and Aini (2022) compared various laser wavelengths for illumination during etching, reporting that the green laser (532 nm) produced the most homogeneous and densest PSi network on *n*-type <100> silicon substrates.

Harb and Mutlak (2022) explored the relationship between current density and Raman spectral features of PSi-based, observing that increasing the current density broadened Raman peaks and caused redshifts, with the full width at half maximum (FWHM) expanding from 20 cm^{-1} to 26 cm^{-1}. This was attributed to optical phonon confinement in the nanoscale silicon domains. Razali et al. (2019) employed incandescent lamp illumination combined with a DCPEC (Double Cell Photo Electrochemical Cell) technique, which produced deeper pores and larger crystallite

sizes, ultimately enhancing both Raman and photoluminescence responses. Abdullah et al. (2019) utilized a 10 W lamp to compare etching outcomes between *n*-type and *p*-type wafers, concluding that both Raman peak symmetry and FWHM were strongly dependent on etching duration. Lastly, Zhang et al., (2012) proposed that *n*-type PSi with resistivity in the range of 1-10 Ω·cm represents a promising new material for the fabrication of highly sensitive SERS substrates, combining favourable electronic properties with structural tunability.

In summary, the reviewed findings collectively underscore that three interdependent parameters which are the type of silicon wafer used, the precise electrochemical etching settings applied and the specific illumination method employed during processing exert decisive influence over both the structural characteristics and optical responses of PSi-based. These factors not only determine pore morphology, size distribution and crystallite dimensions, but also directly impact photoluminescence intensity, Raman spectral features and overall suitability for sensing applications. In the present study, careful consideration has been given to these variables in order to design an optimized fabrication protocol for SERS-active PSi substrates. An *n*-type <100> silicon wafer, chosen for its optimal electronic properties and structural uniformity, is employed. The wafer possesses a resistivity within the range of 1 Ω·cm to 10 Ω·cm and a uniform thickness of 285 μm, ensuring consistency across all experimental runs. The fabrication process utilizes the DCPEC technique, chosen for its ability to simultaneously achieve controlled pore formation and maintain substrate integrity. Illumination is provided by a stable incandescent lamp source, which promotes uniform carrier generation across the wafer surface. During etching, the applied electrical parameters are kept constant at 10 V and 10 mA to ensure reproducibility of results and to minimize variation due to electrical instabilities. The electrolyte bath consists of a HF and ethanol mixture in a 4:1 volumetric ratio, with ethanol serving to improve wettability and promote uniform dissolution of the silicon surface. A key focus of this investigation lies in systematically varying the etching duration, allowing for a detailed evaluation of how processing time influences pore depth, surface area and optical enhancement capabilities in the resulting PSi layers.

Table 2.6
Summary of Key Research on PSi Fabrication and Applications

Reference	**Silicon Material Parameters** *(Si-type, crystal orientation, resistivity, thickness)*	**Electrochemical Setting Parameter** *(electrolyte ratio, current density, etching time, method of current supply)*	**Illumination Method**	**Key Observations**
Jakubowicz (2007)	*n*-type <100>, 0.02-0.1 Ω.cm (l), 525µm *n*-type <100>, 2-10 Ω.cm (h), 525µm *n*-type <100>, 2-10 Ω.cm (h), 525µm *n*-type <111>, 0.02-0.1 Ω.cm (l), 525µm note: (h) - high resistivity (l) - low resistivity	HF:Ethanol:DI water = 2:20:78 50:20:30 Current density = 2 mA/cm^2 Etching time = 5 min	Halogen lamp Backside illumination Topside illumination immerse electrolyte Without illumination	*n*-Si <111> 10 times current is observed than *n*-Si <100>. for (h), higher critical current density. Increase HF, increase critical current density. Topside illumination gives the highest critical current density. The largest pores observe from the topside illumination. The smallest pores observe from the without illumination. Without illumination, the critical current density is very low.
Abood and Mutlak (2020)	*n*-type <111>, 0.015 Ω.cm, 508 µm	HF:Ethanol = 1:5 Current density = 6-56 mA/cm^2 Etching time = 5 min Room temperature DC current	Laser wavelength = 532 nm Power = 200 mW	Varying current density is possible to control the porosity and photoluminescence properties.
Suryana and Aini (2022)	*n*-type <100>, 1-5 Ω.cm, 508 µm	HF:Ethanol = 1:3 Current density = 20 mA/cm^2 Etching time = 15 min DC current	Laser wavelength = 650 nm (red) 532 nm (green) 405 nm (purple)	The homogenous and highest density of PSi was obtained using green laser.
Harb and Mutlak (2022)	*n*-type <100>, 0.1-100 Ω.cm	Current density = 6, 13, 20, 27 and 34 mA/cm^2 Etching time = 10 min	Laser wavelength = 532 nm	Increasing current density shift. The structural characteristic of PSi samples modified by varying the apply current density.

Reference	Silicon Material Parameters *(Si-type, crystal orientation, resistivity, thickness)*	Electrochemical Setting Parameter *(electrolyte ratio, current density, etching time, method of current supply)*	Illumination Method	Key Observations
		Room temperature		The Raman peaks become broader and shift to lower wavenumbers compared to the reference bulk Si peak at 520 cm^{-1} as the applied current density increases. The full width half maximum (FWHM) increases from 20 cm^{-1} to 26 cm^{-1}, indicating that optical phonons are confined within the walls of the nano-sized silicon structures.
Razali et al. (2019)	*n*-type <100>	HF:Ethanol = 1:4 Current density = 20 mA/cm^2 Etching time = 20 min Room temperature DC current Integrated pulse	Incandescent lamp	The sample prepared by the DCPEC technique produces a nanostructure and deeper pore, resulting in larger crystallite size and better intensity in the Raman and PL spectra.
Abdullah et al. (2019)	*n*-type <100>, 1 Ω.cm, 300 µm *p*-type <111>, 1 Ω.cm, 300 µm	HF:Ethanol = 1:4 Current density = 50 mA/cm^2 Etching time = 10 min and 13 min DC current	10W lamp	Raman analysis demonstrated the sharp symmetric peak position with slightly different in the intensity and width. The intensity and values of FWHM increases proportionally to the etching time.
H. Zhang et al. (2012)	*n*-type <100>, 1-10 Ω.cm, 420 µm	HF:Ethanol = 1:3 Current density = 2-20 mA/cm^2 Etching time = 8 min 55 ºC	Not available	It is suggested that *n*-type (1 Ω·cm to 10 Ω·cm in resistivity) PSi is proposed as a new material for the fabrication of sensitive substrates for SERS.

2.3.4 Plasmonic Metals for Raman Signal Enhancement

The function of plasmonic metals in SERS is to amplify the Raman signal molecules located near their surface. This enhancement is primarily due to the LSPR effect. LSPR is the key electromagnetic mechanism behind SERS signal enhancement, occurring when conduction electron on the surface of plasmonic metal nanoparticles such as Ag, Au and Cu oscillate collectively in resonance with incident light (Le Ru & Etchegoin, 2009).

In solid-based SERS, LSPR arises from nanostructured metal coatings on solid surface. The interaction of light with these metallic features leads to intends local electric fields. The resonance condition modified by the solid dielectric environment results in field amplification governed by the polarizability of the metal solid interface.

The general dipole resonance condition defines by

$$Re[\varepsilon(\omega)] = -n_{eff} \tag{2.6}$$

where, ε_m is dielectric metal of metal, n_{eff} is effective refractive index of the surrounding medium including substrate and air voids.

The polarizability α of a metallic nanoparticles is given by,

$$\alpha = 4\pi R^3 \left(\frac{\varepsilon_m(\omega) - \varepsilon_s}{\varepsilon_m(\omega) + 2\varepsilon_s} \right) \tag{2.7}$$

where, R is characteristic radius of the nanostructure, ε_s is dielectric constant of the surrounding solid.

The polarizability governs the localized electric field enhancement,

$$\left|\vec{E}_{loc}\right|^2 = |M(\omega)|^2 \left|\vec{E}_0\right|^2 \tag{2.8}$$

where, $\left|\vec{E}_{loc}\right|^2$ is the intensity (squared magnitude) of the local electric field at a point near the plasmonic surface or hotspot, $|M(\omega)|^2$ is the field enhancement factor which depends on the frequency of the incident light and $\left|\vec{E}_0\right|^2$ is the intensity of the incident electric field.

There are various methods used to apply plasmonic metals onto solid-based SERS substrates. Table 2.7 summarizes several studies utilizing such substrates, highlighting their plasmonic metals, probe molecules and analytical performance. AuNPs and AgNPs are the most commonly employed plasmonic materials due to their strong LSPR properties and greater resistance to oxidation (Markin et al., 2018).

Table 2.7
Plasmonic Metals for SERS

Reference	Plasmonic Metal	Deposition Method	Raman Mrobe Molecules	Key Findings
Stankevičius et al. (2021)	AuNPs Size: 5-20 nm	NA	4-Mercaptobenzoic Acid (4-MBA)	The highest EF is achieved with pure AuNPs made from a single gold layer with additional coating of 5 nm gold layer.
Amador-Martínez et al. (2023)	CuNPs Size: 3-10 nm	Drop casting	Pyridine	The maximum EF reported is 19.89.
Çelik and Kurt (2021)	AgNPs Size: NA	Compressed pellets	Rhodamine 6G (R6G)	The EG/AgNPs substrate showed a detection limit of 10^{-11} M for Rhodamine 6G (R6G) with an enhancement factor of 2.7×10^6. R6G peaks at this low concentration were still visible after one month, showing the substrate's high stability and long shelf life. Its excellent sensitivity, stability, low-cost and simple production make it highly promising for routine SERS applications.
Mao et al. (2023)	AuNPs Size: AuNPs - 5 nm Ag@SiO2 NPs - 200 nm	Drop casting	Rhodamine B (RhB)	At 532 nm excitation, the SERS signal of RhB at 1647 cm^{-1} shows a linear trend with the logarithm of RhB concentrations from 10^{-4} M to 10^{-7} M, with a detection limit as low as 5×10^{-9} M. The substrate demonstrated good uniformity and stability, maintaining strong signals even after four weeks of storage. It also proved reusable after cleaning with anhydrous ethanol, it still effectively enhanced RhB signals. The substrate successfully detected real samples with satisfactory recovery.
Y. Liu et al. (2022)	AuNPs Size: 100 nm	Drop casting	Malachite green (MG), crystal violet (CV) and methylene blue (MB)	The substrate enabled simple detection of MG, achieving a low LOD of 1.5×10^{-9} M.

In the investigation conducted by Stankevičius et al. (2021), AuNPs with diameters ranging from approximately 5 nm to 20 nm were generated through a nanosecond laser treatment process, a technique that offers precise size control without the need for chemical reducing agents. Among the various configurations tested, the optimal SERS performance was obtained from a single uniform Au layer that was further coated with an additional ultra-thin 5 nm Au overlayer. Using

4-mercaptobenzoic acid (4-MBA) as the model Raman probe molecule, this configuration yielded the highest measured EF, demonstrating the importance of fine-tuning nanoparticle layering for signal amplification.

Similarly, Amador-Martínez et al. (2023) synthesized AgNPs in the size range of 3 nm to 10 nm via a straightforward chemical reduction route employing rongalite as the reducing agent and gelatin as a stabilizing matrix to prevent aggregation. This approach resulted in a maximum EF of 19.89 for pyridine detection, highlighting the combined effects of nanoparticle size control and colloidal stability on SERS activity.

In another study, Çelik and Kurt (2021) reported that compressed composite pellets formed from AgNPs and expanded graphite (EG) produced a highly sensitive and mechanically stable SERS substrate. This hybrid configuration achieved an exceptionally low detection limit of 10^{-14} M for R6G, showcasing the synergistic enhancement provided by the conductive graphite framework and well-dispersed metallic nanoparticles.

Mao et al. (2023) fabricated silver-silica ($Ag@SiO_2$) core-shell nanoparticles that were further decorated with 5 nm AuNPs, resulting in a bimetallic structure combining the high plasmonic activity of silver with the chemical stability of gold. These hybrid nanoparticles exhibited not only excellent signal enhancement but also remarkable stability, reusability over multiple detection cycles and a well-defined linear SERS response for Rhodamine B (RhB) quantification.

Most recently, Y. Liu et al. (2022) developed an innovative "sea urchin-like" $Au@SiO_2$ nanoparticle morphology, referred to as $SG@SiO_2$ NPs, characterized by radially protruding Au branches on a silica core. This unique structure created a dense array of electromagnetic "hot spots" that significantly boosted SERS sensitivity. The substrate was applied for detecting the synthetic dye malachite green (MG) in tilapia samples, achieving a remarkably low LOD of 1.5×10^{-9} M, underscoring its potential for food safety monitoring. These studies collectively highlight the importance of selecting suitable plasmonic metals and optimizing substrate integration to achieve high-performance SERS detection.

In the present work, AgNPs are selected as the plasmonic material to be deposited onto the surface of the fabricated PSi-based substrates. The choice of AgNPs is motivated by their superior plasmonic properties, including a high extinction coefficient in the visible range, strong LSPR effects and an exceptional ability to generate intense electromagnetic "hot spots" at nanoscale junctions (Katyal, 2019;

Mosier-Boss, 2017). These properties make Ag an ideal candidate for amplifying Raman scattering signals. A systematic investigation is carried out to examine how variations in AgNPs size influence the resulting SERS performance. By employing nanoparticles of different diameters, the study aims to determine the relationship between particle size and the intensity of the Raman spectral response. Understanding this size-dependent behaviour is crucial for optimizing the nanoparticle-PSi interface to achieve maximum signal enhancement, tailored to the specific requirements of targeted NS1 detection.

2.3.5 Surface Functionalization

Surface functionalization of SERS substrates plays a pivotal role in enhancing the sensitivity, selectivity and reproducibility of Raman signal detection (Cialla et al., 2012). This is achieved by tailoring the surface chemistry through the incorporation of specific functional groups, linker molecules or biorecognition elements such as antibodies and aptamers to strengthen the interaction between the analyte and the plasmonic surface. In biological sensing applications, surface functionalization facilitates the selective capture of target biomarkers, including proteins and nucleic acids, from complex biofluids such as saliva, serum or urine (Kahraman et al., 2017). However, detecting analytes from these biological fluids presents several challenges, including the presence of interfering substances, high background signals, non-specific adsorption and the typically low concentration of target molecules. These factors can compromise the reliability and reproducibility of SERS signals. Therefore, the proper design and implementation of surface functionalization strategies are essential for improving analyte binding and signal enhancement.

Table 2.8 provides a comprehensive summary of multiple research studies that have implemented surface functionalization techniques to enhance SERS-based platforms for the detection of a wide range of diseases. These studies collectively underscore the adaptability and broad applicability of SERS in the biomedical diagnostics domain, covering conditions such as Alzheimer's disease, prostate cancer, dengue fever and SARS-CoV-2 infection.

For Alzheimer's disease detection, gold nanowire arrays were functionalized with monoclonal 6E10 antibodies, which exhibit high specificity toward amyloid β (1-42) peptides, a well-established biomarker of the disease (M. Kim et al., 2024). In

the context of prostate cancer diagnostics, polystyrene colloidal spheres coated with a silver shell (PS@Ag) were modified with a combination of thiolated DNA probes and prostate-specific antigen (PSA)-targeting aptamers. This dual-recognition strategy enabled the selective identification of both PSA and its free form (f-PSA), thereby improving diagnostic accuracy (Zhao et al., 2022).

DENV detection was explored in two separate studies that adopted distinct functionalization approaches. In one case, gold nanorods and nanospheres were deposited on a glass substrate and conjugated with DENV NS1 proteins, which served as recognition elements for capturing dengue-specific IgG antibodies from patient samples (Mustapa et al., 2025). The second study employed silver nanorods in combination with hairpin DNA probes specifically engineered for localized catalytic hairpin assembly (LCHA) and hybridization chain reaction (HCR), allowing for the highly sensitive detection of the DENV gene sequence (Song et al., 2020).

For SARS-CoV-2 detection, researchers developed a nanopillar array coated with a silver film and functionalized it with SARS-CoV-2-specific antibodies to enable the capture and identification of viral-like particle (VLP) proteins (Kaladharan et al., 2023). Taken together, these investigations highlight the pivotal role of surface functionalization, whether through antibodies, proteins, aptamers or DNA-based molecular probes in significantly improving the selectivity and sensitivity of SERS platforms. Such strategies enable precise targeting of antibody-based, protein-based and nucleic acid-based biomarkers, thereby expanding the scope of SERS in clinical diagnostics and facilitating rapid, label-free detection of diverse disease indicators.

Table 2.8
Surface Functionalization of SERS Substrates

Reference	**Diseases**	**SERS Substrate**	**Recognition Element**	**Targeted Molecules**
M. Kim et al. (2024)	Alzheimer	Au nanowire array	Monoclonal 6E10 antibody solution	Amyloid β (1-42)
Zhao et al. (2022)	Prostate cancer	Polystyrene colloidal sphere @Ag shell (PS@Ag)	DNA probe (SH-DNA) PSA Aptamer	Prostate-specific antigen (PSA) free prostate-specific antigen (f-PSA)
Mustapa et al. (2025)	Dengue	Au nanorods applied to glass surface + Au nanospheres	DENV NS1 protein	Immunoglobin G antibodies (IgG)
Song et al. (2020)	Dengue	Ag nanorods	Hairpin DNA probes used in LCHA and HCR	DENV gene sequence (nucleic acid from DENV)
Kaladharan et al. (2023)	SARS-CoV-2	Nanopillar arrays and coated with silver film	SARS-CoV-2 antibody	SARS-CoV-2 VLP protein

In the present work, the detection of NS1 is enhanced through the surface functionalization of the SERS substrate with dengue NS1-specific antibodies. This functionalization strategy enables selective binding between the immobilized antibodies and the NS1 antigen present in the sample, thereby improving the capture efficiency and concentrating the target molecules in close proximity to the plasmonic “hot spots”. As a result, the localized electromagnetic field is maximized at the antigen-antibody interface, leading to a stronger Raman signal and improved sensitivity. This approach not only increases the detection limit for NS1 but also enhances the specificity of the assay by minimizing interference from non-target biomolecules commonly present in complex biological fluids.

2.4 Conclusion

This chapter has reviewed the fundamental concepts and recent advancements relevant to the development of a SERS-based biosensor for salivary detection of DENV. It began with an overview of dengue fever, highlighting the limitations of conventional detection methods and the growing interest in non-invasive diagnostic strategies using saliva. The principles of SERS were then discussed, emphasizing its high sensitivity and potential for label-free detection of low-abundance biomarkers. Various aspects of SERS substrates were explored, including the use of silicon-based platforms, electrochemical etching techniques for substrate fabrication and the role of plasmonic metals in enhancing Raman signal intensity. The surface functionalization strategies, which are critical for improving selectivity, signal reproducibility and biofluid compatibility is also reviewed. Through a comparative review of recent studies, the application of SERS for disease diagnosis, particularly for viral targets like DENV and SARS-CoV-2, was demonstrated to be both promising and adaptable. Collectively, the literature provides a solid foundation for the development of a high-performance, solid-based SERS substrate tailored for salivary dengue NS1 detection.

In conclusion, the reviewed literature underscores the critical need for a reliable, non-invasive method for dengue virus detection. While SERS-based techniques have shown substantial potential due to their high sensitivity and molecular specificity, existing studies are constrained by inadequate substrate performance, particularly in detecting low concentrations of the NS1 antigen in saliva. The absence of a purpose-engineered SERS substrate with enhanced affinity toward NS1 constitutes a significant

research gap that necessitates further investigation. Addressing this limitation is essential to advance the development of practical, salivary-based diagnostic tools capable of supporting early and accurate dengue detection.

Accordingly, this study proposes the fabrication and characterization of a AgNPs-coated PSi SERS substrate specifically designed to enhance detection sensitivity and reproducibility for NS1 in saliva. The subsequent chapter delineates the experimental framework, materials, fabrication procedures and characterization techniques employed to achieve the objectives of this research.

CHAPTER 3
RESEARCH METHODOLOGY

3.1 Introduction

This chapter outlines the research design and methodology employed in this study to address the research questions and objectives identified in the previous chapters. Section 3.2 provides an overview of the methodological framework of the SERS substrate. Section 3.3 elucidates the processes involved in the preparation of the silicon wafer, electrochemical fabrication of PSi and plasmonic metal coating. Section 3.4 focuses on the characterization of the AgNPs-coated PSi SERS substrates using Raman spectroscopy and structural analysis, which define the key variables of interest and ensure that the findings are both reliable and relevant. Section 3.5 presents the surface functionalization of the AgNPs-coated PSi SERS substrates for DENV NS1 antigen detection. Finally, Section 3.6 concludes the research methodology by providing a comprehensive overview of the approach taken and contributes to addressing the research questions effectively.

3.2 Research Methodology Overview

The overall step by step process involved in designing the SERS substrate are illustrated in Figure 3.1. The process involves five main steps. First, an extrinsic *n*-type silicon substrate was selected and cleaned with HF dip (Canham, 1990). Second, a PSi layer was fabricated using the photo-assisted electrochemical etching technique, as depicted in Figure 3.1(B). In the third step, AgNPs were deposited onto the PSi surface via the drop casting method to produce the SERS-active substrate, as shown in Figure 3.1(C). Next, surface functionalization was carried out by immobilizing dengue NS1 antibodies onto the AgNPs-coated PSi SERS substrate surface, enabling biological specificity, as illustrated in Figure 3.1(D). Finally, the DENV NS1 antigen was introduced onto the antibody-functionalized substrate to allow antigen-antibody binding for SERS-based detection, as represented in Figure 3.1(E).

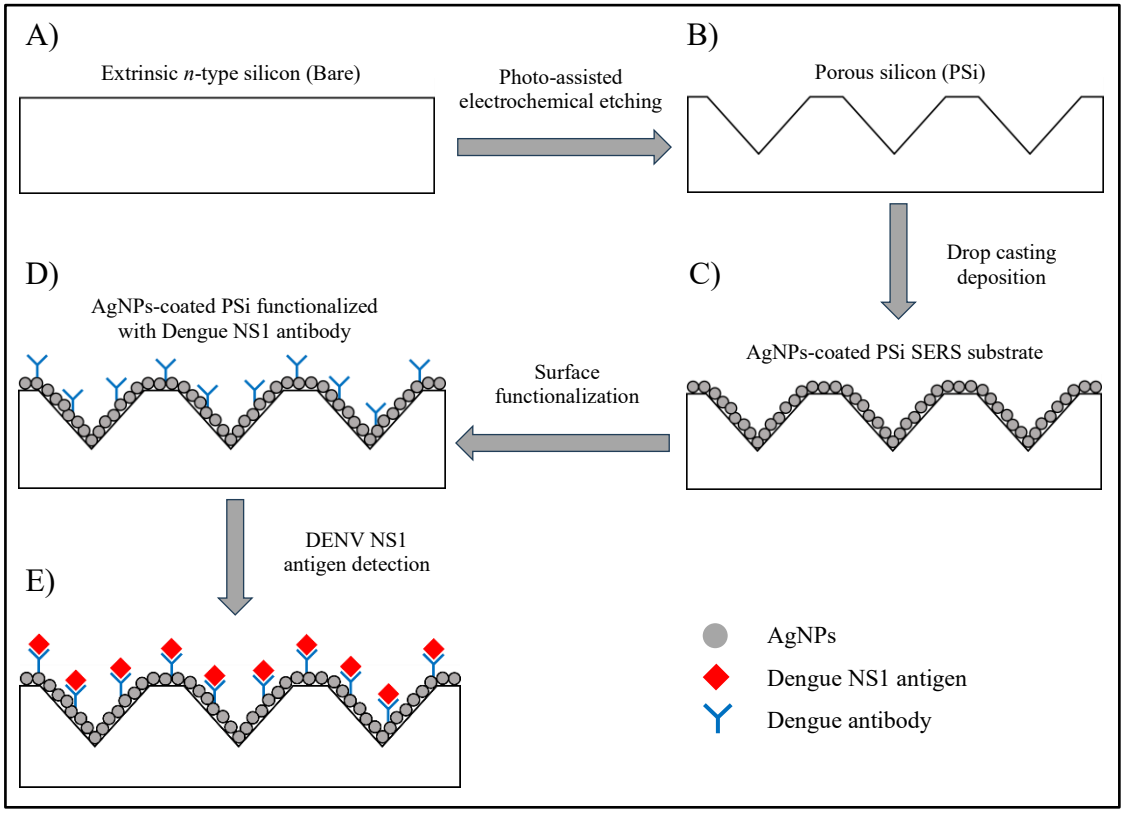

Figure 3.1 Development of a Solid-Based SERS Substrate for The Detection of Low-Concentration NS1: Schematic Illustration of the Five Key Layers Involved in The Fabrication Process

Figure 3.2 shown depicts the overall works involved in this study. This work can be divided into three stages: Stage 1 involves the fabrication of the PSi to serve as the base of AgNPs-coated PSi SERS substrate; Stage 2 focuses on the characterization of the substrate; and Stage 3 evaluates the detection performance of NS1.

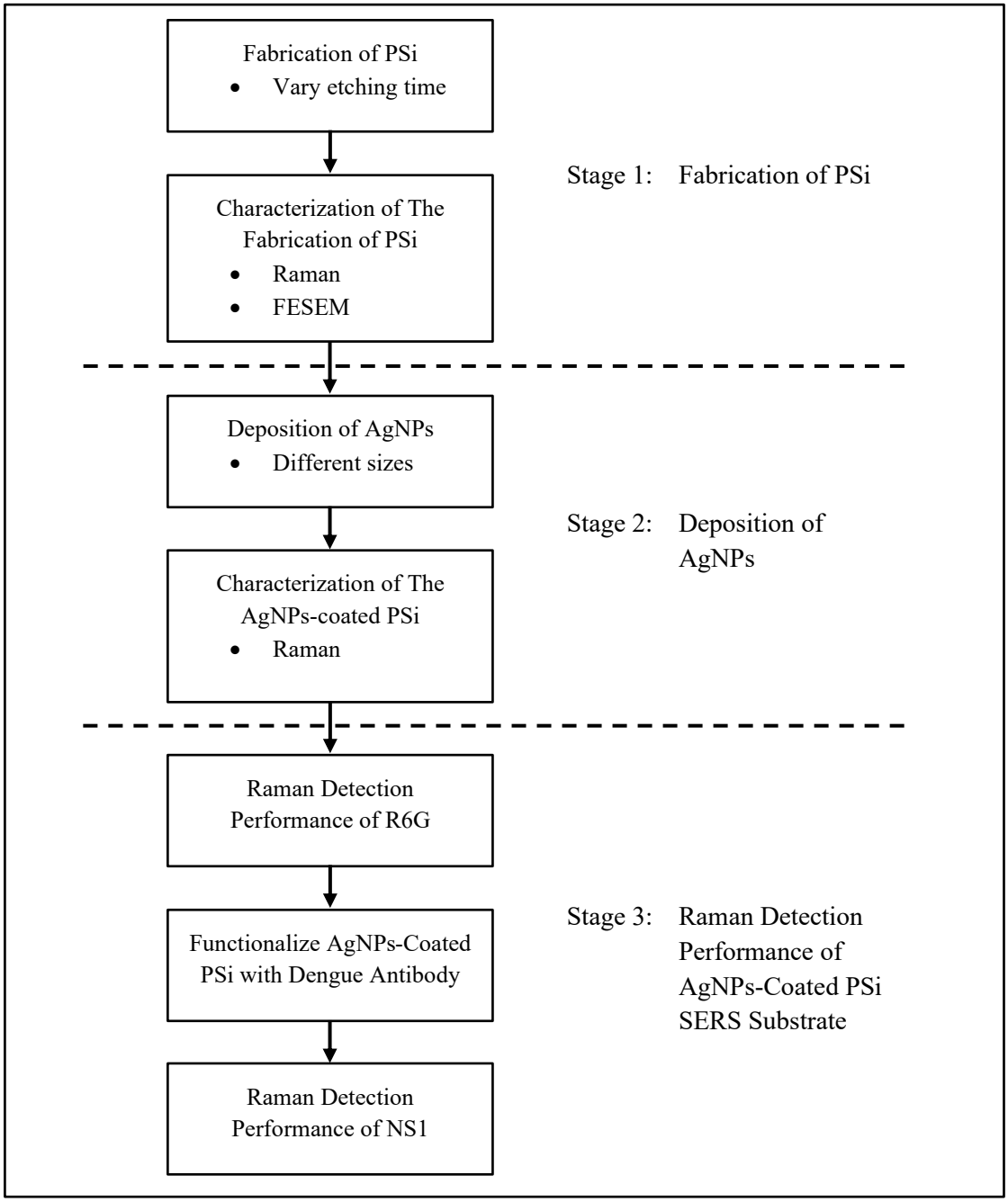

Figure 3.2 Methodology Workflow

Stage 1: Fabrication of PSi

Extrinsic *n*-type silicon doped with phosphorus (P) dopant, with a resistivity of 1-10 Ω·cm, <100> crystal orientation and a thickness of 285 µm, was fabricated using a photo-assisted electrochemical etching technique to produce high-surface-area of PSi. The PSi served as the solid base of the SERS substrate. Etching duration was varied to determine the optimum etching conditions. The fabricated PSi samples were then characterized using FESEM and Raman analysis to observe their properties.

Stage 2: Deposition of AgNPs

Then, the PSi samples were deposited with 30 µL of AgNPs of various sizes using an oven-assisted drop casting technique to enhance Raman scattering. The AgNPs-coated PSi SERS substrates samples were characterized using FESEM for structural analysis and Raman spectroscopy for Raman analysis.

Stage 3: Raman detection performance of AgNPs-coated PSi SERS substrate

Prior to detecting the DENV NS1 antigen, the detection performance of the AgNPs-coated PSi SERS substrate samples was evaluated using R6G as a Raman probe. Different concentrations R6G were deposited onto the AgNPs-coated PSi SERS substrate samples to determine the optimal samples for NS1 detection. The EF and LOD of the samples were evaluated using Raman spectra of R6G. The optimized AgNPs-coated PSi SERS substrates were functionalized with anti-DENV antibodies at a concentration of 0.025 mg/mL chosen based on reported immunosensor studies indicating that antibody concentrations in this range offer a balance between adequate surface coverage and maintained bioactivity (Parkash et al., 2014). The LOD of NS1 detection is established.

3.3 Fabrication of SERS Substrate

3.3.1 Preparation of Silicon Wafer

The experiment began with a 2-inch diameter extrinsic *n*-type silicon wafer doped with phosphorus (P). The wafer had a resistivity of 1-10 Ω·cm, <100> crystal orientation and a thickness of 285 µm. It was diced into smaller samples of approximately 1 cm × 1 cm before being fitted into the Teflon cell. Prior to etching, the silicon samples were cleaned using an aqueous solution prepared from 50 mL of deionized (DI) water and 1 mL of hydrofluoric acid (HF). The overall cleaning process is illustrated in Figure 3.3.

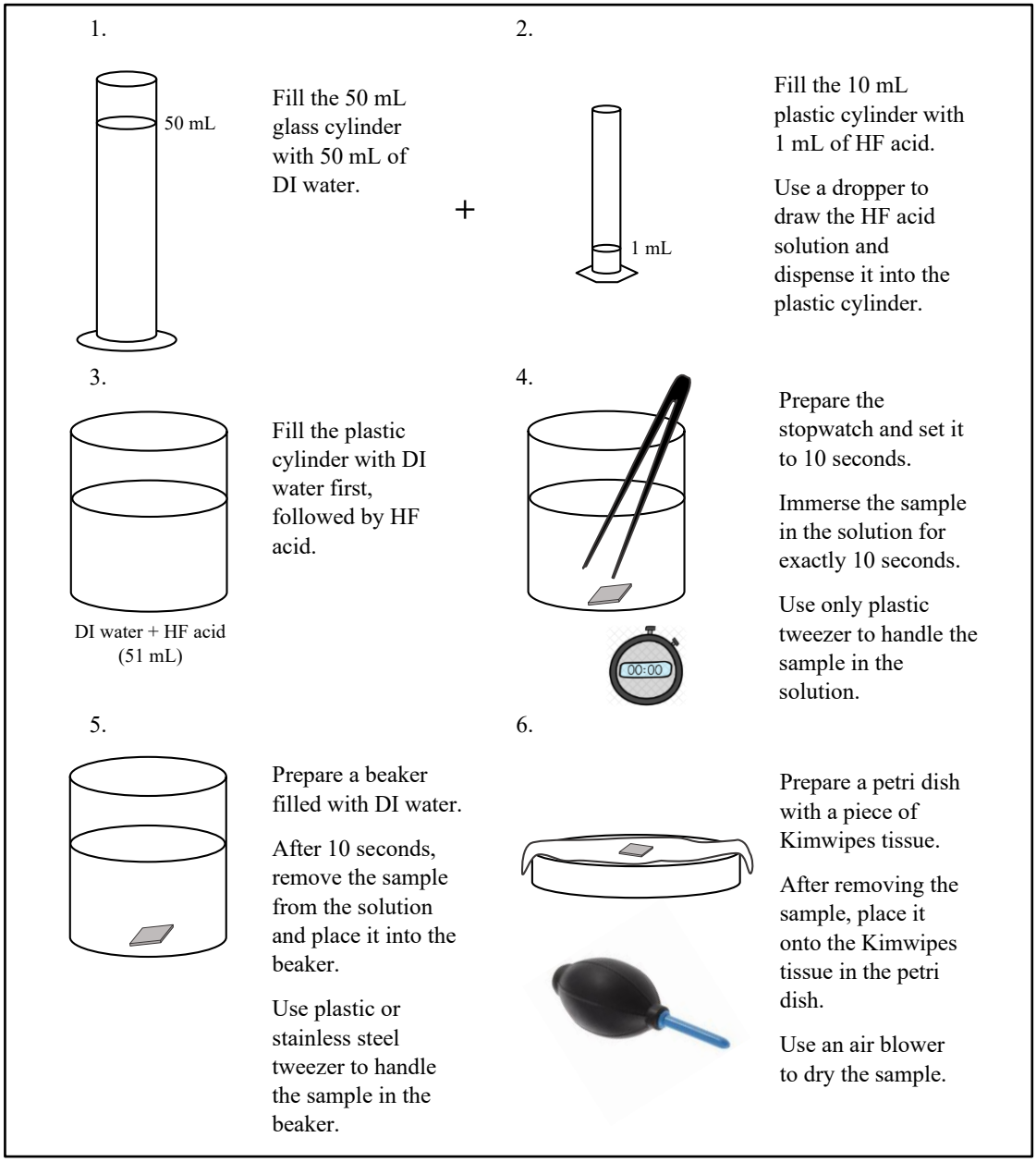

Figure 3.3 Cleaning Process of Silicon Wafers

3.3.2 Electrochemical Fabrication of PSi

The porous structure was fabricated using the direct current electrochemical etching (DCPEC) technique (Razali et al., 2019). Figure 3.4 illustrates the overall fabrication process of PSi. As shown in Figure 3.4(A), the cleaned and diced silicon wafer was carefully mounted in a Teflon cell equipped with an O-ring, ensuring that only the front surface of the wafer was exposed to the electrolyte solution. To avoid leakage during the process, a metal plate was firmly clamped against the cell using two screws.

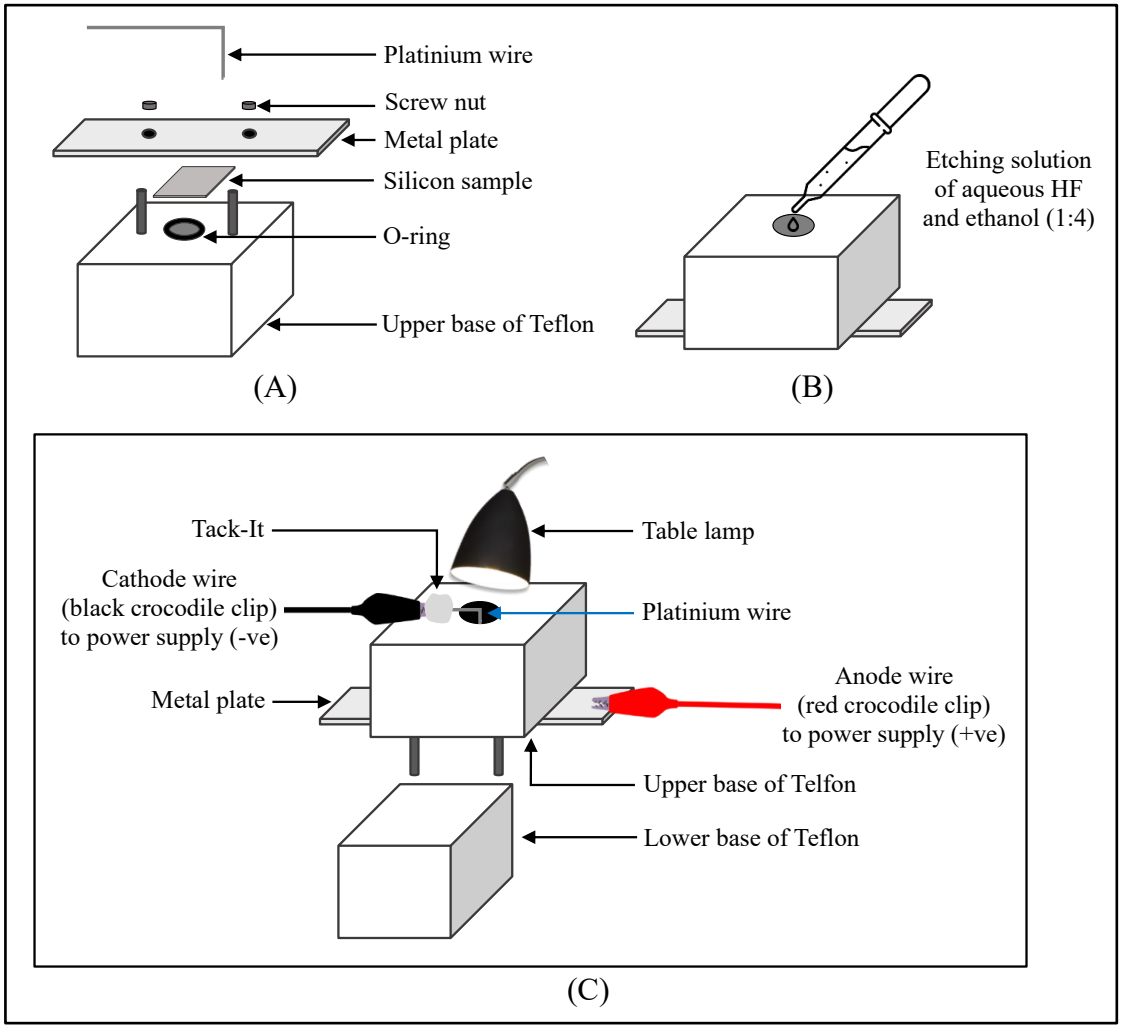

Figure 3.4 Fabrication of The SERS Substrate Using DCPEC Technique: Illustration of The Overall Fabrication Process for Developing PSi-Based Structures

Figure 3.4(B) presents the electrolyte solution, which consisted of a mixture of aqueous hydrofluoric acid (HF) and ethanol (C_2H_5OH) in a 1:4 volume ratio. This solution was filled onto the silicon surface through a hole specifically designed in the Teflon cell. Figure 3.4(C) shows the etching process, which was conducted under illumination from an incandescent lamp to enhance electron-hole pair generation. The etching duration was systematically varied at intervals of 20 minutes, 22 minutes, 24 minutes, 26 minutes, 28 minutes and 30 minutes in order to determine the optimal conditions for PSi formation. Following the etching process, all samples were thoroughly rinsed with DI water to remove residual electrolyte.

The supplied voltage and current are fixed at 10 V and 10 mA, respectively. Using the equation (3.1), the used current density is 20 mA/cm^2.

$$J = \frac{I\,(mA)}{Area\,(cm)} = \frac{x\,(mA)}{\pi\,(0.4)^2} \tag{3.1}$$

J = Current density

I = Applied current at power supply

r = 0.4 (size of O-ring)

3.3.3 Drop Casting Deposition of AgNPs Coating

AgNPs is one of the nanomaterials most frequently used because of its anti-microbial properties (Al-Hosaini & Azhar, 2021), high electrical conductivity (Khodke et al., 2017) and optical properties (Prosyčevas et al., 2007). AgNPs has a high surface area per unit mass and releases a continuous Ag ion level within their environment. Ag is found to be capable of enhancing the Raman intensity of various molecules. AgNPs acts as a shielding layer and provides long-term stability for SERS substrates layer (Markin et al., 2018).

The AgNPs used in this research were purchased from nanoComposix. Based on literature review where various sizes of AgNPs ranging from 3 to 200 nm (Amador-Martínez et al., 2023; Çelik & Kurt, 2021; Y. Liu et al., 2022; Mao et al., 2023; Stankevičius et al., 2021) were used. The selected particle diameters for this study were 5 nm, 25 nm, 50 nm, 75 nm and 110 nm. The surface of the AgNPs was coated with polyvinylpyrrolidone (PVP) with a molecular weight of 40 kDa. PVP is a large polymer that provides excellent steric stability (nanoComposix, n.d.). The 40 kDa version helps prevent the particles from contacting and aggregating when the solution conditions change or when the particles are dried onto a substrate or thin film. Figure 3.5 illustrate the drop casting deposition technique used in this study, in which 30 µL of AgNPs solution was drop cast onto the PSi using a micropipette.

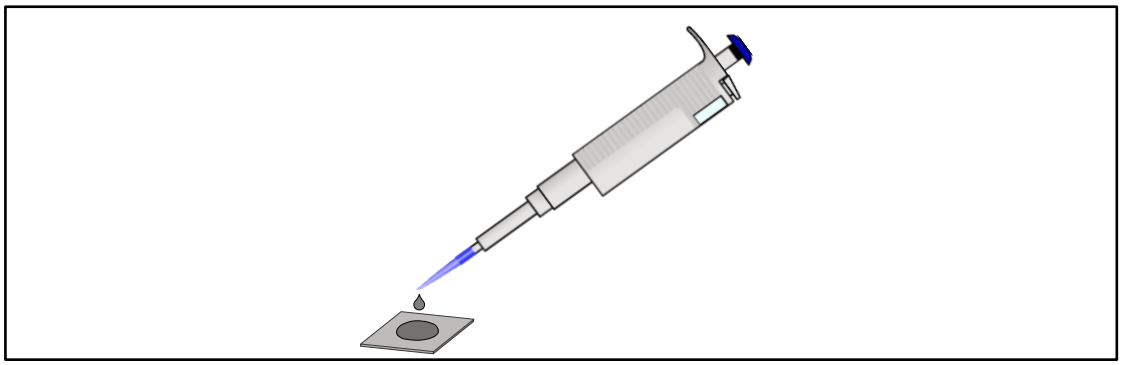

Figure 3.5 Drop-Casting Deposition of AgNPs Coating

3.4 Characterization of SERS Substrate

3.4.1 Raman Characterization

Raman characterization of the samples was conducted using PeakSeeker Raman spectrometer equipped with 785 nm laser source. The spectra were collected using 10× microscope objective over the range 400 cm^{-1} to 1800 cm^{-1}. Initially, the Raman spectra of all the samples were measured without the presence of Raman probe molecule (R6G). This step is to observe the Raman characteristic of the samples. Then, various concentration of R6G were deposited onto the samples to investigate the Raman detection performance of the develop AgNPs-coated PSi SERS substrate. R6G is a cationic dye known for its bright yellow-orange colour and strong fluorescence properties. The dye's unique molecular structure enables it to absorb light at specific wavelengths and emit light at longer wavelengths, making it a valuable Raman probe molecule in Raman analysis (Andreev et al., 1976). Its stability and solubility in various solvents further contribute to its versatility in research and industrial applications (Hildebrandt & Stockburger, 1984). The presence of R6G can be detected with the presence of peaks related to its molecular vibration as tabulated in Table 3.1.

Table 3.1
Raman Peaks of R6G Deposited on AgNPs-Coated PSi SERS Substrate

Peaks *(cm^{-1})*	**Assignation**
611	C-C-C ring in-plane bending
771	C-H out-of-plane bending
1127	C-H in-plane bending
1183	Aromatic C-C stretching
1310	Aromatic C-C stretching
1360	Aromatic C-C stretching
1508	Aromatic C-C stretching
1573	Aromatic C-C stretching
1648	Aromatic C-C stretching

Note: Peak assignments adapted from Andreev et al. (1976), He et al. (2012), Hildebrandt and Stockburger (1984) and L. Liu et al. (2020). Substrate information adapted from Ismail et al. (2024).

The detection performance of R6G is evaluated using EF and LOD where 30 µL of R6G was deposited on the fabricated substrate using a micropipette at different concentrations of 10 mg/mL, 1 mg/mL, 0.1 mg/mL and 0.01 mg/mL. The samples were left to dry at room temperature in a desiccator for 3 hours. Then, the samples were analyzed using a PeakSeeker Raman spectrometer with a 10 seconds exposure time and

100 mW power. The settings were determined through an examination of the Raman spectra of R6G, where exposure time and power are adjusted if required.

The EF serves as a quantitative indicator of the SERS performance and sensitivity of the PSi substrate. Higher EF values signify more efficient Raman signal amplification, arising from enhanced plasmonic effects and improved analyte adsorption. Consequently, EF directly reflects the substrate's capability to detect low-concentration analytes and is used to assess and compare overall SERS substrate performance. Equation 3.2 is used to calculate the EF,

$$EF = \frac{I_{SERS}}{I_{BARE}} \times \frac{C_{BARE}}{C_{SERS}} \tag{3.2}$$

where, I_{SERS} is the intensity of the selected peak height obtained from AgNPs-coated PSi SERS substrate, I_{BARE} is the intensity of the selected peak height obtained from bare silicon, C_{BARE} is the concentration of the R6G deposited on bare silicon, C_{SERS} is the concentration of the R6G deposited on AgNPs-coated PSi SERS substrate.

Meanwhile, LOD is the parameter to indicate the lowest concentration of analytes that can be reliably detected using AgNPs-coated PSi SERS substrate.

3.4.2 Structural Characterization

The surface morphology and topography of the PSi-based structure was characterized by the FESEM (Model: JEOL JSM 7401F). The NanoScope Analysis software was used to analyse the surface roughness and the estimated pore depth of the samples with a scan area of 5 µm × 5 µm and 10 µm × 10 µm. The samples also undergo the energy-dispersive EDX to determine the composition of each material existing on the PSi surface.

3.5 Surface Functionalization of SERS Substrate for DENV NS1 Antigen Detection

In this work, the surface functionalization procedure was adapted and refined from the method described by Hadis (2018), with the objective of chemically modifying the sensing surface to enhance its specificity toward the target analyte, the dengue NS1 antigen. The functionalization was performed on the pre-optimized 75 nm AgNPs-coated PSi SERS substrate, which had previously been identified as the most

suitable configuration. By immobilizing dengue NS1 antibodies on the 75 nm AgNPs-coated PSi SERS substrate surface, the platform was designed to achieve selective antigen recognition while minimizing non-specific interactions.

Prior to the functionalization process, the SERS substrate underwent a cleaning step using a plasma cleaner, a method chosen for its effectiveness in eliminating surface impurities, organic contaminants and adsorbed particles that could interfere with subsequent chemical binding (X. Wang et al., 2008). This cleaning ensured optimal exposure of the surface for silanization. Following the cleaning step, the substrate was immersed for one hour in a solution containing 10 mM acetic acid and 1% (v/v) glycidoxypropyl-trimethoxysilane (GPTS) in ethanol (Carrara et al., 2012; Puppo et al., 2014). The GPTS acts as a silane coupling agent, forming covalent bonds with the hydroxylated silicon surface. After incubation, the substrate was dried with a stream of high-purity nitrogen gas and subsequently baked at 110 °C for 15 minutes to complete the silanization reaction and improve the stability of the surface modification layer (Carrara et al., 2012; Puppo et al., 2014).

Next, a solution of diluted dengue NS1 protein at a concentration of 0.025 mg/mL, prepared in phosphate-buffered saline (PBS), was carefully pipetted onto the silanized substrate surface and incubated for 3 hours in a humid chamber maintained at ambient temperature. This step allowed for covalent binding of the antibodies to the active epoxy groups of the GPTS layer. To prevent any unreacted GPTS groups from binding non-target species, a blocking step was performed using 10 mM ethanolamine, with incubation for 1 hour (Carrara et al., 2012; Patolsky et al., 2004; Puppo et al., 2014). Additional blocking was achieved by treating the substrate with 3% gelatin (Sigma) in PBS for 30 minutes, effectively reducing non-specific protein adsorption (Carrara et al., 2012; Puppo et al., 2014). Finally, the functionalized substrate was gently rinsed with PBS to remove unbound biomolecules and dried under nitrogen flow.

For the detection phase, a series of NS1 antigen solutions with concentrations of 0.1 mg/mL, 0.05 mg/mL, 0.02 mg/mL, 0.01 mg/mL, 0.005 mg/mL, 0.002 mg/mL and 0.001 mg/mL were prepared and deposited onto the fully functionalized 75 nm AgNPs-coated PSi SERS substrates. The samples were left to dry in a desiccator for 1 hour to ensure solvent evaporation without introducing ambient contamination. Raman spectra were then acquired using a PeakSeeker Raman spectrometer under an excitation power of 100 mW, with an integration time of 10 seconds for each

measurement, enabling the evaluation of substrate sensitivity and detection limits for dengue NS1 antigen.

3.6 Conclusion

In this chapter, a comprehensive overview of the research methodology employed in this study was presented. The fabrication of the PSi substrate via photo-assisted electrochemical etching was described, followed by the drop casting process used to coat the PSi surface with AgNPs of various sizes. Structural and Raman characterization techniques were employed to evaluate the properties of the fabricated substrates. Finally, the optimized SERS substrate was functionalized with dengue NS1 antibodies to enable specific detection of the target antigen. Each step in the methodology was designed to ensure the effective preparation and evaluation of the developed SERS substrate for detection of DENV NS1 antigen detection.

CHAPTER 4
RESULTS AND DISCUSSIONS

4.1 Introduction

This chapter presents the results and discussions derived from the experimental investigations conducted in this study, addressing the research objectives outlined in the preceding chapters. Section 4.2 examines the characterization of PSi, focusing on the influence of etching time on both Raman and structural properties. Section 4.3 evaluates the Raman characterization of AgNPs-coated PSi SERS substrates, with emphasis on the effect of varying AgNPs deposition sizes. Section 4.4 analyzes the detection performance of AgNPs-coated PSi SERS substrates, comparing EF for both bare silicon and PSi-based, along with the determination of the LOD. Finally, Sections 4.5 and 4.6 present the detection results for low concentration of dengue NS1 antigen and provide the concluding remarks, thereby linking the experimental findings to the study's overall objectives.

4.2 Characterization of PSi

This section presents the Raman spectra and FESEM images obtained from various PSi samples to investigate the effect of etching time duration on the Raman and structural properties of the substrates. To ensure the repeatability of the results, for each etching time, three samples are prepared and analyzed. The reported spectra in this section are the average from ten separate measurement points taken across different regions of the samples.

4.2.1 Effect of Etching Time on Raman Properties

Figure 4.1 presents the Raman spectrum obtained from extrinsic *n*-type bare silicon, doped with phosphorus (P) atoms, prior to undergoing the PSi fabrication process. The spectrum exhibits a dominant and well-defined sharp peak centered at approximately 520 cm^{-1}, which corresponds to the first-order optical phonon mode associated with Si-Si covalent bond vibrations in crystalline silicon (Xu et al., 2018).

The prominence and narrow linewidth of this peak are characteristic indicators of a highly ordered crystalline lattice with minimal structural defects, confirming the good quality of the starting silicon substrate (Deschaines et al., 2009). From ten separate measurement points taken across different regions of the wafer surface, the average peak intensity is determined to be 2551 a.u. with FWHM of the 7.74 cm^{-1}, signifying excellent uniformity in both crystallinity and optical response throughout the substrate.

In addition to the primary phonon peak at 520 cm^{-1}, the Raman spectrum of silicon displays a broad fluorescence background between approximately 1500 cm^{-1} and 1800 cm^{-1}. This background originates from Si-O bonds in the native oxide layer formed upon air exposure, where the resulting surface states generate broadband photoluminescence under laser excitation (Cullis et al., 1997). The fluorescence intensity is strongly influenced by the excitation wavelength, with a more pronounced response observed at 780 nm (Deschaines et al., 2009). Moreover, the reflective nature of the silicon surface can further enhance the detected background by redirecting both the incident laser light and the emitted fluorescence back into the spectrometer (Vulchi et al., 2024). Such a fluorescence baseline is of particular importance for subsequent SERS measurements, as it can contribute to background noise and potentially mask weak analyte peaks if left unaddressed. Therefore, this observation further justifies the necessity of subsequent surface modifications, including the controlled formation of porous structured network and the deposition of plasmonic nanoparticles, to enhance Raman scattering efficiency while reducing background interference.

Overall, the Raman spectrum obtained here serves as a critical baseline reference against which structural, morphological and optical modifications introduced during later fabrication stages can be quantitatively compared. This baseline allows for direct evaluation of how the transformation from a flat crystalline silicon surface to a nanostructured PSi-based SERS substrate impacts peak position, intensity and spectral background, thereby providing insight into the effectiveness of each fabrication step.

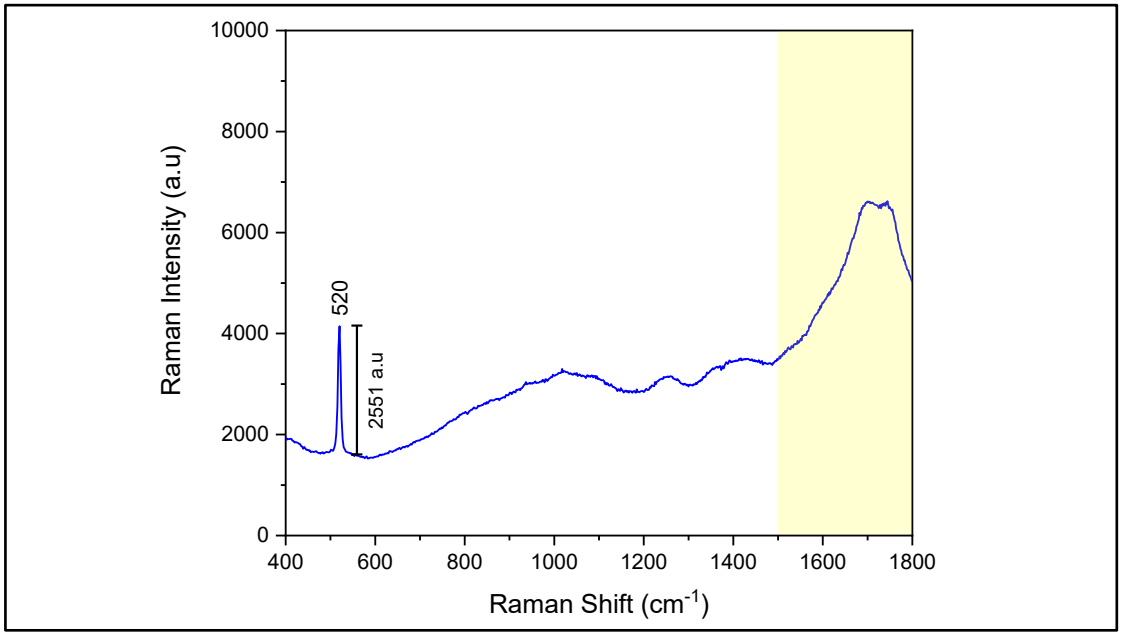

Figure 4.1 Raman Intensity of The PSi Peak in Extrinsic *n*-Type Silicon

Figure 4.2 presents the Raman spectra of PSi samples fabricated using different electrochemical etching durations, specifically ranging from 20 minutes to 30 minutes. Similar to bare silicon spectrum, a cross all measured spectra, a distinct and well-defined Raman peak is observed at approximately 520 cm^{-1}. This peak corresponds to the Si-Si optical phonon vibrational mode, indicating that the crystalline nature of the silicon lattice is preserved even after the formation of the porous structure (Abdullah et al., 2019; Razali et al., 2019). The retention of this vibrational signature suggests that, despite the extensive surface modification induced by the etching process, the underlying silicon framework remains structurally coherent (Zhong et al., 2018).

A notable feature of these spectra is the pronounced increase in peak intensity compared to that of the unetched silicon substrate. This enhancement can be attributed to several contributing factors. Primarily, the significantly enlarged specific surface area of PSi allows for more efficient light-matter interaction (Kuntyi et al., 2022). When light interacts with porous structure it may scatter from the crystallites, penetrate deeper into the material or become confined within the pores, resulting in successive scattering, a process more pronounced in PSi than in crystalline silicon (Dariani & Ahmadi, 2013). This photon trapping effect further intensifies the observed Raman response, making PSi a promising candidate for SERS applications.

It is also important to highlight the absence of the broad, elevated fluorescent background typically observed between 1500 cm^{-1} and 1800 cm^{-1} in the spectra of the

bare crystalline silicon substrate. This suppression of fluorescence is most likely a direct consequence of the rough, non-reflective surface topography of the PSi layer, which minimizes specular reflection and reduces background luminescence (Huang et al., 2014). Such a reduction in unwanted fluorescence is advantageous for Raman-based sensing, as it improves the overall signal-to-noise ratio and enhances the detectability of weak vibrational features.

Figure 4.2 shows that the Raman intensity does not originate from zero a.u. due to inherent detector background, fluorescence and arbitrary intensity scaling. Impurities in the sample or fluorescence from the material at the excitation wavelength generate a broad background signal, causing the Raman peaks to appear as smaller features superimposed on an elevated baseline. In this study, the PSi sample exhibits a high baseline intensity of approximately 30000 a.u., which is attributed to aggressive pore formation resulting from a longer etching time of 30 minutes, leading to enhanced background contributions. By comparison, the bare silicon sample without porosity shows a substantially lower baseline of around 2000 a.u. Nevertheless, neither spectrum reaches zero intensity, as residual instrumental noise, detector offsets, stray light and sample-related luminescence remain present in all measurements.

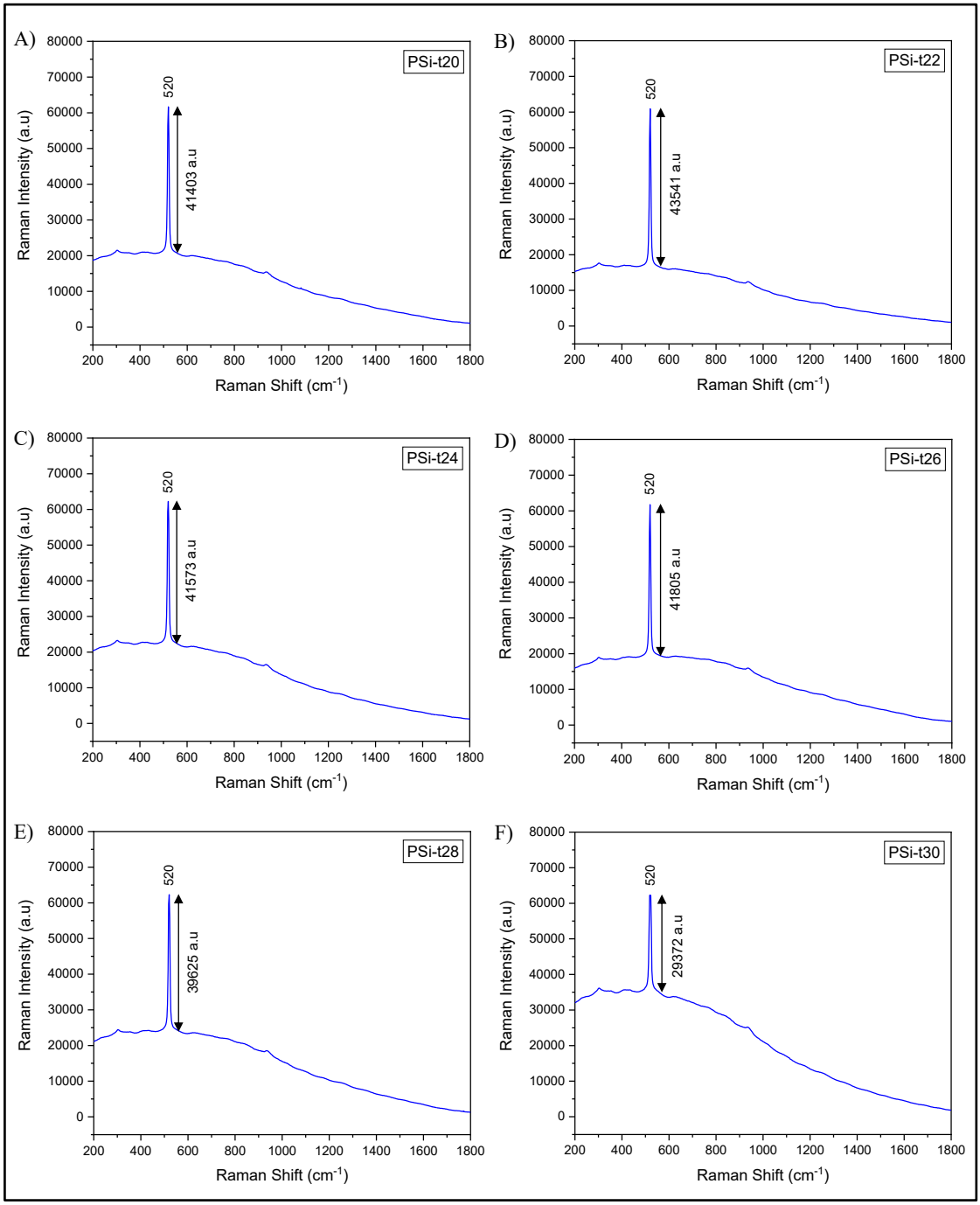

Figure 4.2 Raman Spectra of PSi at Different Etching Durations. (A) 20 minutes, (B) 22 minutes, (C) 24 minutes, (D) 26 minutes, (E) 28 minutes and (F) 30 minutes

Table 4.1 summarizes the effect of etching duration on the Raman peak intensity, FWHM and EF of the silicon peak at 520 cm^{-1}, providing insight into the structural and optical behaviour of PSi substrates fabricated under different etching times.

Table 4.1
Raman Peak Intensity of Silicon (520 cm^{-1}), FWHM and EF Calculations for Various Etching Times

Etching Time *(min)*	**Height of Raman Peak Intensity of Si (520 cm^{-1})** *(a.u.)*	**FWHM** *(cm^{-1})*	**Enhancement Factor for PSi** $EF = \frac{I_{SERS}}{I_{BARE}}$
20	41403	8.193	16.23
22	43541	7.928	17.07
24	41573	8.420	16.30
26	41805	8.001	16.39
28	39625	8.464	15.53
30	29372	10.798	11.51

The data confirm that etching time is a key parameter influencing the quality and SERS performance of PSi. Relative to bare silicon (FWHM = 7.74 cm^{-1}), PSi exhibits slightly broader FWHM values, attributable to variations in nanocrystal size and increased structural disorder compared to bulk crystalline silicon (Ivanda, 2018). Among all samples, the substrate etched for 22 minutes showed the most superior properties, including the highest Raman peak intensity (43541 a.u.), the narrowest FWHM (7.928 cm^{-1}) and the largest EF (17.07). These results suggest a highly crystalline porous structure with minimal defects (Harb & Mutlak, 2022), an optimal condition for strong LSPR and efficient Raman signal enhancement.

In contrast, the sample etched for 30 minutes showed a significant decline in performance, with a notable drop in peak intensity to 29372 a.u. and a substantial broadening of the Raman peak (FWHM = 10.798 cm^{-1}), resulting in the lowest EF (11.51). The broadening of the FWHM is attributed to optical phonons being trapped in nano-dimensional Si nanostructures and a decrease in crystallite size due to the quantum confinement effect (Zhong et al., 2018). This deterioration attributed to over-etching, which can lead to structural collapse, increased surface roughness and loss of effective surface area for nanoparticle interaction Abdullah et al., 2019) all of which may hinder SERS activity. In comparison, samples etched for 20 to 28 minutes maintained consistent Raman performance. Minor fluctuations in intensity and FWHM reflect gradual, controlled changes in porosity and surface morphology, which influence nanoparticle adsorption and distribution without compromising SERS enhancement, demonstrating that etching within this duration produces stable and highly effective nanostructures.

Throughout all etching durations, the Raman peak consistently appeared at 520 cm^{-1}, with no observable peak shift as shown in Figure 4.3. This consistency suggests that the internal crystal structure of silicon remains intact and free from significant strain or quantum confinement effects, even as porosity and surface morphology evolve (Cullis et al., 1997). The lack of peak shift confirms that the variations in FWHM and EF are primarily influenced by changes in surface properties rather than fundamental alterations in the silicon lattice (Cullis et al., 1997).

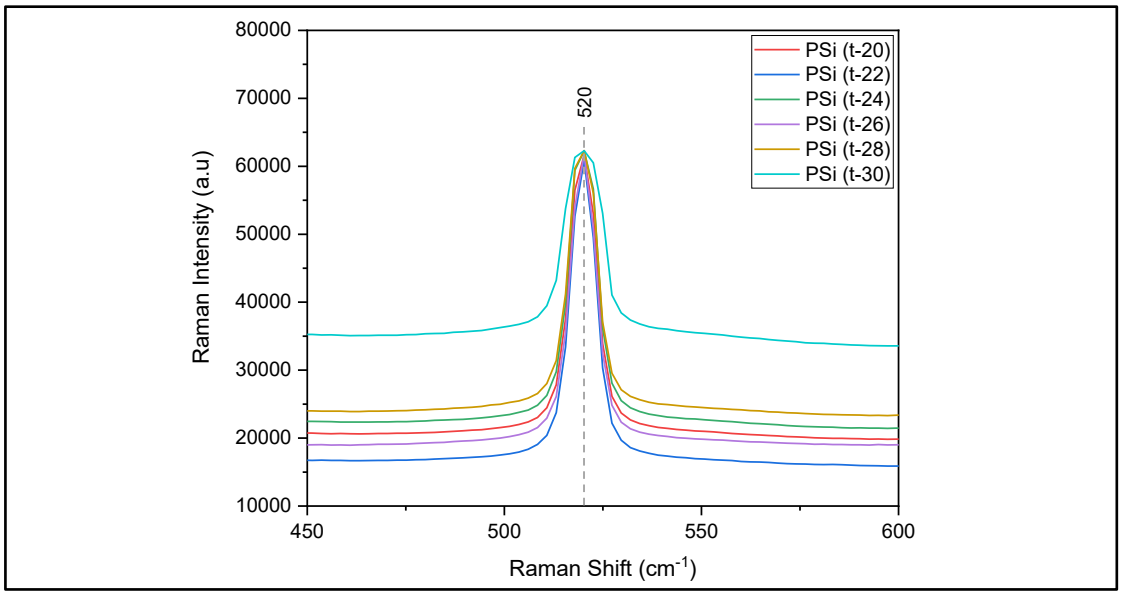

Figure 4.3 Silicon Raman Peak at 520 cm^{-1} for Various Etching Times

Although a non-monotonic trend is observed with increasing etching time, it is evident that an etching duration of 22 minutes yields the optimal PSi structure, exhibiting superior Raman characteristics and the highest enhancement factor. At this etching time, an optimal balance is achieved between adequate porosity, which promotes effective Raman signal amplification and sufficient structural integrity, which prevents excessive lattice disorder and defect formation. Prolonged etching beyond this duration leads to increased surface roughness, pore interconnection and structural degradation, as reflected by the reduced Raman intensity, broadened FWHM and diminished enhancement efficiency.

4.2.2 Effect of Etching Time on Structural Properties of PSi

Figure 4.4 presents the top-view FESEM images of PSi samples fabricated under a constant current density of 20 mA/cm^2, while systematically varying the etching duration. The etching time was adjusted from 20 minutes to 30 minutes in increments of 2 minutes, allowing for a clear comparative analysis of the resulting surface morphologies. At a magnification of 5000×, it is evident that well-defined cross-shaped porous structures are consistently formed across all samples, irrespective of the total etching time applied. Upon closer examination, a progressive change in structure size is observed as the etching duration increases from 20 minutes up to 28 minutes.

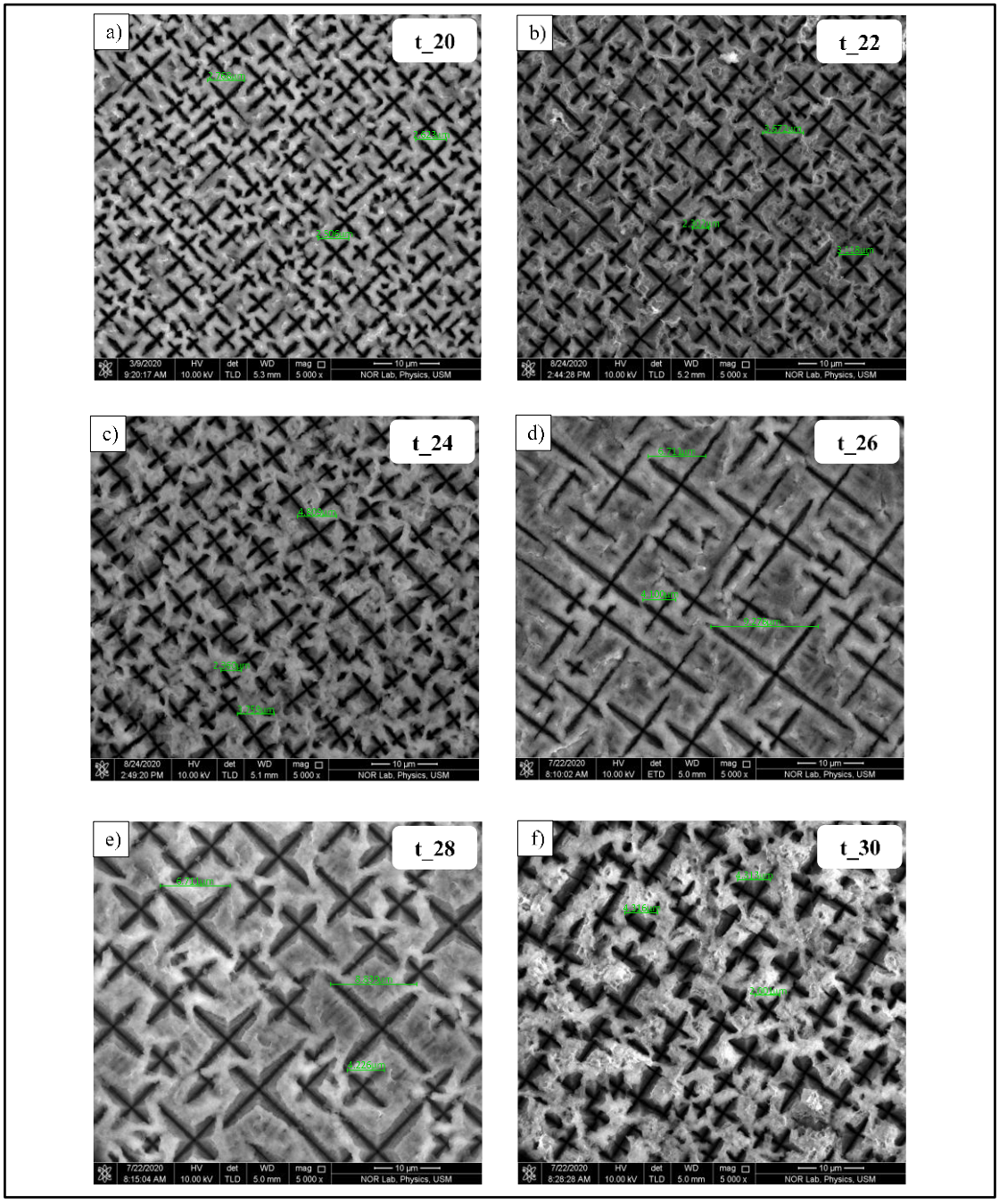

Figure 4.4 FESEM Characterization of The Top-View Surface Morphology of *n*-Type <100> PSi at 5000× Magnification for Different Etching Durations. (A) 20 minutes, (B) 22 minutes, (C) 24 minutes, (D) 26 minutes, (E) 28 minutes and (F) 30 minutes

Besides, the average dimensions of the cross-shaped features also increase, as quantitatively summarized in Table 4.2. However, when the etching time is extended further to 30 minutes, as depicted in Figure 4.4(F), noticeable morphological changes occur. Specifically, several of the previously distinct cross-shaped structures begin to merge with adjacent structures, creating a more interconnected network and resulting in a visibly rougher PSi surface.

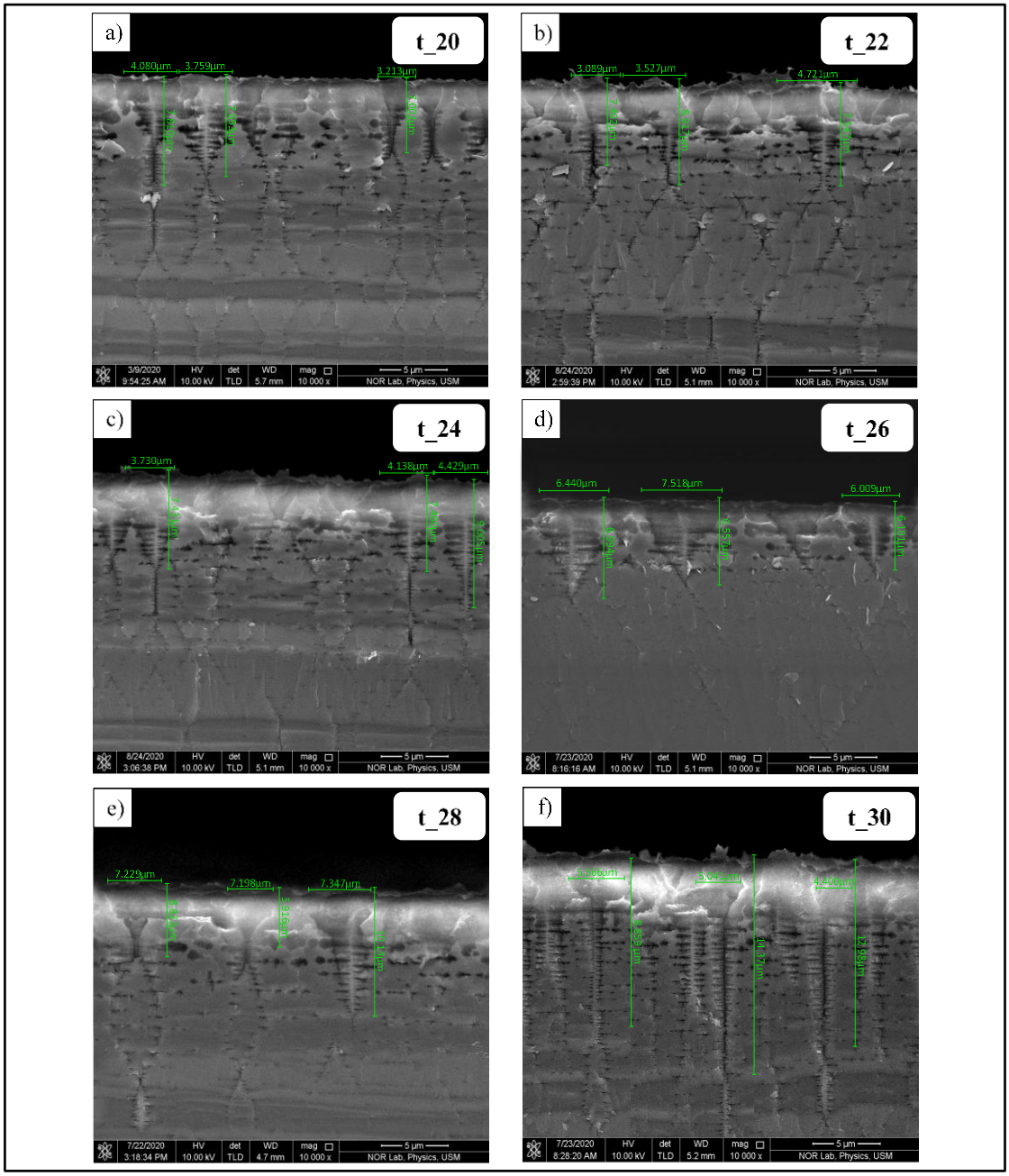

Figure 4.5 FESEM Characterization of The Cross-Sectional Surface Morphology of *n*-Type <100> PSi at 10000× Magnification for Different Etching Durations. (A) 20 minutes, (B) 22 minutes, (C) 24 minutes, (D) 26 minutes, (E) 28 minutes and (F) 30 minutes

Figure 4.5 also shows the cross-sectional view of FESEM images for the other etching times, where triangle-shaped structures are observed at magnification of 10000×. The dimension of the triangular-shaped structures in terms of triangular opening and depth is tabulated in Table 4.2.

Table 4.2
Dimensions of Cross-Shaped PSi Structures at Different Etching Times

Etching Time ***(min)***	**Top-View Average size** ***(μm)***	**Cross Sectional-View Average size** ***(μm)***	
		Triangle opening	**Depth**
20	2.632	3.684	7.502
22	3.031	3.779	7.955
24	3.643	4.099	7.965
26	6.696	6.656	6.551
28	6.592	7.258	8.293
30	NA	5.002	12.070

Analysis of the porosity depth reveals a general trend of increase with prolonged etching time, with the exception of the 26 minute data point. This deviation is likely the result of a gross measurement error, potentially caused by misplacement of the measurement cursor during data acquisition. Examination of the cross-sectional images further indicates that the average triangular opening expands progressively as etching duration increases, reaching its largest dimension at 28 minutes. Interestingly, at an etching time of 30 minutes, the average triangular opening decreases to 5.002 μm. This unexpected reduction can be attributed to the pronounced surface roughness caused by the formation of interconnected cross-shaped structures, as depicted in Figure 4.5(F). The presence of these features obscures the boundaries of the triangular openings, thereby complicating precise measurement. This challenge is further evident in the cross-sectional FESEM image, where the dense structural interconnections disrupt the uniformity of the porous framework. Such irregularities make it difficult to accurately isolate and define measurement regions, resulting in reduced reliability of dimensional assessment at this stage of etching. Consequently, the average size of the cross-shaped structures in the sample etched for 30 minutes could not be reliably determined for direct comparison with the other samples. This finding explains the wider FWHM and lower Raman intensity reported in Section 4.2.1, as the irregular surface topography and increased pore wall interconnection can introduce greater phonon scattering and strain in the material (Cullis et al., 1997; X. G. Zhang, 2004). These effects lead to a loss of vibrational coherence, broadening the Raman peaks, while the reduced uniformity and diminished effective surface area for resonance enhancement lower the overall Raman signal intensity.

Figure 4.6 presents the EDX characterization of PSi. The spectrum in Figure 4.6(A) depicts the primary elemental composition of the PSi structure, which, as expected, consists predominantly of silicon (Si) and oxygen (O). The presence of oxygen is attributed to the electrochemical etching process. Figure 4.6(B) shows the corresponding atomic and weight percentages, with O and Si comprising 33.7% and 66.3% of the atomic composition and 22.45% and 77.55% of the weight composition, respectively. Across different etching times, the elemental composition remains largely consistent.

A)

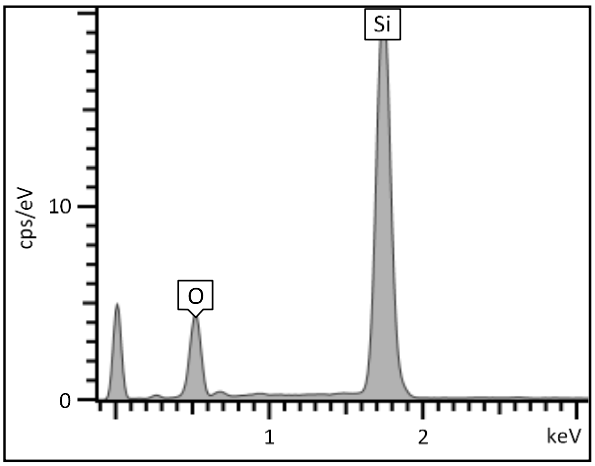

B)

Element	Atomic %	Wt%	Wt% Sigma
O	33.7	22.45	0.45
Si	66.3	77.55	0.45
Total:	100	100	

Figure 4.6 EDX Characterization of PSi. (A) Spectrum Confirming The Elements Present in Porous Structure; (B) Percentage of The Atomic and Weight for Elements Present in Porous Structure

4.3 Raman Characterization of AgNPs-Coated PSi SERS Substrate

In this section, the influence of AgNPs size on the Raman spectra of PSi is systematically examined. The PSi samples were etched for 22 minutes, a condition previously identified as optimal in Section 4.2.1 based on their structural and Raman characteristics. To establish a meaningful comparison, the Raman spectra of AgNPs with varying particle sizes deposited on bare silicon substrates are also measured and compared. This comparison enables a clearer understanding of how particle size affects the Raman spectra in both porous and non-porous silicon-based SERS substrates.

To ensure the repeatability of the results, for each AgNP size, three samples are prepared and analyzed. The reported spectra in this section are the average from ten separate measurement points taken across different regions of the samples.

Figure 4.7(A) and (B) present the Raman spectra of bare silicon and PSi-based substrates coated with various sizes of AgNPs, respectively.

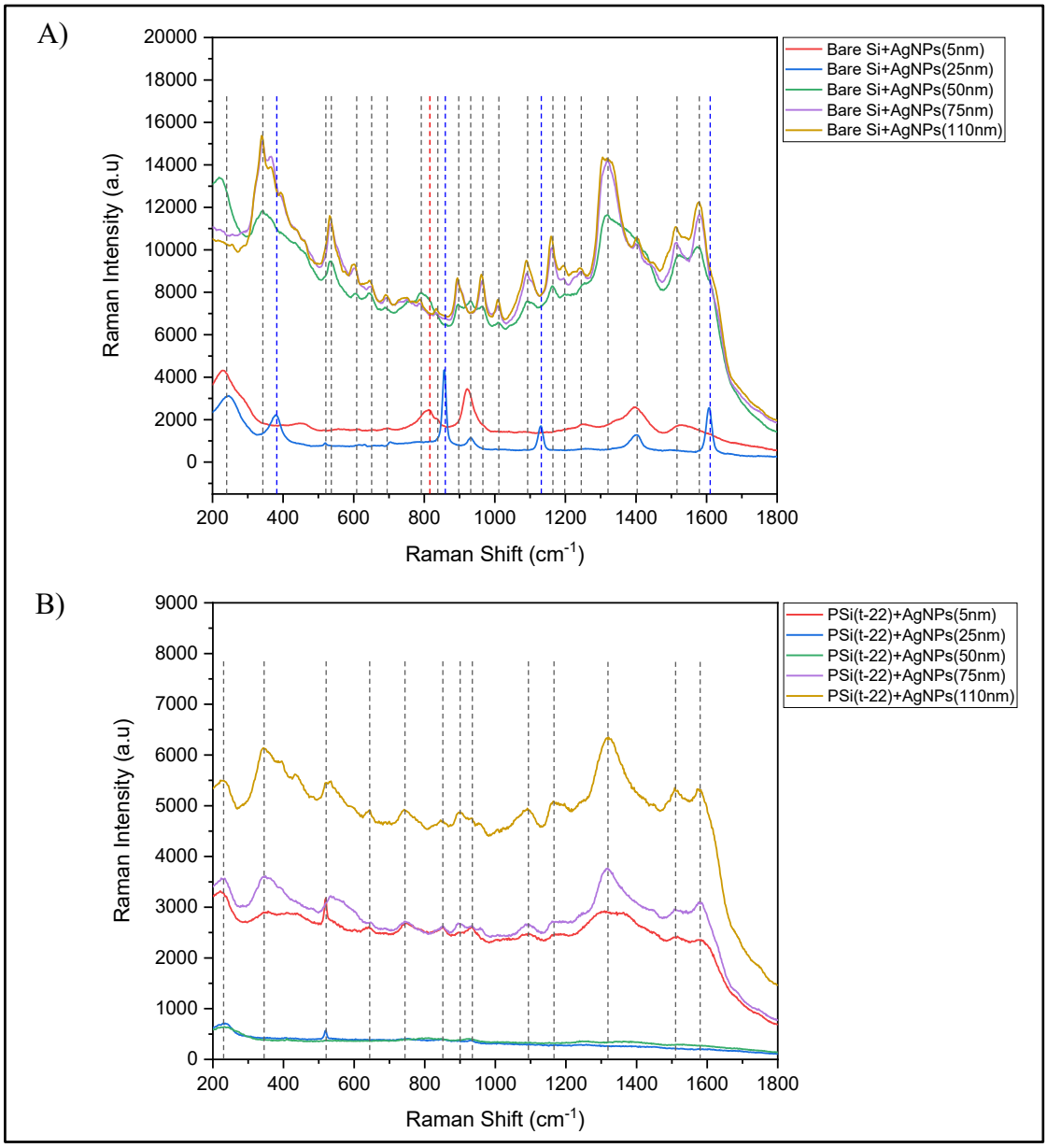

Figure 4.7 Raman Spectra of Substrates Coated with AgNPs of Various Sizes (5 nm, 25 nm, 50 nm, 75 nm and 110 nm). (A) Bare Silicon Substrate and (B) PSi-Based Substrate

From Figure 4.7(A), bare silicon substrates coated with smaller AgNPs (5 nm and 25 nm) produce Raman spectra with lower fluorescence background signals,

which is desirable for reducing spectral interference. In contrast, larger AgNPs (50 nm, 75 nm and 110 nm) generate significantly higher fluorescence background signals. Table 4.3 lists the Raman peaks observed in each spectrum. The spectra for 5 nm and 25 nm AgNPs display fewer Raman peaks compared to those with 50 nm, 75 nm and 110 nm. A lower number of peaks is advantageous as it minimizes the risk of overlap with Raman signals from target analyte molecules, enhancing the accuracy of detection.

Table 4.3
Raman Peaks of Bare Silicon Coated with Different Sizes of AgNPs

Bare + 5 *nm*	**Bare + 25 *nm***	**Bare + 50 *nm***	**Bare + 75 *nm***	**Bare + 110 *nm***
		Raman Shift *(cm^{-1})*		
231	246	218	-	-
-	-	344	341	341
-	378	-	-	-
-	-	536	534	534
-	-	601	604	601
-	-	645	649	645
-	-	690	690	690
-	-	790	790	788
814	-	-	-	-
-	857	-	-	-
-	-	896	894	894
921	932	930	-	-
-	-	963	963	961
-	-	1009	1009	1009
-	-	1090	1090	1090
-	1130	-	-	-
-	-	1162	1160	1160
-	-	-	1246	1240
-	-	1318	1318	1305
1398	1400	-	1400	1400
1529	-	1519	1513	1513
-	-	1575	1580	1576
-	1607	-	-	-

However, the larger AgNPs (50 nm, 75 nm and 110 nm) exhibit peaks of higher intensity, indicating stronger LSPR activity (Mosier-Boss, 2017), with only a subtle

Raman shift observed. This suggests that, despite the increased background, these particle sizes provide better Raman signal enhancement, thereby improving the sensitivity of the substrate. It is also noted that the Raman spectra for 50 nm, 75 nm and 110 nm AgNPs exhibit almost similar characteristics.

Figure 4.7(B) presents the Raman spectra of PSi etched for 22 minutes and subsequently deposited with AgNPs of varying sizes which are 5 nm, 25 nm, 50 nm, 75 nm and 110 nm. The spectra reveal a notable suppression of the silicon peak at 520 cm^{-1}, particularly with the deposition of larger AgNPs. The characteristic silicon peak at 520 cm^{-1} is only observed in the Raman spectra of PSi samples coated with 5 nm and 25 nm AgNPs. This indicates that the Si-Si vibrational mode remains detectable only at smaller nanoparticle sizes. The presence of this peak suggests that the underlying PSi structure is still partially exposed and accessible to the Raman excitation laser, allowing the crystalline silicon vibration to be captured. In contrast, for larger AgNPs sizes (50 nm, 75 nm and 110 nm), the silicon peak is no longer visible. This decrease in peak intensity is likely attributed to the increased surface coverage by the larger AgNPs, which may mask the underlying PSi structure and hinder the interaction between the laser and the Si-Si bonds.

A relatively low baseline intensity is observed in the Raman spectra of PSi coated with AgNPs sized at 25 nm and 50 nm, with baseline values remaining below 1000 a.u. This suggests a cleaner spectral background and reduced fluorescence or scattering noise, which is favourable for signal clarity. In contrast, samples coated with 5 nm and 75 nm AgNPs exhibit elevated baseline intensities ranging from approximately 3000 a.u. to 4000 a.u., indicating increased background signals that may interfere with peak analysis. The highest baseline intensity is recorded for the PSi sample coated with 110 nm of AgNPs, reflecting a substantial increase in background noise. This rise in baseline intensity with larger nanoparticle sizes may be attributed to increased light scattering (Mosier-Boss, 2017), aggregation effects (Kahraman et al., 2017) or enhanced surface plasmon resonance (Cialla et al., 2012) that contributes to higher background fluorescence. These variations in baseline intensity highlight the influence of nanoparticle size on the optical response and signal quality of the SERS substrate.

Table 4.4 lists the distinctive Raman peaks observed from PSi-based substrates coated with various sizes of AgNPs. Compared to the Raman spectra of bare silicon, the PSi-based substrates spectra display a noticeably lower number of peaks.

This reduction in peak occurrence indicates a cleaner spectral background, which is advantageous for future analyte detection. Fewer interfering peaks reduce spectral overlap, thereby enhancing the accuracy and sensitivity of detecting specific target molecules in subsequent analyses. It should also be noted that peak shifts are observable, depending on the nanoparticle sizes. These shifts occur because variations in AgNPs dimensions alter the local electromagnetic environment, modulating the vibrational energy levels detected by the Raman laser. Larger nanoparticles generate stronger localized surface plasmon resonance fields and changes in surface coverage or nanoparticle aggregation further affect coupling with the underlying PSi. The size-dependent peak shifts demonstrate that the optical and electronic environment of the substrate is highly sensitive to nanoparticle dimensions and precise control of AgNPs size is essential to achieve reproducible Raman signals and reliable analyte detection.

Table 4.4
Raman Peaks of PSi Coated with Different Sizes of AgNPs

PSi + 5 *nm*	**PSi + 25 *nm***	**PSi + 50 *nm***	**PSi + 75 *nm***	**PSi + 110 *nm***
		Raman Shift *(cm^{-1})*		
221	233	231	233	221
-	-	-	349	344
520	520	-	-	-
-	-	-	534	534
640	-	-	647	643
748	-	-	744	742
851	-	-	849	844
-	-	-	894	896
932	-	-	957	957
1092	-	-	1090	1090
1170	-	-	1160	1164
1309	-	-	1318	1320
1515	-	-	1506	1508
1582	-	-	1575	1571

4.4 Detection Performance of AgNPs-Coated PSi SERS Substrates

This section presents and discusses the Raman analysis results of SERS substrates deposited with varying concentrations of R6G, aimed at evaluating their performance in detecting low-concentration analytes. The performance of

AgNPs-coated PSi substrates is compared with that of AgNPs-coated bare silicon substrates in terms of EF. Then, the LOD of the optimum SERS substrate is evaluated. The AgNPs used for coating varied in size: 5 nm, 25 nm, 50 nm, 75 nm and 110 nm. For the PSi samples, etching duration of 22 minutes was selected for its superior performance reported in Section 4.2.1. To ensure result repeatability, the spectra reported in this section represent the average of ten measurements taken at different regions of the samples. For each AgNP size, three independent samples were prepared and analyzed.

4.4.1 Enhancement Factor (EF) of AgNPs-Coated Bare Silicon Substrate

Figure 4.8 shows the Raman spectra of R6G deposited on AgNPs-coated bare silicon substrate for different AgNPs sizes. The concentration of R6G is 0.01 M. The presence of R6G at a concentration of 0.01 M is confirmed by the appearance of characteristic Raman peaks corresponding to R6G, as mentioned in Table 3.1 in Section 3.4.1. The Raman intensity of these peaks varies significantly depending on the size of the AgNPs used to coat the bare silicon substrate. For uncoated bare silicon (black line) and bare silicon coated with 5 nm AgNPs (red line), no detectable R6G peaks are observed. However, when the AgNPs size is increased to 25 nm (blue line), the characteristic R6G peaks become visible, demonstrating improved signal enhancement. This indicates that the 5 nm particle size is insufficient for effective SERS enhancement at this concentration. A further increase in AgNPs size to 50 nm (green line) results in a substantial increase in Raman intensity, with this size yielding the highest signal among all tested samples. Beyond 50 nm, a decline in Raman intensity is observed. Specifically, substrates coated with 75 nm and 110 nm AgNPs exhibit reduced signal strength, suggesting a decrease in SERS enhancement efficiency at larger nanoparticle sizes. This trend highlights the critical influence of AgNPs size on the performance of the bare silicon-based SERS substrate, with 50 nm emerging as the most effective for detecting R6G at low concentrations.

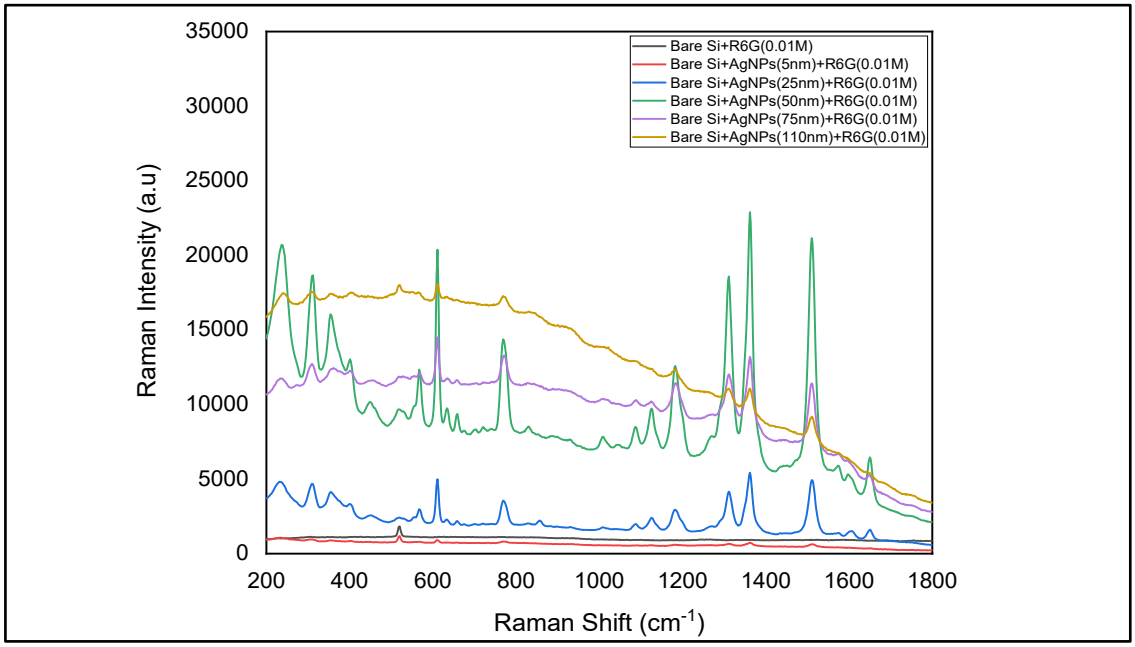

Figure 4.8 Raman Spectra of R6G (0.01 M) Deposited on AgNPs-Coated Bare Silicon Substrates with Different AgNPs Sizes

Table 4.5 tabulates the EF of bare silicon coated with different sizes of AgNPs to evaluate the Raman enhancement. The EF is calculated using equation (3.2) in Section 3.4.1 where, I_{SERS} is the intensity of the selected peak height at 611 cm^{-1} obtained from AgNPs-coated bare silicon substrate. C_{SERS} is the concentration of the R6G (0.01 M) deposited on AgNPs-coated bare silicon substrate. I_{BARE} is the intensity of the same peak (611 cm^{-1}) measured from uncoated bare silicon, which is 430 a.u. C_{BARE} refers to the concentration of R6G deposited on bare silicon, which is 0.0209 M. These values enable the comparison of SERS performance across different AgNPs sizes. The highest EF of 55.38 is obtained from bare silicon coated with 50 nm AgNPs.

Table 4.5
Enhancement Factor (EF) of Bare Silicon-Based SERS Substrates

Substrate	**Raman Peak Height (611 cm^{-1})**	**EF**
Bare Si + R6G (0.01M)	Not detectable	-
Bare Si + AgNPs (5 nm) + R6G (0.01M)	177.62	0.86
Bare Si + AgNPs (25 nm) + R6G (0.01M)	2852.64	13.86
Bare Si + AgNPs (50 nm) + R6G (0.01M)	11393.07	**55.38**
Bare Si + AgNPs (75 nm) + R6G (0.01M)	2931.32	14.25
Bare Si + AgNPs (110 nm) + R6G (0.01M)	998.95	4.86

4.4.2 Enhancement Factor (EF) of AgNPs-Coated PSi Substrate

Figure 4.9 displays the Raman spectra of R6G at a concentration of 0.01 M deposited on PSi-based substrates coated with AgNPs of various sizes. Similar to the uncoated bare silicon, the absence of AgNPs (black line), no detectable R6G peaks are observed, confirming that the PSi alone does not provide sufficient enhancement for Raman detection. This highlights the crucial role of AgNPs in facilitating SERS (Katyal, 2019; Mosier-Boss, 2017).

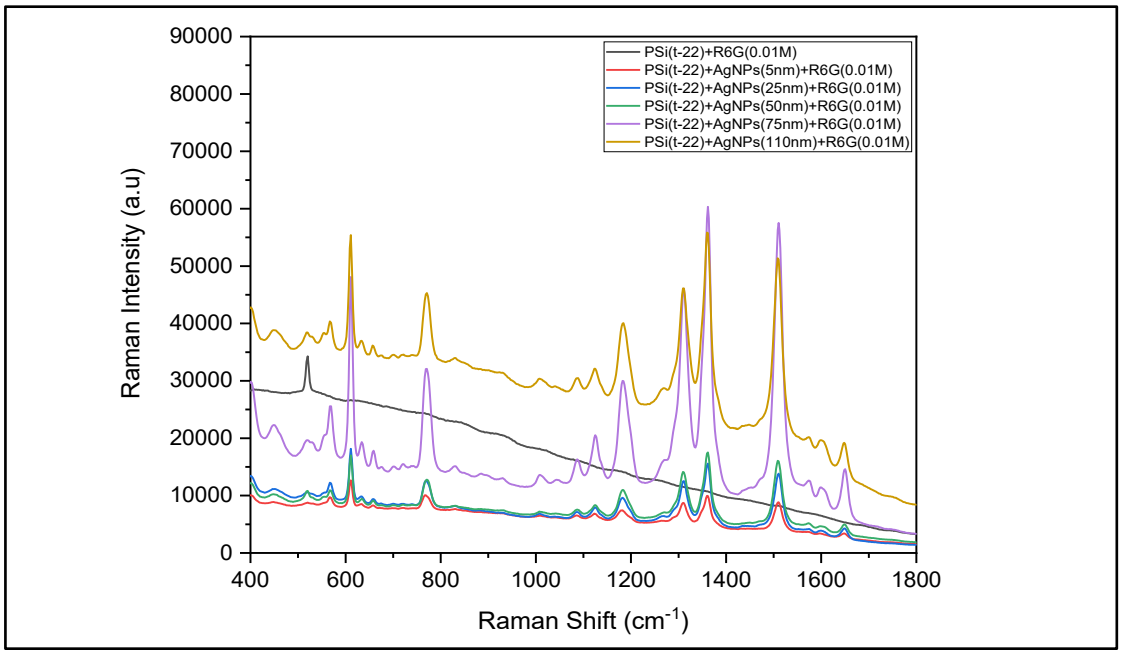

Figure 4.9 Raman Spectra of R6G (0.01 M) Deposited on AgNPs-Coated PSi Substrates with Different AgNPs Sizes

Table 4.6
Enhancement Factor (EF) of PSi-Based SERS Substrates

Substrate	**Raman Peak Height (611 cm^{-1})**	**EF**
PSi(t-22) + R6G (0.01M)	Not detectable	-
PSi(t-22) + AgNPs (5 nm) + R6G (0.01M)	4464.66	21.70
PSi(t-22) + AgNPs (25 nm) + R6G (0.01M)	8645.29	42.02
PSi(t-22) + AgNPs (50 nm) + R6G (0.01M)	8035.22	39.05
PSi(t-22) + AgNPs (75 nm) + R6G (0.01M)	30564.03	**148.56**
PSi(t-22) + AgNPs (110 nm) + R6G (0.01M)	19490.00	94.73

When comparing the SERS performance of PSi-based substrates to those based on bare silicon, the PSi-based substrates exhibit significantly better Raman signal enhancement across all AgNPs sizes tested. Among them, the PSi substrate coated

with 75 nm AgNPs demonstrates the highest Raman intensity, corresponding to an EF of 148.56 as tabulated in Table 4.6. This superior performance can be attributed to the synergistic interaction between the porous structure, the AgNPs and the R6G molecules (Bandarenka et al., 2018). The porous architecture of PSi provides a high surface area, enabling more effective nanoparticle loading and facilitating stronger LSPR effects from successive scattering of the trapped photons (Dariani & Ahmadi, 2013). These factors collectively contribute to enhanced electromagnetic field generation at the surface, which amplifies the Raman signal of the analyte (Zhong et al., 2018).

Overall, the results confirm that both the porous structure of the substrate and the size of the AgNPs significantly influence the enhancement of Raman signal intensity. These factors play a critical role in determining the detection performance of the SERS substrate toward target analytes. The PSi provides a high surface area for nanoparticle attachment and analyte interaction, while the size of the AgNPs affects the LSPR behaviour, which is key to signal amplification. Among all the tested configurations, the PSi-based substrate coated with 75 nm of AgNPs demonstrated the highest EF, indicating its superior SERS performance.

Moreover, FESEM images of the 75 nm AgNP-coated PSi SERS substrate are presented in Figure 4.10 to depict its structural properties. As a result of the electrochemical etching process, cross-shaped PSi structures are formed, which are subsequently coated with 75 nm AgNPs, as shown in Figure 4.10(A). The cross-sectional view in Figure 4.10(B) reveals triangle-shaped features, with the AgNPs coating clearly visible. However, the distribution of the nanoparticles is uneven, which is expected due to the drop-casting method used for their deposition on the PSi surface. Based on these results, this specific substrate configuration was selected for further evaluation. The next section examines the LOD of the PSi-based SERS substrate coated with 75 nm AgNPs to assess its sensitivity in detecting low-concentration analytes.

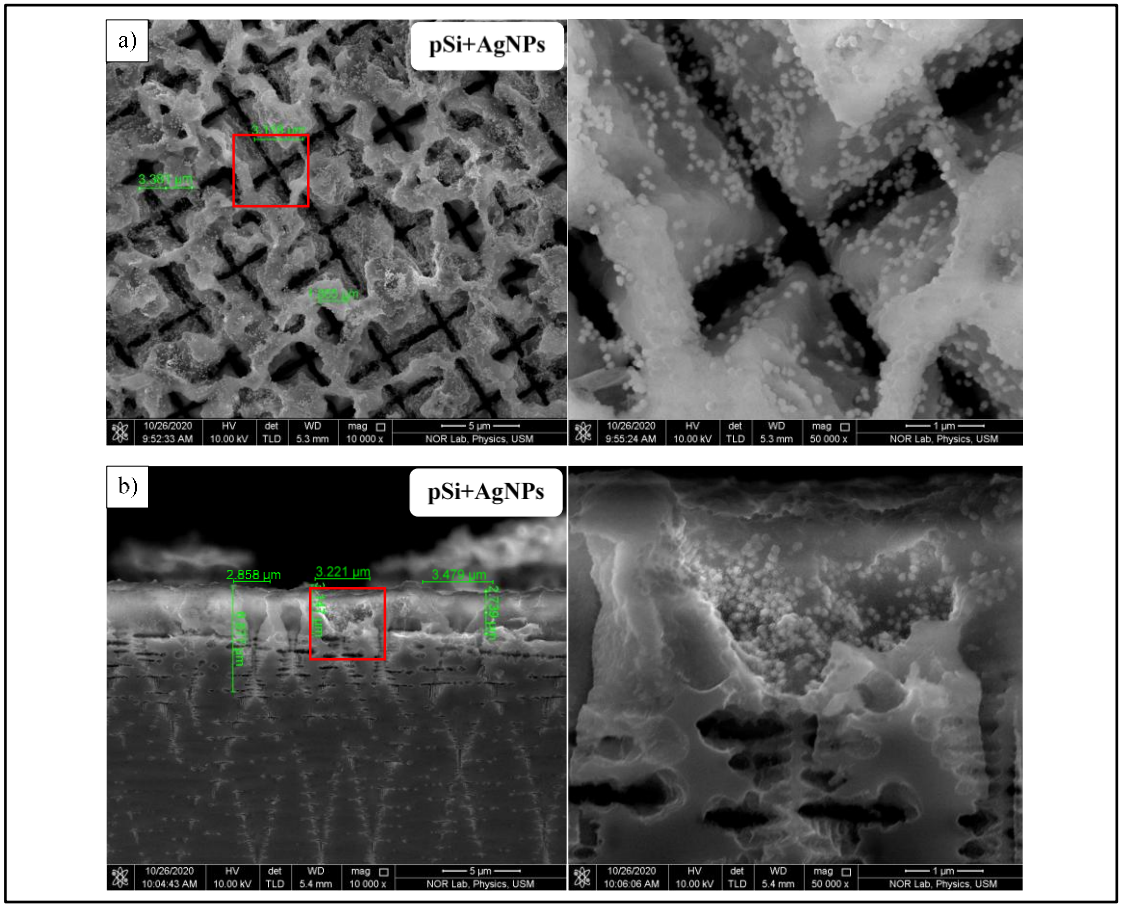

Figure 4.10 FESEM Images of AgNPs-Coated PSi SERS Substrate (75 nm). (A) Top-View at 10000× Magnification (Left) and 50000× Magnification (Right, Zoomed from The Red Box); (B) Cross-Sectional View at 10000× Magnification (Left) and 50000× Magnification (Right, Zoomed from The Red Box)

Figure 4.11 presents the EDX characterization of the 75 nm AgNPs-coated PSi SERS substrate. The spectrum in Figure 4.11(A) shows distinct peaks for carbon (C), oxygen (O), silicon (Si) and silver (Ag), confirming the presence of these elements in the AgNPs-coated PSi SERS substrate. The detection of Ag is consistent with the expected incorporation from the AgNPs layer on the PSi surface. Quantitative analysis in Figure 4.11(B) indicates that Si accounts for the highest proportion, with 47.76% atomic composition and 49.56% weight composition, reflecting the underlying porous silicon framework. O with 30.67% atomic composition and 18.13% weight composition, is likely related to native oxide formation on the silicon surface. Meanwhile, C comprising 15.14% atomic composition and 6.72% weight composition, may originate from surface contamination or residual organics. The Ag signal, measured at 6.42% atomic composition and 25.59% weight composition, confirms the successful deposition of AgNPs, which is critical for SERS activity. The relatively high

weight percentage of Ag compared to its atomic percentage can be attributed to its higher atomic mass. Overall, the results verify the elemental composition and successful fabrication of the AgNPs-coated PSi substrate.

A)

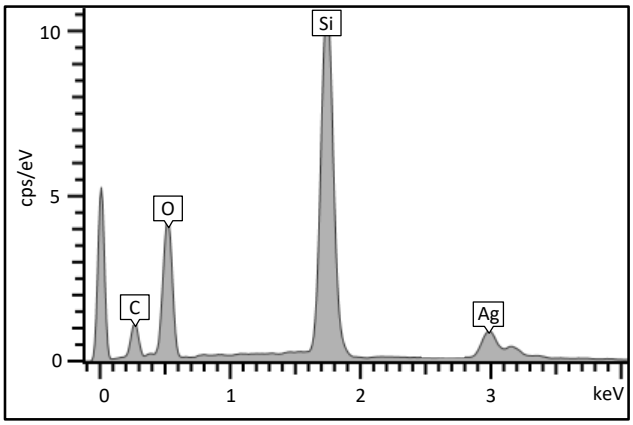

B)

Element	Atomic %	Wt%	Wt% Sigma
C	15.14	6.72	0.4
O	30.67	18.13	0.45
Si	47.76	49.56	0.74
Ag	6.42	25.59	0.92
Total:	100	100	

Figure 4.11 EDX Characterization of 75 nm AgNPs-Coated PSi SERS Substrate. (A) Spectrum Confirming The Elements Present in Substrate; (B) Percentage of The Atomic and Weight for Elements Present in Substrate

Finally, Figure 4.12 compares the Raman spectrum of R6G obtained from the optimum PSi SERS substrate coated with 75 nm AgNPs against that from bare silicon substrate. This comparison underscores the role of the porous structure and AgNPs deposition in enhancing Raman signal intensity, thereby improving detection effectiveness. The spectrum acquired from the fabricated SERS substrate (red line) displays distinct and well-defined R6G Raman peaks, whereas the spectrum from bare silicon, lacking surface modification and plasmonic metal deposition (black line), exhibits only weak and barely discernible peaks.

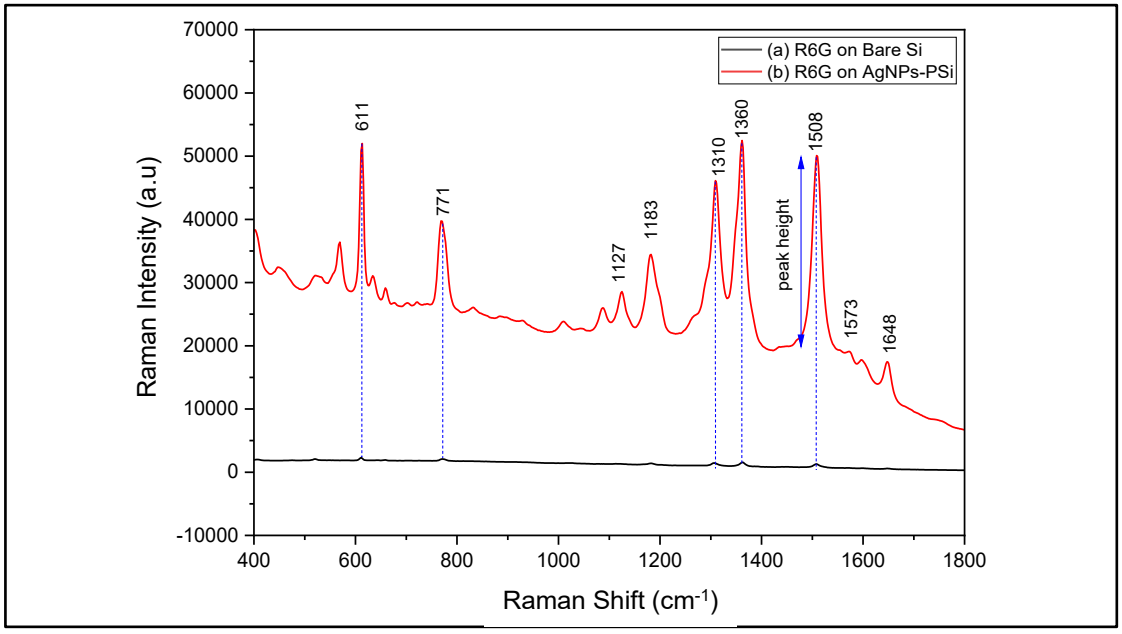

Figure 4.12 Raman Spectrum of R6G (0.02 M) Deposited on (A) Bare Silicon Substrate and (B) 75nm AgNPs-Coated PSi SERS Substrate

4.4.3 Limit of Detection (LOD)

To evaluate the LOD of R6G, several concentrations of R6G which are 1 mg/mL, 0.1 mg/mL and 0.01 mg/mL were deposited on the 75 nm AgNPs-coated PSi SERS substrate. Concentration values in mg/mL were used instead of molar units to maintain consistency with the concentration format applied for NS1 in the following section. Since the exact molar mass of NS1 is not definitively established due to variations in glycosylation and structure, expressing concentrations in molar terms is less usual. Therefore, mg/mL was chosen as the preferred unit for both analytes. Figure 4.13 clearly shows the R6G signature peaks at 611 cm^{-1}, 773 cm^{-1}, 1183 cm^{-1}, 1310 cm^{-1}, 1360 cm^{-1} and 1507 cm^{-1} on 1 mg/mL and 0.1 mg/mL concentrations, as highlighted in yellow. However, as the concentration was reduced to 0.01 mg/mL, most of the signature peaks could be noted, but a few were ambiguous. The peaks may not be obvious if the concentration were reduced further. Thus, 0.01 mg/mL was selected as the LOD of R6G.

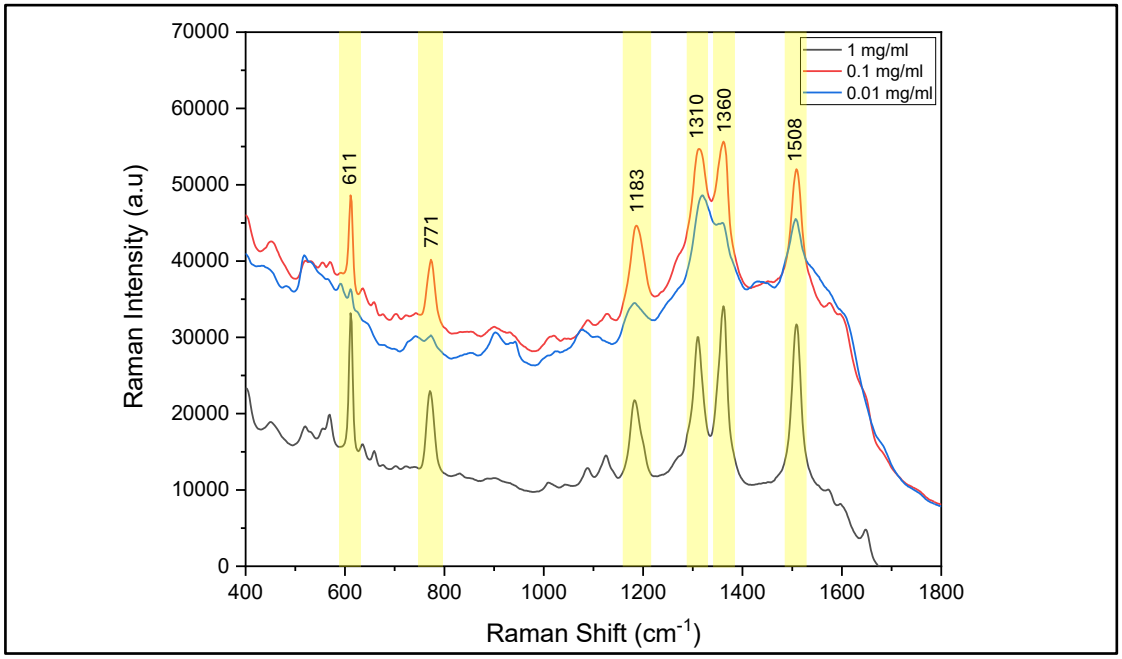

Figure 4.13 Raman Spectra of R6G at Concentrations of 1, 0.1 and 0.01 mg/mL Deposited on 75 nm AgNPs-Coated PSi SERS Substrate

4.5 Detection of Low-Concentration Dengue NS1 Antigen

Prior to detection of NS1 antigen, the 75 nm AgNPs-coated PSi SERS substrate are functionalized with dengue antibody as described in Section 3.5. Figure 4.14 shows the Raman spectra acquired from two samples of functionalized 75 nm AgNPs-coated PSi substrates: S1 and S2. The peaks are observed and labelled. Raman-shifts of the peaks are consistent for every spectrum. It is essential to identify peaks related to the substrate prior to the detection of the low-concentration NS1, to ensure the peaks detected originate from the NS1 molecules and not from the substrate.

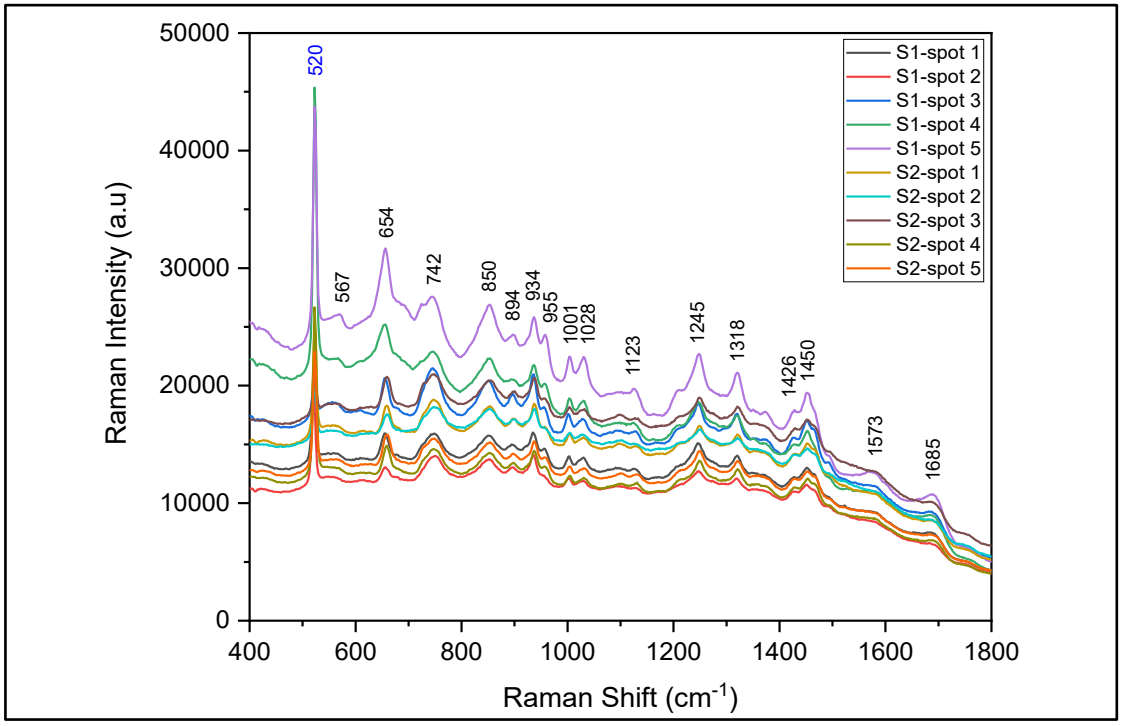

Figure 4.14 Raman Spectra of The Functionalized 75 nm AgNPs-Coated PSi SERS Substrates Sampled from Different Spots on S1 and S2

The performance of 75 nm AgNPs-coated PSi SERS substrate in detecting NS1 is illustrated in Figure 4.15. It compares the Raman spectra of NS1 at 0.01 mg/mL deposited on different functionalized substrates, obtained from 75 nm AgNPs-coated PSi SERS substrate, PSi-based without AgNPs and bare silicon substrates. No peaks are observed on the functionalized PSi (red line) and bare silicon (blue line) spectra, except at Raman shift 520 cm^{-1}, which corresponds to the silicon crystalline structure of the substrates. This indicates that the PSi-based and bare silicon substrates are unable to detect the presence of NS1 at 0.01 mg/mL.

It is noted that the peak intensity of 520 cm^{-1} from functionalized PSi substrate (red line) has a significantly higher intensity than bare silicon substrate (blue line). This result just shows that the formed porous structures have improved the occurrence of Raman scattering in the vicinity of the substrate surface. A similar observation was also found in unfunctionalized PSi reported in Section 4.2.2 and published in (Ismail et al., 2022). Functionalized PSi coated with 75 nm AgNPs produced a Raman spectrum (black line) with significant peaks indicating its capability to detect the presence of NS1. This finding shows that the presence of AgNPs significantly improved the performance of the SERS substrate in detecting NS1.

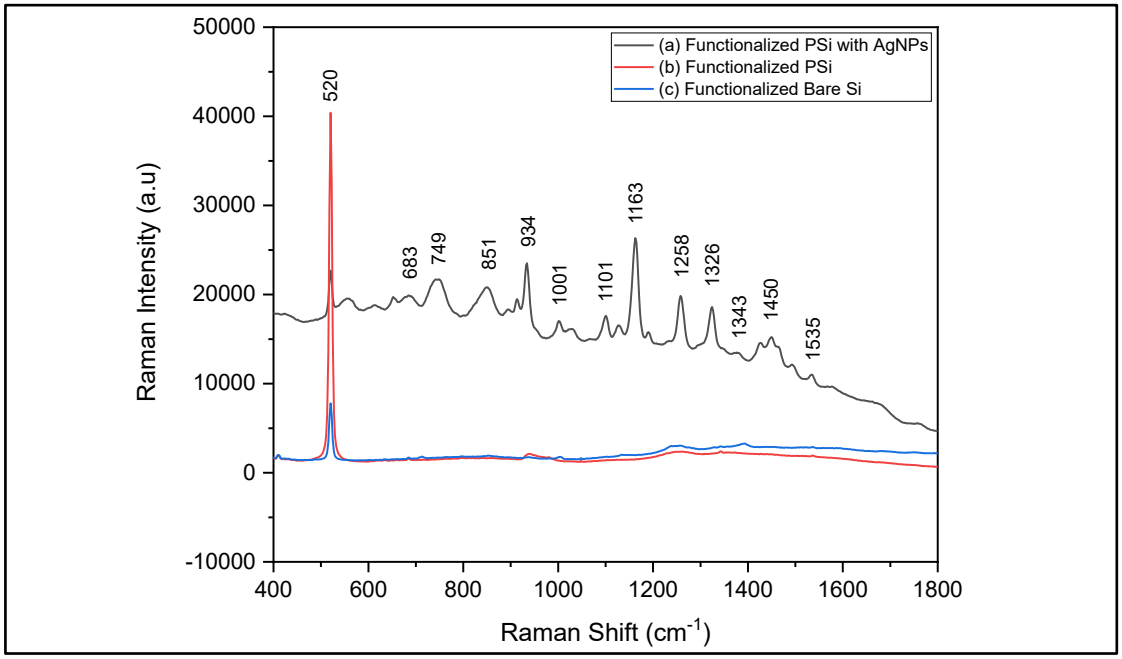

Figure 4.15 Raman Spectra of 0.01 mg/mL NS1 Deposited on (A) Functionalized AgNPs-Coated PSi SERS Substrate, (B) Functionalized PSi Substrate without AgNPs and (C) Functionalized Bare Silicon Substrate

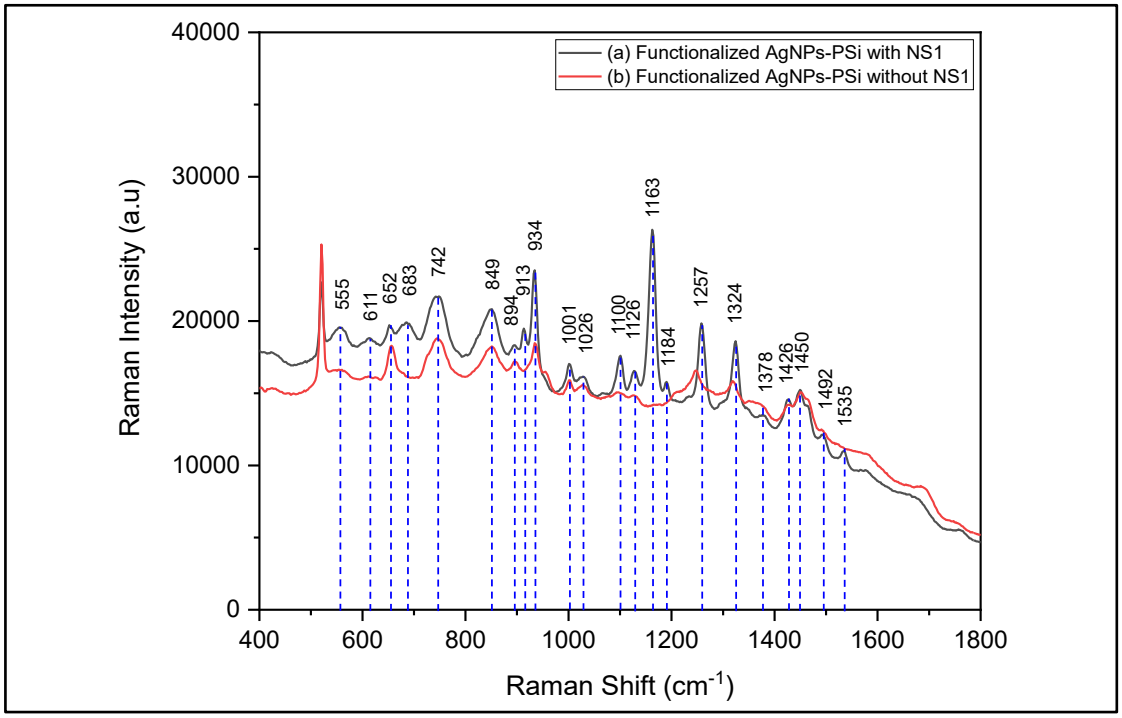

Figure 4.16 Raman Spectra of AgNPs-Coated PSi SERS Substrate Functionalized (A) With 0.01 mg/mL NS1 and (B) Without NS1

Figure 4.16 compares the Raman spectra of 75 nm AgNPs-coated PSi SERS substrates functionalized with NS1 and without NS1. Additional peaks are observed at 611 cm^{-1}, 686 cm^{-1}, 913 cm^{-1}, 1163 cm^{-1}, 1184 cm^{-1}, 1378 cm^{-1} and 1535 cm^{-1}.

Meanwhile, peaks at 555 cm^{-1}, 934 cm^{-1}, 1100 cm^{-1} and 1126 cm^{-1} are increased in intensity. Peaks at 1257 cm^{-1} and 1324 cm^{-1} are observed to have slightly shifted to the right. Despite the lack of absolute assignment of the Raman peaks, some of the peaks and their corresponding assignment are found from previous studies (Adar, 2022; Kengne-Momo et al., 2012; Movasaghi et al., 2007; Rygula et al., 2013) and the studies listed in Table 4.7. Some peaks are not reported in the previous studies since Raman spectroscopy is not well established in biological sample analysis including protein antigen binding. Thus, it is a potential research area that needs further exploration.

Table 4.7
Raman Peaks Acquired from 0.01 mg/mL of NS1 Deposited on AgNPs-Coated PSi SERS Substrate and Their Corresponding Assignments

Peaks (cm^{-1})	**Origin (Intensity)**	**Assignment**
555	NS1(w)	NA
611	NS1(w)	NA
652	Substrate(m)/ NS1(w)	NA
683	NS1(w)	Tyrosine (Kengne-Momo et al., 2012)
742	Substrate (s)/ NS1(s)	NA
849	Substrate(m)/ NS1(s)	C-O-C skeletal mode of α-anomer (Movasaghi et al., 2007)
894	Substrate(vw)/ NS1(vw)	NA
913	NS1(w)	ρCH2 (Movasaghi et al., 2007)
934	Substrate(m)/ NS1(s)	Rocking vibration of CH_3 (δCH_3) (Kengne-Momo et al., 2012)
1001	Substrate(w)/ NS1(w)	Benzene ring breathing (Phe) (Kengne-Momo et al., 2012; Movasaghi et al., 2007)
1026	Substrate(vw)/ NS1(vw)	NA
1100	Substrate(vw)/ NS1(s)	C-C vibration mode of the gauche-bonded chain (Movasaghi et al., 2007)
1126	Substrate(vw)/ NS1(w)	C-N stretching vibration (protein vibration) (Rygula et al., 2013)
1163	NS1(vs)	Tyrosine (Movasaghi et al., 2007)
1184	NS1(vw)	Cytosine, guanine, adenine (Movasaghi et al., 2007)
1244	Substrate(m)	One of the two distinct peaks for RNA (Movasaghi et al., 2007)
1257	NS1(s)	Amide III, adenine, cytosine (Movasaghi et al., 2007)
1324	Substrate(m), NS1(s)	Vibration of CH_3 (Movasaghi et al., 2007)
1378	NS1(vw)	CH rocking (Movasaghi et al., 2007)
1426	Substrate(vw)/NS1(vw)	NA
1450	Substrate(m)/NS1(m)	CH2 bending (Rygula et al., 2013)
1492	Substrate(vw)/NS1(vw)	NA
1535	NS1(w)	Amide carbonyl group vibration and aromatic hydrogens, Tryptophan-v side chain (Adar, 2022)

Note: Adapted from Ismail et al. (2024). Intensity level: Very weak (vw), weak (w), medium (m), strong (s) and very strong (vs); NA novel application

To determine the LOD for NS1 using the functionalized 75 nm AgNPs-coated PSi SERS substrate, NS1 was deposited on the substrates at different concentration levels. Figure 4.17 shows the Raman spectra obtained from several concentration of NS1 which are 0.1 mg/mL, 0.05 mg/mL, 0.02 mg/mL and 0.01 mg/mL. A few of the peaks appear consistently for all concentrations but reduce in intensity with the increased concentration of NS1. The peaks that remain visible at 0.01 mg/mL of NS1 are 683 cm^{-1}, 1163 cm^{-1}, 1257 cm^{-1} and 1535 cm^{-1}.

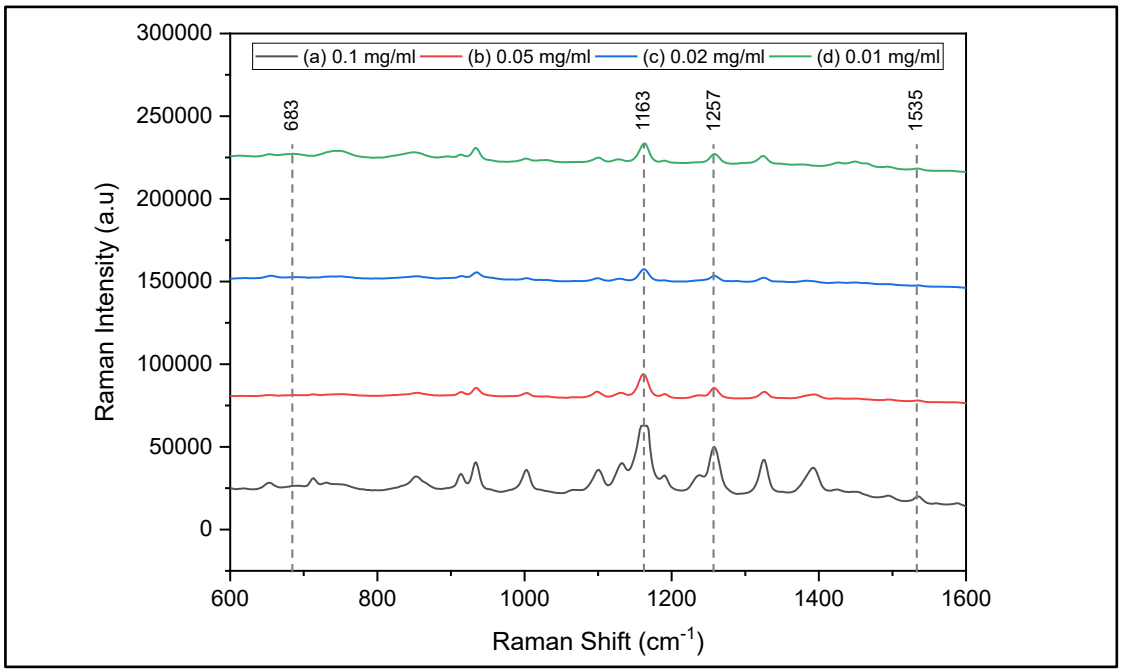

Figure 4.17 Raman Spectra of NS1 at Different Concentrations. (A) 0.1 mg/mL, (B) 0.05 mg/mL, (C) 0.02 mg/mL and (D) 0.01 mg/mL

Figure 4.18 shows the Raman spectra of NS1 at even lower concentrations (0.005 mg/mL, 0.002 mg/mL and 0.001 mg/mL). The Raman spectrum of the substrate without NS1 (the black line) is also included to differentiate between peaks associated with the substrate and NS1. With reference to the NS1 at 0.001 mg/mL spectrum (the blue line), very weak peaks are observed at 684 cm^{-1}, 934 cm^{-1}, 1138 cm^{-1}, 1340 cm^{-1} and 1535 cm^{-1}. With reference to Figure 4.16, peak 934 cm^{-1} belongs to the substrate, while peaks 683 cm^{-1} and 1535 cm^{-1} are present in the NS1 Raman spectrum at 0.01 mg/mL. Hence, the fabricated functionalized 75 nm AgNPs-coated PSi SERS substrate can actually detect the presence of NS1 up to 0.001 mg/mL. This achievement comes as a surprise since only electrochemical fabrication and drop casting methods

were used, due to limitations in facilities, which are simple and perhaps inadequate relative to the qualitative performance of SERS. The result is promising for the detection of NS1 using the proposed substrate. The EF and LOD values can be improved further with more advanced, expensive fabrication and deposition methods.

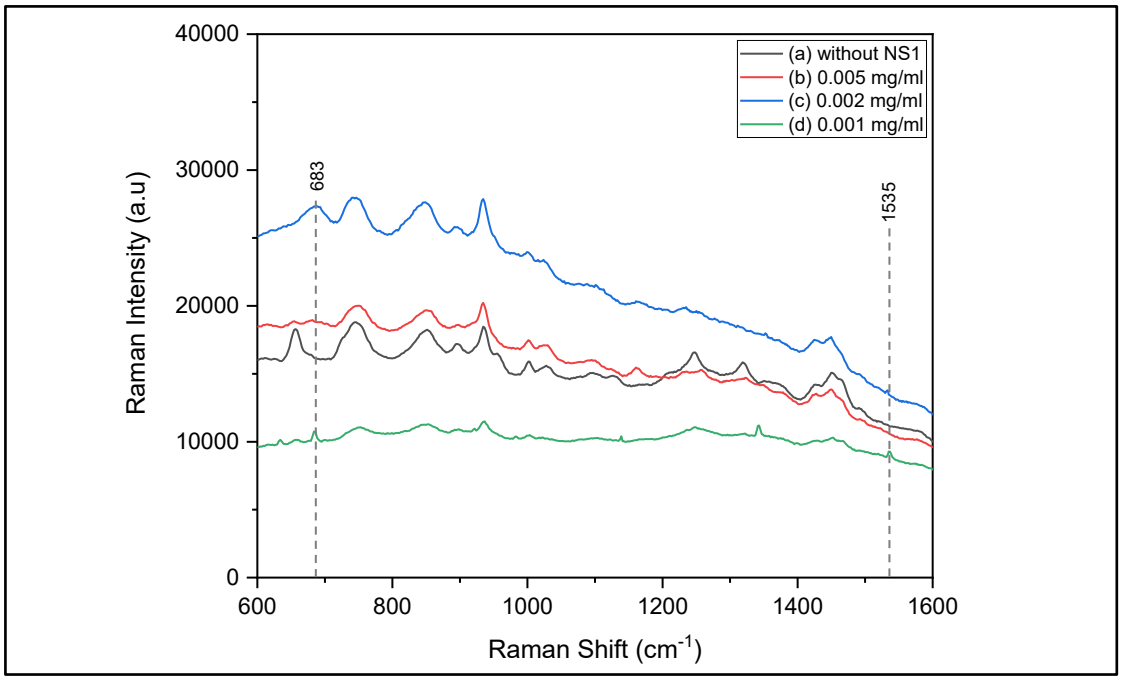

Figure 4.18 Raman Spectra of The Substrate (Black Line) and NS1 at Much Lower Concentrations: (B) 0.005 mg/mL, (C) 0.002 mg/mL and (D) 0.001 mg/mL

4.6 Conclusion

Overall, the findings presented in this chapter demonstrate the significant impact of varied parameters, particularly etching time and AgNPs deposition size on the structural, optical and sensing performance of PSi-based SERS substrates. The optimized AgNPs-coated PSi substrate exhibited superior EF compared to their bare silicon counterparts, enabling the sensitive detection of low-concentration dengue NS1 antigen. These results validate the effectiveness of the proposed substrate design and fabrication approach, aligning closely with the research objectives.

CHAPTER 5
CONCLUSION

5.1 Introduction

The primary objective of this study was to develop a SERS substrate capable of detecting low concentrations of DENV NS1 protein, aiming to facilitate a non-invasive saliva-based diagnostic method. This was achieved through the fabrication and characterization of AgNPs-coated PSi SERS substrates followed by performance evaluation using R6G and NS1 as analytes.

Among the fabricated substrates, the one coated with 75 nm AgNPs emerged as the most effective, demonstrating significantly enhanced Raman signal intensity. The substrate achieved a maximum EF of 148.56, indicating its strong capability to amplify Raman signals and its effectiveness in enhancing molecular detection sensitivity. This high EF value validates the substrate's LSPR efficiency from the interaction of the AgNPs and high surface area architecture of the PSi as critical factors for optimal SERS performance.

In terms of analytical sensitivity, the 75 nm AgNPs-coated PSi substrate achieved a LOD of 0.01 mg/mL for R6G, a widely used Raman marker, confirming its competence in detecting low-abundance molecules. More importantly, it demonstrated an even lower LOD of 0.001 mg/mL for NS1, a key biomarker for early DENV infection. This substantial sensitivity to NS1 is particularly significant, as it underscores the substrate's potential for real-world application in early-stage dengue diagnosis through saliva samples, a method that is both non-invasive and patient-friendly compared to conventional blood-based assays.

The findings from this study contribute meaningful insights into the design and optimization of SERS substrates, emphasizing the importance of nanoparticle size and surface morphology in determining performance. The 75 nm AgNPs-coated PSi SERS substrate provided an optimal balance between surface area, plasmonic activity and analytes interaction on the PSi template, resulting in superior enhancement and detection capability.

In conclusion, the study successfully fulfilled its research objectives and established that a 75 nm AgNPs-coated PSi SERS substrate fabricated via electrochemical methods and simple drop casting deposition technique is a highly sensitive and promising platform for detecting low concentrations of NS1. The demonstrated LOD and EF values support its potential as early, non-invasive dengue detection using salivary diagnostics. These findings initiate for further development of portable, low-cost and rapid diagnostic devices that could significantly improve public health surveillance and clinical outcomes in dengue-endemic regions.

5.2 Future Work

Building on the promising results of this study, several future works are recommended to further enhance the performance, reliability and practical applicability of the AgNPs-coated PSi SERS substrate for NS1 dengue detection:

a) Optimization of Fabrication and Deposition Techniques

While the electrochemical method used in this study proved effective, employing more advanced fabrication technique, such as electron-beam lithography, nanosphere lithography or atomic layer deposition could significantly improve the uniformity, nanostructure control and reproducibility of the SERS substrates. Enhanced structural precision would likely contribute to higher enhancement factors, reduced variability between batches and better signal stability in practical applications.

b) Clinical Validation Using Saliva Samples from Dengue Patients

To establish real-world diagnostic potential, future studies should involve the analysis of actual saliva samples from dengue-positive patients. This will help evaluate the substrate's sensitivity and specificity in complex biological matrices, assess potential interference from salivary components and verify its practical feasibility for non-invasive, point-of-care testing. Benchmarking against standard diagnostic techniques like ELISA or RT-PCR in terms of sensitivity, cost, processing time and user-friendliness would provide valuable insights into its competitive advantages and areas for improvement.

c) Long-Term Stability and Reusability Testing

Investigating the chemical and structural stability of the SERS substrates over time is essential for practical deployment. Future work should evaluate substrate shelf-life, resistance to oxidation and potential for repeated use without significant loss of signal intensity or sensitivity.

d) Integration into Portable Diagnostic Platforms

For field and clinical applications, the SERS substrate should be integrated into a compact and user-friendly device. Future work could focus on coupling the optimized substrate with miniaturized Raman spectrometers, microfluidic sample handling systems and automated data analysis software to create a rapid, portable diagnostic tool suitable for deployment in low-resource settings.

5.3 Summary

This study presents several key academic contributions in the development of SERS-based biosensing for low-concentration dengue NS1 detection.

1. A 75 nm AgNPs-coated porous silicon (PSi) substrate was successfully fabricated using an electrochemical technique, providing a reproducible and stable nanostructured platform.
2. The substrate demonstrated strong enhancement performance, achieving a maximum EF of 148.56 and a LOD of 0.01 mg/mL using the Raman marker Rhodamine 6G (R6G).
3. Most notably, it enabled ultrasensitive detection of the DENV NS1 antigen with a limit of detection of 0.001 mg/mL, highlighting its potential for non-invasive, salivary-based diagnostics.

REFERENCES

Abdullah, N. H. (2022). *Situasi semasa demam denggi, zika dan chikungunya di Malaysia tahun 2021*.

Abdullah, N. H. (2023). *Situasi semasa demam denggi di Malaysia tahun 2022*.

Abood, H. K., & Mutlak, F. A. H. (2020). Structural, morphological and optical properties of *n*-type porous Silicon-effect of etching current density. *IOP Conference Series: Materials Science and Engineering*, *757*(1).

Hassan, M. R. A. (2024). *Situasi semasa demam denggi di Malaysia: Minggu epidemiologi 52 (24 Disember - 30 Disember 2023)*.

Hassan, M. R. A. (2025). *Situasi semasa demam denggi di Malaysia tahun 2024*.

Adar, F. (2022, February). Interpretation of Raman spectrum of proteins. *Spectroscopy*, *37*(2), 9–13, 25.

Albrecht, M. G., & Creighton, J. A. (1977). Anomalously intense Raman spectra of pyridine at a silver electrode. *Journal of the American Chemical Society*, *99*(15), 5215–5217.

Alcon, S., Talarmin, A., Debruyne, M., Falconar, A., Deubel, V., & Flamand, M. (2002). Enzyme-linked immunosorbent assay specific to dengue virus type 1 nonstructural protein NS1 reveals circulation of the antigen in the blood during the acute phase of disease in patients experiencing primary or secondary infections. *Journal of Clinical Microbiology*, *40*(2), 376–381.

Al-Hosaini, K., & Azhar, A. (2021). Silver nanoparticle and their antimicrobial properties. *EC Pharmacology and Toxicology*, *9*(3), 1–8.

Al-Syadi, A. M., Faisal, M., Harraz, F. A., Jalalah, M., & Alsaiari, M. (2021). Immersion-plated palladium nanoparticles onto meso-porous silicon layer as novel SERS substrate for sensitive detection of imidacloprid pesticide. *Scientific Reports*, *11*, 9174.

Amador-Martínez, J. D., Flores-López, N. S., Hernandez-Martínez, A. R., Calderón-Ayala, G., Bocarando-Chacon, J., Cayetano-Castro, N., Martínez-Suarez, F., Leal-Pérez, J. E., Cortez-Valadez, M., & Britto Hurtado, R. (2023). Experimental and DFT studies of copper nanoparticles as SERS substrates. *Applied Physics A: Materials Science and Processing*, *129*(4).

Anand, A. M., Sistla, S., Dhodapkar, R., Hamide, A., Biswal, N., & Srinivasan, B. (2016). Evaluation of NS1 antigen detection for early diagnosis of dengue in a

tertiary hospital in Southern India. *Journal of Clinical and Diagnostic Research*, *10*(4), DC01–DC04.

Anders, K. L., Nguyet, N. M., Quyen, N. T. H., Ngoc, T. Van, Tram, T. Van, Gan, T. T., Tung, N. T., Dung, N. T., Chau, N. V. V., Wills, B., & Simmons, C. P. (2012). An evaluation of dried blood spots and oral swabs as alternative specimens for the diagnosis of dengue and screening for past dengue virus exposure. *American Journal of Tropical Medicine and Hygiene*, *87*(1), 165–170.

Andreev, R. B., Bobovich, Ya. S., Bortkevich, A. V., Volosov, V. D., & Tsenter, M. Ya. (1976). Raman spectra of rhodamine 6G molecules in intense and weak resonance fields. *Journal of Applied Spectroscopy*, *25*, 1013–1015.

Banavar, S. R., & Vidya, G. S. (2014). Diagnostic efficacy of saliva for dengue - A reality in near future? A piloting initiative. *Journal of Clinical and Diagnostic Research*, *8*(3), 229–232.

Bandarenka, H. V., Girel, K. V., Zavatski, S. A., Panarin, A., & Terekhov, S. N. (2018). Progress in the development of SERS-active substrates based on metal-coated porous silicon. *Materials*, *11*(5).

Canham, L. T. (1990). Silicon quantum wire array fabrication by electrochemical and chemical dissolution of wafers. *Applied Physics Letters*, *57*(10), 1046–1048.

Carrara, S., Sacchetto, D., Doucey, M. A., Baj-Rossi, C., De Micheli, G., & Leblebici, Y. (2012). Memristive-biosensors: A new detection method by using nanofabricated memristors. *Sensors and Actuators, B: Chemical*, *171–172*, 449–457.

Çelik, Y., & Kurt, A. (2021). Three dimensional porous expanded graphite/silver nanoparticles nanocomposite platform as a SERS substrate. *Applied Surface Science*, *568*, 150946.

Abdullah, C. A. C., Razak, D. F. A., Yunus, M. B. M., & Zaki, M. Y. M. (2019). Structural and optical properties of *n*-type and *p*-type porous silicon produced at different etching time. *International Journal of Electroactive Materials*, *7*, 28–37.

Chen, H., Park, S. K., Joung, Y., Kang, T., Lee, M. K., & Choo, J. (2022). SERS-based dual-mode DNA aptasensors for rapid classification of SARS-CoV-2 and influenza A/H1N1 infection. *Sensors and Actuators B: Chemical*, *355*.

Chen, Y., Zheng, S., Tang, X., Wang, F., Wang, L., & Li, C. (2023). Recent research progress of surface-enhanced Raman scattering dominated analysis strategies in early diagnosis of diseases. *Chemistry – An Asian Journal*, *18*(12).

Cialla, D., März, A., Böhme, R., Theil, F., Weber, K., Schmitt, M., & Popp, J. (2012). Surface-enhanced Raman spectroscopy (SERS): Progress and trends. *Analytical and Bioanalytical Chemistry*, *403*, 27–54.

Cullis, A. G., Canham, L. T., & Calcott, P. D. J. (1997). The structural and luminescence properties of porous silicon. *Journal of Applied Physics*, *82*(3), 909–965.

Costa, V. G. da, Marques-Silva, A. C., & Moreli, M. L. (2014). A meta-analysis of the diagnostic accuracy of two commercial NS1 antigen ELISA tests for early dengue virus detection. *PLoS ONE*, *9*(4).

Dariani, R. S., & Ahmadi, Z. (2013). Study of porous silicon structure by Raman scattering. *Optik*, *124*(22), 5353–5356.

Das, S., Saxena, K., Tinguely, J. C., Pal, A., Wickramasinghe, N. L., Khezri, A., Dubey, V., Ahmad, A., Perumal, V., Ahmad, R., Wadduwage, D. N., Ahluwalia, B. S., & Mehta, D. S. (2023). SERS nanowire chip and machine learning-enabled classification of wild-type and antibiotic-resistant bacteria at species and strain levels. *ACS Applied Materials and Interfaces*, *15*(20), 24047–24058.

Dengue and severe dengue. (2014). *World Health Organization*, 1–4.

Deschaines, T., Hodkiewicz, J., & Henson, P. (2009). Characterization of amorphous and microcrystalline silicon using Raman spectroscopy. *Thermo Fisher Scientific*.

Dussart, P., Labeau, B., Lagathu, G., Louis, P., Nunes, M. R. T., Rodrigues, S. G., Storck-Herrmann, C., Cesaire, R., Morvan, J., Flamand, M., & Baril, L. (2006). Evaluation of an enzyme immunoassay for detection of dengue virus NS1 antigen in human serum. *Clinical and Vaccine Immunology*, *13*(11), 1185–1189.

Fisher, R., Lustig, Y., Sklan, E. H., & Schwartz, E. (2023). The role of NS1 protein in the diagnosis of flavivirus infections. *Viruses*, *15*(2).

Fleischmann, M., Hendra, P. J., & Mcquillan, A. J. (1974). Raman spectra of pyridine adsorbed at a silver electrode. *Chemical Physics Letters*, *26*, 163–166.

Gardiner, D. J., & Graves, P. R. (1989). *Practical Raman Spectroscopy* (D. J. Gardiner & P. R. Graves, Eds.; 1st ed.). Springer Berlin, Heidelberg.

Gu, Y., Wang, J., Luo, Z., Luo, X., Lin, L. L., Ni, S., Wang, C., Chen, H., Su, Z., Lu, Y., Gan, L. Y., Chen, Z., & Ye, J. (2024). Multiwavelength surface-enhanced Raman scattering fingerprints of human urine for cancer diagnosis. *ACS Sensors*, *9*(11), 5999–6010.

Hadis, N. S. M. (2018). *Development of fluidic-based memristor sensor for biosensing application* (Doctoral dissertation). Universiti Sains Malaysia.

Harb, N. H., & Mutlak, F. A. H. (2022). Effect of etching current density on spectroscopic, structural and electrical properties of porous silicon photodetector. *Optik*, *249*, 168298.

He, X. N., Gao, Y., Mahjouri-Samani, M., Black, P. N., Allen, J., Mitchell, M., Xiong, W., Zhou, Y. S., Jiang, L., & Lu, Y. F. (2012). Surface-enhanced Raman spectroscopy using gold-coated horizontally aligned carbon nanotubes. *Nanotechnology*, *23*(20), 205702.

Hildebrandt, P., & Stockburger, M. (1984). Surface-enhanced resonance Raman spectroscopy of Rhodamine 6G adsorbed on colloidal silver. *The Journal of Physical Chemistry*, *88*(24), 5935–5944.

Huang, S., Zhang, H., Wu, Z., Kong, D., Lin, D., Fan, Y., Yang, X., Zhong, Z., Huang, S., Jiang, Z., & Cheng, C. (2014). Large-area ordered *p*-type Si nanowire arrays as photocathode for highly efficient photoelectrochemical hydrogen generation. *ACS Applied Materials and Interfaces*, *6*(15), 12111–12118.

Humaidi, M., Tien, W. P., Yap, G., Chua, C. R., & Ng, L. C. (2021). Non-invasive dengue diagnostics – The use of saliva and urine for different stages of the illness. *Diagnostics*, *11*(8).

Ismail, N. F., Lee, K. Y., Ismail, L. N., Rahim, A. F. A., Hadis, N. S. M., & Radzol, A. R. M. (2022). Structural, electrical and Raman characterization of AgNP-coated porous silicon SERS substrate for detection of dengue NS1 protein. *2022 IEEE-EMBS Conference on Biomedical Engineering and Sciences (IECBES)*, 78–83.

Ismail, N. F., Lee, K. Y., Hadis, N. S. M., Ismail, L. N., Rahim, A. F. A., Abdullah, M. H., & Radzol, A. R. M. (2024). Nano silver-coated porous silicon-based surface-enhanced Raman spectroscopy substrate for low-concentration dengue NS1 protein detection. *Journal of Applied Spectroscopy*, *91*(2), 480–488.

Ivanda, M. (2018). Raman spectroscopy of porous silicon. In L. Canham (Ed.), *Handbook of Porous Silicon* (3rd ed., pp. 611–620). Springer, Cham.

Jakubowicz, J. (2007). Nanoporous silicon fabricated at different illumination and electrochemical conditions. *Superlattices and Microstructures*, *41*(4), 205–215.

Jeanmaire, D. L., & Van Duyne, R. P. (1977). Surface Raman spectroelectrochemistry: Part I. Heterocyclic, aromatic, and aliphatic amines adsorbed on the anodized silver electrode. *Journal of Electroanalytical Chemistry and Interfacial Electrochemistry*, *84*(1), 1–20.

Kahraman, M., Mullen, E. R., Korkmaz, A., & Wachsmann-Hogiu, S. (2017).

Fundamentals and applications of SERS-based bioanalytical sensing. *Nanophotonics*, *6*(5), 831–852.

Kaladharan, K., Chen, K. H., Chen, P. H., Goudar, V. S., Ishdorj, T. O., Santra, T. S., & Tseng, F. G. (2023). Dual-clamped one-pot SERS-based biosensors for rapid and sensitive detection of SARS-CoV-2 using portable Raman spectrometer. *Sensors and Actuators B: Chemical*, *393*.

Katyal, J. (2019). Comparative study between different plasmonic materials and nanostructures for sensor and SERS application. In C. D. Geddes (Ed.), *Reviews in Plasmonics 2017* (1st ed., pp. 77–108). Springer, Cham.

Kengne-Momo, R. P., Daniel, Ph., Lagarde, F., Jeyachandran, Y. L., Pilard, J. F., Durand-Thouand, M. J., & Thouand, G. (2012). Protein interactions investigated by the Raman spectroscopy for biosensor applications. *International Journal of Spectroscopy*, *2012*, 1–7.

Khodke, P. B., Popat, R. R., Burakale, P. V., Chinchole, P. P., & Shrikhande, V. N. (2017). Silver nanoparticles - A review. *Research Journal of Pharmacy and Technology*, *10*(6), 1820–1833.

Kim, M. G., Jue, M., Lee, K. H., Lee, E. Y., Roh, Y., Lee, M., Lee, H. J., Lee, S., Liu, H., Koo, B., Jang, Y. O., Kim, E. Y., Zhen, Q., Kim, S. H., Kim, J. K., & Shin, Y. (2023). Deep learning assisted surface-enhanced Raman spectroscopy (SERS) for rapid and direct nucleic acid amplification and detection: Toward enhanced molecular diagnostics. *ACS Nano*, *17*(18), 18332–18345.

Kim, M., Huh, S., Park, H. J., Cho, S. H., Lee, M. Y., Jo, S., & Jung, Y. S. (2024). Surface-functionalized SERS platform for deep learning-assisted diagnosis of Alzheimer's disease. *Biosensors and Bioelectronics*, *251*.

Kumar, K., M, M. S., Kumar, P., Munjal, R., Mukhopadhyay, S., Mondal, D. P., Khan, M. A., & Vandana, V. (2024). Detection of water pollutants using super-hydrophobic porous silicon-based SERS substrates. *Microchimica Acta*, *191*, 357.

Kuntyi, O., Zozulya, G., & Shepida, M. (2022). Porous silicon formation by electrochemical etching. *Advances in Materials Science and Engineering*, *2022*(1), 1482877.

Lan, W., Zhao, J., Zhai, X., Gu, C., Jiang, T., & Wang, J. (2025). PCA-assisted direct diagnosis of Aβ proteins for Alzheimer's disease using non-metallic SERS platform of graphitic carbon nitride@metal-organic framework. *Colloids and Surfaces B: Biointerfaces*, *252*.

Le Ru, E. C., & Etchegoin, P. G. (2009). *Principles of Surface-Enhanced Raman Spectroscopy*. Elsevier.

Lin, D., Wu, Z., Li, S., Zhao, W., Ma, C., Wang, J., Jiang, Z., Zhong, Z., Zheng, Y., & Yang, X. (2017). Large-area Au-nanoparticle-functionalized Si nanorod arrays for spatially uniform surface-enhanced Raman spectroscopy. *ACS Nano*, *11*(2), 1478–1487.

Lin, H., Mock, J., Smith, D., Gao, T., & Sailor, M. J. (2004). Surface-enhanced Raman scattering from silver-plated porous silicon. *Journal of Physical Chemistry B*, *108*(31), 11654–11659.

Liu, L., Hou, S., Zhao, X., Liu, C., Li, Z., Li, C., Xu, S., Wang, G., Yu, J., Zhang, C., & Man, B. (2020). Role of graphene in constructing multilayer plasmonic SERS substrate with graphene/agnps as chemical mechanism - Electromagnetic mechanism unit. *Nanomaterials*, *10*(12), 1–16.

Liu, Y., Lei, L., Wu, Y., Chen, Y., Yan, J., Zhu, W., Tan, X., & Wang, Q. (2022). Fabrication of sea urchin-like Au@SiO2 nanoparticles SERS substrate for the determination of malachite green in tilapia. *Vibrational Spectroscopy*, *118*, 103319.

Low, S. P., & Voelcker, N. H. (2018). Biocompatibility of porous silicon. In L. Canham (Ed.), *Handbook of Porous Silicon* (3rd ed., pp. 533–545). Springer, Cham.

Machado, M. A. de A. M., Barbério, G., & Rios, D. R. (2012). Detection of dengue virus infection NS1 antigen using human saliva. *IADR General Session*.

Madalli, V. B. (2013). Saliva - A diagnostic tool. *IOSR Journal of Dental and Medical Sciences*, *11*(6), 96–99.

Malaysia Health Technology Assessment Section (MaHTAS). (2015). *Clinical practice guidelines Management of dengue infection in adults* (3rd ed.). Malaysia Health Technology Assessment Section (MaHTAS).

Mao, S., Pei, F., Feng, S., Hao, Q., Zhang, P., Tong, Z., Mu, X., Lei, W., & Liu, B. (2023). Detection of trace Rhodamine B using stable, uniformity, and reusable SERS substrate based on Ag@SiO2-Au nanoparticles. *Colloids and Surfaces A: Physicochemical and Engineering Aspects*, *657*, 130595.

Markin, A. V., Markina, N. E., Popp, J., & Cialla-May, D. (2018). Copper nanostructures for chemical analysis using surface-enhanced Raman spectroscopy. *Trends in Analytical Chemistry*, *108*, 247–259.

Mittal, S., Bansal, V., Garg, S., Atreja, G., & Bansal, S. (2011). The diagnostic role of

saliva - A review. *Journal of Clinical and Experimental Dentistry*, *3*(4), 314–320.

Mizuno, Y., Kotaki, A., Harada, F., Tajima. S, Kurane, I., & Takasaki, T. (2007). Confirmation of dengue virus infection by detection of dengue virus type 1 genome in urine and saliva but not in plasma. *Transactions of the Royal Society of Tropical Medicine & Hygiene*, *101*(7), 738–739.

Moi, M. L., Omatsu, T., Tajima, S., Lim, C. K., Kotaki, A., Ikeda, M., Harada, F., Ito, M., Saijo, M., Kurane, I., & Takasaki, T. (2013). Detection of dengue virus nonstructural protein 1 (NS1) by using ELISA as a useful laboratory diagnostic method for dengue virus infection of international travelers. *Journal of Travel Medicine*, *20*(3).

Mosier-Boss, P. A. (2017). Review of SERS substrates for chemical sensing. *Nanomaterials*, *7*(6).

Movasaghi, Z., Rehman, S., & Rehman, I. U. (2007). Raman spectroscopy of biological tissues. *Applied Spectroscopy Reviews*, *42*(5), 493–541.

Muller, D. A., & Young, P. R. (2013). The flavivirus NS1 protein: Molecular and structural biology, immunology, role inpathogenesis and application asadiagnostic biomarker. *Antiviral Research*, *98*(2), 192–208.

Mustapa, M. A., Latif, A. A., Awang, N. A., Muhammad, F. D., & Amir Hamzah, A. S. (2025). Modulating surface-enhanced Raman scattering with hybrid-gold nanostructures: PCA-driven insights into ultrasensitive detection of dengue virus NS1 IgG. *Microchemical Journal*, *210*.

nanoComposix. (n.d.). *Polyvinylpyrrolidone (PVP) Surface*. Retrieved April 30, 2024.

Nazarovskaia, D. A., Domnin, P. A., Gyuppenen, O. D., Tsiniaikin, I. I., Ermolaeva, S. A., Gonchar, K. A., & Osminkina, L. A. (2025). Bimetallic AuAg-coated porous silicon nanowire platform for rapid SERS-based antibiotic susceptibility testing. *Results in Surfaces and Interfaces*, *19*, 100524.

Nirala, N. R., Sadhasivam, S., Singh, R. K., Sionov, E., & Shtenberg, G. (2025). Sensitive ratiometric detection of Fumonisin B1 using a reusable Ag-pSi SERS platform. *Food Chemistry: X*, *25*, 102151.

Costrada, A. N., Felicia, Nina Siti Aminah, Masduki, F. F., Herman, Dessy Natalia, & Djamal, M. (2024). Detection of envelope glycoprotein domain III (ED III) based on Surface-Enhanced Raman Scattering for dengue diagnosis. *Journal of Physics: Conference Series*, *2696*(1).

Parkash, O., Yean, C. Y., & Shueb, R. H. (2014). Screen printed carbon electrode based

electrochemical immunosensor for the detection of dengue NS1 antigen. *Diagnostics*, *4*(4), 165–180.

Patolsky, F., Zheng, G., Hayden, O., Lakadamyali, M., Zhuang, X., & Lieber, C. M. (2004). Electrical detection of single viruses. *Proceedings of the National Academy of Sciences of the United States of America*, *101*(39), 14017–14022.

Poloni, T. R., Oliveira, A. S., Alfonso, H. L., Galvão, L. R., Amarilla, A. A., Poloni, D. F., Figueiredo, L. T., & Aquino, V. H. (2010). Detection of dengue virus in saliva and urine by real time RT-PCR. *Virology Journal*, *7*.

Prosyčevas, I., Juraitis, A., Puišo, J., Niaura, G., Guobienė, A., Tamulevičius, S., Balčaitis, G., & Šileikaitė, A. (2007). Synthesis and characterization of silver nanoparticles. In S. Ašmontas & J. Gradauskas (Eds.), *Advanced Optical Materials, Technologies, and Devices*. Society of Photo-Optical Instrumentation Engineers (SPIE).

Puppo, F., Doucey, M. A., Di Ventra, M., De Micheli, G., & Carrara, S. (2014). Memristor-based devices for sensing. *Proceedings 2014 - IEEE International Symposium on Circuits and Systems (ISCAS)*, 2257–2260.

Raman, C. V., & Krishnan, K. S. (1928). A new type of secondary radiation. *Nature*, *121*.

Razali, N. S. M., Rahim, A. F. A., Radzali, R., Mahmood, A., Yusuf, Y., Zulkifli, F., & Bakar, A. A. (2019). Investigation on the effect of direct current and integrated pulsed electrochemical etching of *n*-type (100) silicon. *Acta Physica Polonica A*, *135*(4), 697–701.

Radzol, A. R. M., Khuan, Y. L., Peng, S. W., Looi, I., & Mansor, W. (2024). Surface-enhanced raman spectroscopy with machine learning in non-invasive detection of dengue-NS1 fingerprint. *ESTEEM Academic Journal*, *20*(March), 65–81.

Rusli, N., Abdullah, N. H., & Chong, C. K. (2020). *Situasi semasa demam denggi, zika dan chikungunya di Malaysia (Minggu 51/2020)*.

Rygula, A., Majzner, K., Marzec, K. M., Kaczor, A., Pilarczyk, M., & Baranska, M. (2013). Raman spectroscopy of proteins: A review. *Journal of Raman Spectroscopy*, *44*(8), 1061–1076.

Sailor, M. J. (2011). *Porous Silicon in Practice: Preparation, Characterization and Applications*.

Schenkels, L. M., Veerman, E. C. I., & Nieuw Amerongen, A. V. (1995). Biochemical composition of human saliva in relation to other mucosal fluids. *Critical Reviews*

in Oral Biology & Medicine, *6*(2), 161–175.

Shlaga, R. A., Alwan, A. M., & Mohammed, M. S. (2025). Performance comparison of plasmonic sensors via ion reduction and KOH methods. *Journal of Applied Sciences and Nanotechnology*, *5*(2), 24–33.

Song, C., Zhang, J., Liu, Y., Guo, X., Guo, Y., Jiang, X., & Wang, L. (2020). Highly sensitive SERS assay of DENV gene via a cascade signal amplification strategy of localized catalytic hairpin assembly and hybridization chain reaction. *Sensors and Actuators, B: Chemical*, *325*.

Srivastava, S., Wang, W., Zhou, W., Jin, M., & Vikesland, P. J. (2024). Machine learning-assisted surface-enhanced Raman spectroscopy detection for environmental applications: A review. *Environmental Science and Technology*, *58*(47), 20830–20848.

Stankevičius, E., Ignatjev, I., Petrikaitė, V., Selskis, A., & Niaura, G. (2021). Gold nanoparticles generated using the nanosecond laser treatment of multilayer films and their use for SERS applications. *ACS Omega*, *6*(49), 33889–33898.

Suryana, R., & Aini, N. Q. (2022). Analysis of porous silicon formation on *n*-type Si (100) using laser-assisted electrochemical anodization method. *Journal of Physics and Its Applications*, *4*(2), 28–32.

Terry, L. R., Sanders, S., Potoff, R. H., Kruel, J. W., Jain, M., & Guo, H. (2022). Applications of surface-enhanced Raman spectroscopy in environmental detection. *Analytical Science Advances*, *3*(3–4), 113–145.

Vazquez, S., Ruiz, D., Barrero, R., Ramirez, R., Calzada, N., Peña, B. del R., Reyes, S., & Guzman, M. G. (2010). Kinetics of dengue virus NS1 protein in dengue 4-confirmed adult patients. *Diagnostic Microbiology and Infectious Disease*, *68*(1).

Vendamani, V. S., Sunkaranam, V. S. N. R., Pathak, A. P., & Soma, V. R. (2022). Silicon nanostructures for molecular sensing: A review. *ACS Applied Nano Materials*, *5*(4), 4550–4582.

Vulchi, R. teja, Morgunov, V., Junjuri, R., & Bocklitz, T. (2024). Artifacts and anomalies in Raman spectroscopy: A review on origins and correction procedures. *Molecules*, *29*(19), 4748.

Wang, S. M., & Sekaran, S. D. (2010). Early diagnosis of dengue infection using a commercial dengue duo rapid test kit for the detection of NS1, IgM, and IgG. *American Journal of Tropical Medicine and Hygiene*, *83*(3), 690–695.

Wang, X., Chen, Y., Gibney, K. A., Erramilli, S., & Mohanty, P. (2008). Silicon-based

nanochannel glucose sensor. *Applied Physics Letters*, *92*(1), 013903.

Wasik, D., Mulchandani, A., & Yates, M. V. (2018). Salivary detection of dengue virus NS1 protein with a label-free immunosensor for early dengue diagnosis. *Sensors*, *18*(8), 2641.

Xu, J., Wang, C., Wang, T., Wang, Y., Kang, Q., Liu, Y., & Tian, Y. (2018). Mechanisms for low-temperature direct bonding of Si/Si and quartz/quartz: Via VUV/O3 activation. *RSC Advances*, *8*(21), 11528–11535.

Zeng, Y., Koo, K. M., Trau, M., Shen, A. G., & Hu, J. M. (2019). Watching SERS glow for multiplex biomolecular analysis in the clinic: A review. *Applied Materials Today*, *15*, 431–444.

Zhang, H., Lv, X., Lv Changwu, & Jia, Z. (2012). *N*-type porous silicon as an efficient surface enhancement Raman scattering substrate. *Optical Engineering*, *51*(9), 099003.

Zhang, X. G. (2004). Morphology and formation mechanisms of porous silicon. *Journal of the Electrochemical Society*, *151*(1), C69.

Zhao, J., Wang, J., Liu, Y., Han, X. X., Xu, B., Ozaki, Y., & Zhao, B. (2022). Detection of prostate cancer biomarkers via a SERS-based aptasensor. *Biosensors and Bioelectronics*, *216*.

Zhong, F., Wu, Z., Guo, J., & Jia, D. (2018). Porous silicon photonic crystals coated with Ag nanoparticles as efficient substrates for detecting trace explosives using SERS. *Nanomaterials*, *8*(11), 872.

AUTHOR'S PROFILE

Noor Fadzilah binti Ismail obtained Bachelor of Science in Electrical & Electronics (Hons.) from Faculty of Electrical Engineering, Universiti Teknologi MARA, Cawangan Pulau Pinang Malaysia in 2020. Since March 2020, she has been pursuing MSc in Electrical Engineering at Faculty of Electrical Engineering, Universiti Teknologi MARA, Shah Alam. Her primary research interests focus in the field of Surface-Enhanced Raman Spectroscopy (SERS) and bio-sensing applications, with a particular focus on the design and fabrication of porous structured SERS substrates. Her MSc thesis is titled "Unravelling Porous Silicon (PSi)-Based Surface-Enhanced Raman Spectroscopy (SERS) Substrate Fabrication Formula Sensitive to Salivary Dengue Non-Structural Protein 1 (NS1)", explore on the development of PSi-based SERS platforms for the early, non-invasive detection of dengue biomarkers using salivary samples. Currently, she is actively engaged in advancing electrochemical fabrication techniques to enhance the sensitivity and reproducibility of SERS substrates for biosensing applications, particularly in the context of infectious disease diagnostics.

LIST OF PUBLICATIONS

Ismail, N. F., Ismail, L. N., Lee, K. Y., Zulhanip, A. Z., Hadis, N. S. M., & Radzol, A. R. M. (2021). Etching time on structural and electrical properties of porous

silicon SERS substrates for non-invasive dengue-NS1 detection. *International Journal of Integrated Engineering*, *13*(5), 119–126.

Ismail, N. F., Lee, K. Y., Hadis, N. S. M., Ismail, L. N., Rahim, A. F. A., Abdullah, M. H., & Radzol, A. R. M. (2024). Nano silver-coated porous silicon-based surface-enhanced Raman spectroscopy substrate for low-concentration dengue NS1 protein detection. *Journal of Applied Spectroscopy*, *91*(2), 480–488.

Ismail, N. F., Lee, K. Y., Ismail, L. N., Rahim, A. F. A., Hadis, N. S. M., & Radzol, A. R. M. (2022). Structural, electrical and Raman characterization of AgNP-coated porous silicon SERS substrate for detection of dengue NS1 protein. *2022 IEEE-EMBS Conference on Biomedical Engineering and Sciences (IECBES)*, 78–83.

Ismail, N. F., Radzol, A. R. M., Ismail, L. N., Lee, K. Y., Zulhanip, A. Z., & Hadis, N. S. M. (2022). Effect of current density on porous silicon (pSi) for non-invasive dengue detection SERS substrates: Electrical and structural property. *Journal of Electrical and Electronic Systems Research*, *20*, 59–65.

Ismail, N. F., Radzol, A. R. M., Zulhanip, A. Z., Ismail, L. N., Hadis, N. S. M., & Lee, K. Y. (2021). Effect of etching time variation on porous Si of SERS substrate for NS1 detection. *2020 IEEE EMBS Conference on Biomedical Engineering and Sciences (IECBES)*, 147–151.